THE EFFECTS OF AIR CONDENSATION ON PROPERTIES OF FLOW AND THEIR MEASUREMENT IN HYPERSONIC WIND TUNNELS

Thesis by

Jerry Grey

In Partial Fulfillment of the Requirements

For the Degree of

Doctor of Philosophy

California Institute of Technology

Pasadena, California

1952

ACKNOWLEDGMENTS

The author wishes to extend his sincerest thanks to Dr. Henry T. Nagamatsu for suggesting this investigation and patiently guiding its progress. The assistance of the staff of the GALCIT 5" Hypersonic Wind Tunnel was invaluable in the collection of data and in its analysis. In particular, the author wishes to express his appreciation to Mr. Manfred Eimer and Mr. Donald Coles, and to Miss Fae Scheinis for her help in the necessary computations. Discussions with Mr. Coles and Mr. Rolf Buhler were of great help in clarifying some of the problems of two-phase fluid flow. Miss Gerry Ellis and Miss Jean Mainwaring have the author's everlasting gratitude for their assistance in the preparation of the final copy of the thesis.

ABSTRACT

Some of the fundamental problems encountered in the measurement of flow properties in condensing air have been discussed, and were investigated experimentally in the GALCIT 5" Hypersonic Wind Tunnel. The saturated expansion theory of flow in a condensing fluid as developed by Buhler was corroborated, and some of the unknown properties of the theory have been clarified by analysis of the wind tunnel tests. Several experimental techniques for the measurement of two-phase fluid properties were developed, and the results were used to supply additional information concerning the nature of phenomena such as supersaturation and normal and oblique shock waves. No definite conclusions could be reached with regard to future application of condensed air wind tunnel data on the basis of these tests, but the subject of similarity parameters comparable to the Mach number in flow of a perfect gas has been discussed at some length.

TABLE OF CONTENTS

I. INTRODUCTION

The expansion of gas to high velocities in a wind tunnel results in a decrease in pressure and temperature of the gas. In subsonic and low supersonic tunnels, this expansion is very nearly isentropic, following the perfect gas laws, but as the supersonic area ratio is increased the free-stream pressure and temperature decrease until the condensation point of the gas is reached. At this point, one or a combination of two things may occur. The gas may continue to expand isentropically into a supersaturated condition, introducing some degree of irreversibility when the supersaturated state breaks down, or the gas properties may undergo no abrupt discontinuities, merely departing from the perfect gas relationships to some other type of expansion during which the condensation process occurs continuously. Full thermodynamic equilibrium is, of course, a special case of the latter.

Many theories have been advanced in attempting to describe the process by which condensation occurs under these conditions. Although much valuable data, both theoretical and experimental, have been gathered on the occurrence of water condensation, the problem of condensation of the air itself has shown many discrepancies from theories developed on the basis of water condensation studies. Despite interesting contributions to this problem by many investigators (Cf. Refs. 1 through 6, for example), the exact mechanism by which condensation of air is triggered and continued has not as yet been discovered. Recent GALCIT experiments by Nagamatsu and Willmarth (Ref. 7) and Arthur and Nagamatsu (Ref. 8) have shed much light on the subject from the standpoint of the effects of impurities in the wind tunnel gas, but a complete treatment of the

inception and evolution of air condensation with and without foreign particles still remains to be made.

The present paper does not attempt to discuss the merits or deficiencies of the various theories, but rather to describe and analyze a series of experiments performed in the GALCIT 5" Hypersonic Wind Tunnel whose aim is to investigate the effects of air condensation on wind tunnel measurements.

The present trend in hypersonic tunnel operation has been to avoid the condensation problem completely by preheating the air, and, if it were possible to obtain large amounts of supersaturation, this method might prove satisfactory. Nagamatsu and Willmarth (Ref. 7) and Arthur and Nagamatsu (Ref. 8) have shown, however, that even with commercially pure nitrogen, only moderate amounts of supersaturation (of the order of 18°C or about 1.2 Mach number) can be reached. The attainment of Mach numbers of, say, 15 and higher is extremely difficult by heating, particularly if it is remembered that local expansions in the neighborhood of the models often exceed the nominal test section air speeds by appreciable amounts. Another method of avoiding the condensation problem, namely the use of low-boiling point gases such as helium, appears to show definite promise, but involves certain problems which must be solved before this type of testing can be applied to wind-tunnel measurements.

In view of these difficulties facing wind tunnel operation at high Mach numbers, the possibility of utilization of condensed-air data, which offers the simplest mechanical solution, is not to be ignored. The present investigation has thus been made with the purpose of clarifying some of the problems encountered in making wind-tunnel measurements in the condensing air.

II. DISCUSSION

In order to devise a method whereby condensing-air data may be used in wind-tunnel testing, it is of prime importance that a simple set of flow equations valid for the two-phase fluid be developed. Of all the theories advanced to describe air condensation phenomena, only one deals with the region of most interest to this investigation: the region of fully-developed condensation well below the dew point. Buhler's postulation of expansion along the saturation curve (Ref. 9) appears to approximate closely the experimental results to date. Nagamatsu and Willmarth's results using commercial nitrogen (Ref. 7) and early data from the GALCIT 5" tunnel (Ref. 10) offered definite indications that the saturated expansion theory predicted two-phase gas properties in hypersonic tunnels with a better than fair degree of accuracy. The first task of the present investigation, then, was to obtain further experimental verification of this theory in order to justify later analysis based on Buhler's flow equations.

A. Theory

The basic premise of the saturated expansion theory is that the expansion takes place in the presence of a number of condensed air droplets sufficiently numerous to act as an infinite plane. The air is treated as diatomic vapor with a single saturation curve (to be discussed later) rather than as a mixture of two or more individual gases.

1. The Significance of "Mach number" in the Flow of a Condensing Gas

The details of the theory as derived by Buhler (Ref. 9) are outlined in Appendix A. The major deficiency in its present state is the absence of a significant flow parameter comparable to the Mach number in single-phase gas flow, and, although this absence offers few obstacles to the parametric use of the theory in reducing wind tunnel data, it will be required for a complete understanding of the phenomena of two-phase flow. The following discussion will serve to outline the difficulties.

In ordinary aerodynamic theory, the Mach number M has two fundamental characteristics: (a) it is a direct measure of the characteristic angle of infinitesimally weak waves, and hence of their speed of propagation, and (b) it is a measure of the ratio of inertia forces and pressure forces in the flow. Now if the speed of propagation of a sound wave in condensing flow is functionally different from that in a perfect gas (i.e., if the passage of an infinitesimally weak wave is not isentropic with respect to the vapor phase alone) then the same Mach number can no longer have both of these fundamental characteristics.

In attempting to select the significant Mach number, then, it is first necessary to decide which is the more significant quantity in hypersonic flow: speed of sound or dynamic-static pressure ratio. Buhler (Ref. 11) has shown that, for example, in the determination of the pressure coefficient on slender bodies, it is necessary to know the propagation speed of a weak wave (Cf. Appendix C-5). The application of the theory of characteristics, as well, is dependent on the definition of this propagation speed. Hence, although the quantity $\tilde{M}$ (defined in Appendix A), which is an indication of dynamic-static pressure ratio,

has been defined and measured, it is necessary that a true speed of propagation of an infinitesimally weak wave be defined for the two-phase air.

The question of the speed of sound in condensing air has been approached by Buhler by considering the character of the mixture of vapor and droplets. The quantity $\tilde{a}$ is defined in Appendix A on the assumption that, although the droplet and vapor temperatures are equal in continuous regions of flow, no heat transfer takes place between the liquid and vapor with the passage of an infinitesimal wave (i.e., $\tilde{a}$ is an isentropic sound velocity in the vapor phase alone). This essentially means that thermal equilibrium does not exist in the neighborhood of a disturbance; i.e., that the wave frequency is too high to enable the droplet temperature fluctuations to follow those of the vapor. This would be a reasonable assumption in the case of fairly large droplets and low density vapor.

Now, suppose the droplets are so large and the vapor density so low that the droplets, in addition to not following the vapor temperature fluctuations, do not follow the velocity fluctuations caused by the passage of a sound wave. Then the fluid behaves as a perfect gas containing inert particles, and the significant sound velocity would be $\check{a} = \sqrt{\gamma RT}$.

At the other end of the scale, when the droplets are so small that thermodynamic as well as mechanical equilibrium exists during passage of a sound wave, a different characteristic velocity is derived. This quantity, $\mathring{a}$, is often called the zero-frequency velocity of sound, since this state of equilibrium (i.e., isentropic passage of a wave in

the vapor-droplet system) will occur in any case provided the disturbance frequency is sufficiently low. $\mathring{a}$ is thus an isentropic sound velocity of the vapor-droplet system, and is calculated in Appendix A on this assumption.

Thus, the quantities $\mathring{a}$ and $\check{a}$ bracket all possible speeds of propagation of a sound wave in the two-phase fluid. $\tilde{a}$ falls somewhere between the two, and although $\tilde{a}$ may not be the physically significant velocity from this standpoint, its importance as the parameter which relates static and dynamic pressures makes it convenient to use as a wind tunnel parameter to aid in describing the properties of condensing air flow.

A one-dimensional calculation (Cf. Appendix A) of the characteristic sound velocity (i.e., the quantity which determines the lines of discontinuous velocity derivatives in the flow) shows that this velocity may always be defined as the square root of $dp/d\rho$ for passage of an infinitesimal wave, regardless of any assumptions about the interaction of vapor and droplets. Thus, a determination of $dp/d\rho$ would completely resolve the problem of determining a significant sound velocity for the two-phase fluid. Experiments performed in the GALCIT 5" tunnel (Ref. 10), in which the angle of a weak wave was measured and corrected for wave strength, indicate that the propagation speed in fully-developed condensing flow falls somewhere between $\mathring{a}$ and $\tilde{a}$. Experiments to determine $dp/d\rho$ in a different manner, by surveying along the length of the wind tunnel nozzle, were performed in connection with the present investigation and are discussed later in the text. In comparing these two measurements, however, it must be remembered that

the true characteristic velocity is determined by $dp/d\rho$ for passage of an infinitesimal wave, and consequently, the two determinations will be equal only if the equilibrium time delay during passage of such a wave is small.

In summarizing this discussion, there exist two physically significant reference velocities in condensing air. The primary one, the actual speed of propagation of an infinitesimally weak wave, is at present unknown. However, the velocity $\tilde{a}$, which is related by what shall be called the pseudo-Mach number $\tilde{M}$ to the dynamic-static pressure ratio*, is easily defined and measured.

2. Saturation Curve for Air

Data for the saturation curve used in the investigation were obtained from saturation vapor pressures of air calculated by Wagner (Ref. 12). The Clausius-Clapeyron equation in the form

$$\frac{dP}{P} = \frac{L}{RT}\,\frac{dT}{T}$$

was used to approximate Wagner's curve in order to permit computation of the saturation curves for any given set of stagnation conditions. Buhler (Ref. 9) used this same principle, but his plot of the logarithm of pressure vs. temperature required an approximation to Wagner's data in order for him to be able to match the data and the Clausius-Clapeyron

---

* The pseudo-Mach number $\tilde{M}$ is based on the quantity $\tilde{a}$ as defined by Equation (A-11) of Appendix A. Actually, $\tilde{M}$ is very close to the Rayleigh Mach number $M(P/P_o')$, the correction to $M(P/P_o')$ to obtain $\tilde{M}$ being given in Fig. 26 (Ref. 11).

equation with constant L/R. If, however, the logarithm of the pressure is plotted against the reciprocal of the temperature, Wagner's data plots to a straight line over an appreciable region, (Cf. Fig. 20) and enables an accurate determination of L/R to be made. The value of L/R as obtained from Fig. 20 is 828.26°K as compared to Buhler's determination of 823.64°K.

3. Oblique Shock Waves

The fundamental theory of oblique shock waves in a two-phase fluid has been derived by Buhler (Ref. 13) as a direct consequence of the saturated expansion theory outlined in Appendix A. Several complications not present in perfect gas theory occur here due to the two-phase nature of the air. The gas downstream of an oblique shock may or may not contain some condensed phase, depending on the strength of the shock, whereas in the case of a normal shock wave all the condensed phase must evaporate, since the downstream flow is always subsonic.

The case of incomplete reevaporation, for weak oblique shocks, requires consideration of the vapor pressure equation in addition to the fundamental flow equations in order to describe the flow downstream of the shock. In the case of wind tunnel analysis, this means that an additional measurement is required for partial evaporation shocks than would be required to obtain equivalent information for the case of full reevaporation. For this reason, the present experimental study deals chiefly with the shocks strong enough to cause complete reevaporation and waves so weak that the amount of condensed

phase may be considered nearly constant during its passage through the wave. The approximate criteria for oblique shocks with full reevaporation are reproduced in Fig. 21. An outline of the oblique shock theory, including calculations on which the data of Fig. 21 are based, is given in Appendix B.

4. Wind Tunnel Methods of Detecting Air Condensation

As is well known from tests on subsonic and low supersonic tunnels, the free-stream Mach number may be determined by several methods. Those in common use are by the measurement of various pitot, static, and stagnation pressure ratios, measurement of area ratio (in conjunction with the determinations of the boundary layer displacement thickness), and, in supersonic tunnels, measurement of the wave angles and surface pressures of wedges or cones.

Consider the use of the pressure ratios p/p_o, p_o'/p_o, and p/p_o'. Down to the condensation point of the air, the Mach numbers as determined by all three of these ratios will be very nearly equal, and will fall very close to the perfect gas isentrope. Now, if any supersaturation along the perfect gas isentrope occurs, these ratios will continue to give the same Mach number, but as soon as condensation begins, whether it be evidenced as a sudden breakdown of the supersaturated state or merely as a gradual departure from the perfect gas laws, the heat of vaporization released to the gas phase will cause changes in the pressure to occur.

The ratio of pitot to stagnation pressure possesses a property which is of great importance in the analysis of measurements made in

two-phase air. Although the theoretical reasons are somewhat obscure, experimental results of Wegener and collaborators (Ref. 14) using heated and unheated air, and the more recent data of Nagamatsu and Willmarth (Ref. 7) indicate that this ratio is negligibly affected by the presence of condensation. In fact, the effect of condensation on p_o'/p_o is considered to be sufficiently small that this quantity has been used generally as a measure of effective area ratio when boundary layer displacement thickness measurements were not available (Refs. 7 and 10).

The ratio of static to stagnation pressure, however, will obviously be increased as a result of the heat released by condensation, as a brief study of the momentum, energy, and state equations of Appendix A will show. In consequence of the increase in static pressure, one would expect the greatest deviation from the perfect gas isentrope to occur in the ratio of static to pitot pressure, since this increase is a much greater per cent of the pitot pressure than of the stagnation pressure.

These pressure ratios offer a mechanically-simple means of detecting the onset of condensation. The method by which this is done will be illustrated later in the text, along with additional analysis based on the experimental results.

Surface pressure and wave angle measurements on wedges or cones will also be affected by the air condensation. Wegener and collaborators (Ref. 14) have used this method in determining the effect of stagnation temperature on the Mach number measurements, and their results indicate that the condensation affects these measurements to the same order of magnitude as it does the static-pitot pressure ratio. The use of wedges and cones as detectors of condensation for constant stagnation

conditions is, however, unsatisfactory. First, if a cone or wedge is translated through the suspected region of the expansion, it will be subject to appreciable pressure gradients which probably render the measurements inaccurate or ambiguous, since a very small model is subject to boundary layer effects, while a large one will be in an excessively non-uniform flow field. Second, there exists the disadvantage of not having a comparison measurement which is essentially unaffected by the condensation, such as is supplied in the case of pressure probe detection measurements by the pitot-stagnation pressure ratio.

The light-scattering method, although excellent for qualitative indications of condensation (Ref. 7), does not lend itself readily to accurate quantitative measurements of the type required for this investigation, and will not be considered here.

B. General Method of Attack

The verification of the saturated expansion theory and the computation of the flow parameters by means of experimental results may be done by several different methods. One of the foremost of these is to make corresponding tests in heated and unheated air, attempting to keep all conditions other than stagnation temperature identical for both runs. This procedure was used by Wegener (Ref. 14) in his condensation investigations and by Nagamatsu and Willmarth (Ref. 7) and Arthur and Nagamatsu (Ref. 8) to a somewhat lesser extent. However, although powerful, this method has the disadvantages of uncertainties in the effect of the temperature and/or Reynolds number on (a) boundary layer, and hence on effective area ratio, (b) friction losses in the

throat, (c) heat transfer characteristics, and (d) nozzle dimensions. To avoid the necessity of estimating the error introduced by these uncertainties, an attempt has been made in the present investigation to conduct experiments such that the desired gas properties could be obtained by the local measurements or by the tunnel centerline surveys with constant stagnation conditions. Thus, only one set of "heated" data is included here for comparison purposes; the major part of the experimentation having been carried out at room stagnation temperatures.

The first objective of the experimental investigation was to corroborate the saturated expansion theory and to roughly define its limits and its accuracy. Additional measurements were made to determine the facility of computing obscure but necessary flow parameters such as free-stream temperature, at the same time acting as a further check on the theory. Experimental techniques applicable to testing in the condensing fluid have been developed, and some clarification of the problem of similarity parameters, based on experimental results, has been made.

III. EXPERIMENTAL EQUIPMENT AND PROCEDURE

A. Description of the Wind Tunnel

All testing was carried out in the GALCIT 5" Hypersonic Wind Tunnel, which is of the continuously operating closed-return type. The required compression ratios were obtained with five stages of Fuller rotary compressors, and, when necessary, an additional stage of Ingersoll reciprocating compressors. The compressors and all valving were operated remotely from a master control panel (Cf. Fig. 1) located adjacent to the test section.

Oil removal was partially accomplished by Cyclone separators after each compression stage, finely-divided carbon canisters (for oil vapor) and two porous carbon filter blocks. Installation of an additional Goetz-type molecular filter was made late in the program, but the major part of the testing was done using air which contained approximately 2.5 parts per million (ppm) of oil fog by weight.

Water was removed by a 2200 pound bed of silica gel in the main air circuit, which was reactivated by a built-in blower-heater-condenser system prior to each run. The maximum water content of the air was kept below 100 ppm by weight at all times, the usual value being approximately 25 ppm. The dew point was measured at the beginning and end of each run using a standard type carbon dioxide-cooled indicator.

Tests were conducted at two area ratios, using two different sets of nozzle blocks. The blocks were designed for nominal Mach numbers of 9 and 6 by the Foelsch method with corrections applied for the estimated boundary layer displacement thickness. The original intention

was to operate at the design Mach numbers (based on area ratio) for each set of nozzle blocks; however, preliminary testing revealed many instrumentation problems at nominal M = 9 (e.g., extremely low test section pressures, very small Mach angles, which left only tiny working areas behind oblique shock waves, disturbances in the test section, etc.). Since fully-developed condensing flow was required for the experiments, it was decided, in the interest of expediency, to operate at a nominal M = 7.5 with the blocks originally designed for M = 8.9. The major difficulty entailed by this was, of course, the non-parallel test-section flow which resulted. However, it was felt that since the major part of this series of tests consisted of either local measurements or tunnel centerline surveys, the source-type test-section flow (Cf. Fig. 22) would not create an insurmountable problem.

The tunnel was equipped with a hydraulically-operated throat plug to facilitate starting. Several model drive mechanisms permitted axial traversing (two separate drives) rotation about the tunnel axis, vertical traversing, and variation of angle of attack. Several additional special drives were used for this phase of testing, and will be described below in connection with the particular experiments concerned.

A 32-tube vacuum-referenced manometer (Fig. 2) using DC-200 silicone fluid was used to measure all static pressures, and an 8-tube vacuum-referenced mercury manometer was used for pitot pressure measurements. The vacuum system reference pressure was measured with a McLeod gage. Stagnation pressure in the settling tank was measured with a Tate-Emery nitrogen-balanced gage, and stagnation temperature was assumed to be equal to the settling-tank air temperature as measured by

a thermocouple. Static pressure orifices at one-inch intervals in top and bottom nozzle blocks permitted a check to be made with the original nozzle calibration on each run.

An optical system using a BH-6 steady source could be used for schlieren or shadow photographs of the flow. The steel test-section doors were fitted with circular glass observation ports as shown in Fig. 4. Photographs of the test section as arranged for testing at nominal Mach numbers of 7.5 and 6 are shown in Figs. 3 and 4 respectively. The overall schematic diagram (without heaters) is given in Fig. 5 in a somewhat simplified form.

B. Test Program and Special Equipment

1. Wind Tunnel Calibration

The first phase of the test program was to obtain and survey a disturbance-free test section. It was discovered in early operation of the GALCIT 5" tunnel that leakage around the throat seals at the tunnel sidewalls created strong waves in the tunnel test section, but the use of different sealing techniques was successful in reducing the strength of these waves to a negligible value.

Once a disturbance-free test section had been attained the tunnel doors were sealed shut, and were never opened for the duration of testing at that nominal Mach number. The reason for this was to prevent any changes in throat dimensions between tests and to avoid any alteration of the throat seals. Access to the test section for the purposes of model changes and adjustment was had through the twelve round observation ports in the doors (Cf. Fig. 4).

Tests at the nominal Mach number of 7.5, encompassing the major portion of the program, were made at nominal stagnation conditions of P_o = 140 psig and T_o = 300°K. The throat setting was .0363", which gave an uncorrected area ratio of 138.

Testing at nominal M = 6 was done at a stagnation pressure of 60 psig and stagnation temperatures ranging from 298 to 375°K. The throat setting was .082" with the corresponding area ratio of 61.0.

Before proceeding with the condensation investigation proper, the test section for nominal M = 7.5 was surveyed for pitot pressure, flow inclination, and static pressure on the centerline. These were accomplished as follows:

(a) Pitot Pressure

A seven-tube pitot rake with a 2-1/2" span was constructed and sting-mounted on the axial traversing drive (Cf. Fig. 6). Test section pitot pressures were measured on vertical and horizontal planes through the tunnel centerline, spanning the full length of the proposed test section. The results of this survey are presented in Figs. 23 and 24.

(b) Static Pressure

The correct dimensions for a free-stream static pressure probe at hypersonic Mach numbers had to be determined before making the survey. This was done by constructing eight one-sixteenth-inch diameter probes of varying dimensions, mounting them three at a time in the tunnel on a support which could be translated vertically and rotated (Cf. Fig. 7) and comparing pressures measured by each of the different probes at a

number of fixed locations in the test section. The probe lengths varied from 10 to 30 diameters between the static pressure orifices and the support, and from 10 to 40 diameters between the pressure orifices and the nose. Seven probes were of the cone-cylinder type with 5° half-angle cone tips, and one was ogive-shaped for comparison. The three pressure orifices in each probe were spaced equally around the circumference of the probe in one vertical plane.

At the Reynolds number of these tests, it was found that less than 1% difference in measured static pressure existed between cone-cylinder probes with nose-to-orifice dimensions of 30 and 40 diameters, and that no consistent difference existed between probes with orifice-to-support distances of 10, 20, and 30 diameters, even when blunt supports were used. The readings of the ogive-shaped probe showed no consistent differences from those of the equivalent cone-cylinder probe. It was also determined at this time that probe angles of attack up to $2\frac{1}{2}^{\circ}$ caused no change in measured pressure, and an angle of attack of 5° caused a maximum of 2% change in the static pressure reading.

The free-stream static pressure survey of the test-section centerline was thus made with a one-sixteenth-inch diameter 5° half-angle cone-cylinder probe whose nose-to-orifice length was 30 diameters and whose orifice-to-support length was 10 diameters. The results of this survey are shown in Fig. 25.

(c) Flow Inclination

A 10° half-angle brass wedge (Cf. Fig. 8) was installed in the

tunnel so that, with the wedge nose position fixed, the angle of attack could be varied. The wedge could also be moved vertically, but could not be translated axially, limiting the survey to a single vertical plane. Only the flow inclination to the horizontal was measured, it being assumed that the inclination angle to the vertical plane was negligibly small.

A row of four static pressure orifices was located down the centerline of each face of the wedge symmetric with the leading edge. Thus, if the pressure difference Δp of two corresponding orifices is plotted against angle of attack, the $\Delta p = 0$ intercept is the flow inclination at that point. The results of the survey are indicated in Fig. 22, which shows the tunnel flow to be essentially a two-dimensional source flow symmetric about the centerline, with a linear flow deflection of $2\frac{1}{2}^{\circ}$ per vertical inch.

The remainder of the testing was directly concerned with the condensation investigation. This section describes only the experimental equipment and methods of obtaining data, leaving discussion of the results to a later portion of the text.

2. Pitot-Static Pressure Surveys

The primary test of the series was a simultaneous survey of pitot and static pressures down the tunnel centerline. A one-sixteenth-inch static probe of standard dimensions (see above discussion) and a one-sixteenth-inch diameter pitot probe (Cf. Fig. 9) were sting-mounted on the axial traversing drive, and the tunnel centerline surveyed at both Mach number settings.

3. Validity of the Pitot Probe Measurements

In order to determine the effect of reevaporation downstream of the bow wave of a pitot tube on the indicated pressure measurement, the model of Fig. 10 was used. This model consisted of a one-inch diameter hollow cylinder, the downstream end of which was fitted with an adjustable cone. After establishing supersonic flow in the cylinder, the cone was moved upstream to choke the flow through the cylinder and to produce a bow wave upstream of its mouth. Then, by retracting the cone to permit a greater flow of air through the channel, the bow wave could be flattened to a nearly plane normal shock standing at the entrance of the channel. A .042" diameter pitot probe was then traversed through the normal shock in both directions to determine the effect of the reevaporation process on measured pitot pressure. Schlieren photographs were taken to obtain the approximate location of the normal shock with respect to the channel mouth.

4. Simple Wedge Measurements

The first of the oblique shock tests was performed with the 10° half-angle wedge of Fig. 8. These tests consisted of varying the wedge angle of attack, and taking readings of wedge surface pressures in conjunction with schlieren photographs to estimate shock wave angles.

5. Pitot and Static Pressures Behind Oblique Shock Waves

Further oblique shock wave testing was performed with a 40° full-angle wedge, fitted with a drive mechanism which enabled a pitot rake to traverse the flow field behind an oblique shock wave standing on the

upper surface of the wedge leading edge (Cf. Fig. 11). The rake consisted of five probes of .018" outside diameter spaced approximately .070" apart* on centers. The wedge itself was equipped with four static pressure orifices down the centerline of the top surface, and was mounted so that its angle of attack could be adjusted.

Readings of the wedge surface pressures and a complete pitot traverse of the flow field behind the oblique shock wave were taken for free-stream flow inclination angles to the wedge top surface of from 20° to 40°.

The pitot rake was replaced with a one-sixteenth-inch diameter static pressure probe of standard dimensions (Cf. page 17) in order to measure static pressure ratio across the oblique shock. It was found, however, that the extreme length of this probe caused it to be subject to interaction with the shock wave, thus rendering its readings useless. An attempt to correct this by inducing transition to turbulence in the probe boundary layer was unsuccessful, and the standard probe was replaced with one whose nose-to-orifice dimension was 10 diameters** (Cf. Fig. 12). Using this probe, a survey of the flow field behind the shock was made at the various wedge angles. Since the Mach number in the region behind the shock was always less than 4.5, it was possible

---

* The exact locations of the probes were of prime importance in these tests. The spacings as measured with an optical comparator are given in Fig. 37.

** One apparent solution to this problem would have been a reduction in diameter of the probe. However, because of the low pressures being measured, the time lag involved in these measurements increases enormously with reduction in the probe passage area.

to make the small (approximately 1%) adjustment necessary to correct these static pressure measurements for insufficient length of the probe.

6. Flow Inclination Behind Oblique Shock Waves

Tests to determine the flow inclination behind an oblique shock were performed with the equipment of Fig. 13. A flat plate was mounted on adjustable supports, allowing changes in angle of attack and vertical position of the plate. A 5° half-angle wedge one-half inch long with opposing static pressure orifices 5/16" from the leading edge was mounted behind the plate in such a way as to permit axial and vertical traversing and variation in the angle of attack.

The plate was set at angles to the flow of 20° and 30°, and the field behind the oblique shock wave was surveyed for flow inclination in each case by moving the wedge so as to balance its surface pressures at various points in the field. The location of the shock wave was determined for each plate angle by substituting a .042" pitot probe for the wedge (Cf. Fig. 14) and traversing the shock region at several points along its length.

IV. DISCUSSION OF RESULTS

A. Pitot-Static Survey

The first and most important aim of the experimental investigation was to substantiate the saturated expansion theory and to define its limits and its accuracy. The primary tests in this phase consisted of pitot-static pressure surveys down the tunnel centerline using the model of Fig. 9.

As pointed out in Part A of Section II, the pressure ratios p/p_o, p_o'/p_o, and p/p_o' offer an excellent check on the theory and on the order of the effects of condensation on air flow parameters. The data obtained from the pitot-static surveys is plotted in two different ways in Figs. 27 and 28.

Fig. 27a plots Mach number as determined by the pressure ratios p/p_o and p/p_o' against effective area ratio as determined by p_o'/p_o, and compares them with the theoretical values as computed in Appendix C-1 using the saturated expansion theory. Fig. 27b presents the same type of plot for a lower stagnation pressure, but differs from Fig. 27a in that the computed Mach numbers are plotted against geometric area ratio for comparison purposes. These plots actually have very little physical significance, but offer a convenient way of illustrating the good comparison with theory and the marked deviation of the various methods and the isentrope in the neighborhood of its intersection with the saturation curve.

Fig. 28, however, is much more interesting, and supplies a good deal of additional information concerning the character of the flow. Experimental values of static-pitot pressure ratio are plotted against

the corresponding values of pitot-stagnation pressure ratio on a sheet which also includes the theoretical isentrope and saturation curve for test stagnation conditions. This plot clearly shows that at a nominal Mach number of 7.5 the air in the tunnel test section was very close to the theoretical saturated expansion, while data taken at nominal M = 6 indicates that the tunnel air supersaturates by approximately three-quarters of a Mach number (about 12°C) before leaving the isentrope.

The data of Fig. 28 may help to throw some light on the question of the mechanism by which condensation occurs and its effects on gas properties in the neighborhood of the condensation point from a sorely-needed experimental standpoint. As may be seen from this figure, there is an appreciable lag both in time and distance between the time the expansion leaves the isentrope until it arrives at the saturation curve. This behavior shows clearly why no "condensation shocks" (or abrupt changes in flow properties) appear in condensing air flows as compared with the case of condensing water in supersonic tunnels. In the early work on hypersonic tunnels, Bogdonoff and Lees (Ref. 15) based their conclusion that the air never did condense on this absence of the expected "condensation shock".

No conclusion can as yet be drawn as to the reason for this time delay between the beginning of the condensation and the saturation of the air. It is fairly certain that impurities such as carbon dioxide or oil droplets act as original condensation nuclei in this case (Refs. 7 and 8) rather than the spontaneous "germ formation", as indicated by the experiments of Ref. 8. Thus, it might at first be concluded that, since the number of these nuclei remains essentially constant, the delay is solely due to the rate of capture of vapor molecules by the

droplets up to the saturation point. However, it must be remembered that, although the condensation process appears to be triggered by impurity nuclei, nothing is known of the rate of germ formation after the onset of condensation. Hence, the magnitude of the time delay may depend on both the rate of capture of vapor molecules by the impurity-triggered droplets and on the rate of formation of new droplets by spontaneous nucleation.

Although the reason for this time delay is still undefinable, some conclusions can be drawn from the experimental data concerning the nature of the flow parameters which affect the delay. There are several parameters which could conceivably have some effect, any or all of which may be of importance in determining the characteristics of the time delay. First, it may be a characteristic time of the condensation process itself, in which case the delay should depend on the distance and air velocity only. Second, it may depend on the temperature and pressure gradients, and third, on the local temperature and pressure themselves.

Fortunately, some experiments made by Arthur and Nagamatsu (Ref. 8) in the GALCIT 1" x 1" hypersonic tunnel, using air from the settling tank of the 5" tunnel, help to resolve the problem. Arthur and Nagamatsu's data on these tests are nearly identical to those of Fig. 28. This completely rules out the second possibility, since gradients with respect to both time and distance in the 1" tunnel are much higher than those in the 5" tunnel. Also, the first possibility does not seem likely, in view of the fact that the time delay in question occupies over six inches of axial distance in the 5" tunnel and only about an inch and a half in the 1" tunnel, the air velocities being of the same

order of magnitude in both tunnels. Since the coordinates of Fig. 28 are local pressure ratios, and since the 1" tunnel results are so close to these, it appears highly probable that local pressure and temperature are the primary factors in determining the rate at which condensation proceeds once the process has been triggered. Further discussion of this subject in somewhat greater detail may be found in Ref. 8.

The character of the flow in this region (i.e., from the point at which the expansion leaves the isentrope until it reaches the saturation curve) cannot be described by the equations of motion in any consistent manner at the present time. Until this region is carefully investigated for the effect of parameters such as pressure and temperature levels, per cent and character of impurities, time, etc., the theory of flow in unheated hypersonic tunnels must of necessity be restricted to regions of low p_o'/p_o (i.e., high pseudo-Mach number), which, as Fig. 28 shows, are quite close to the theoretical saturation curve.

Once this "region of uncertainty" has been passed, the experimental data follows the theoretical saturation curve quite closely. The slight departure at very low values of p_o'/p_o is probably caused by the error involved in assuming a constant value of L in the Clausius-Clapeyron equation over the entire length of the saturation curve, and may easily be corrected by using different values of L to match Wagner's data over each region of the saturated expansion.

To summarize the above, these first experiments indicate that the saturated expansion theory will be valid and quite accurate at points well downstream of the supersaturation and collapse region, but that it cannot be applied at lower area ratios. An upper limit for the theory has not been established by these experiments, but good correspondence

has been demonstrated at least up to an area ratio corresponding to about Mach number 7.5.

Another method by which the saturated expansion theory may be checked by means of pitot-static pressure survey data was used by Nagamatsu and Willmarth (Ref. 7) in their experiments with nitrogen, and involved a calculation of the free-stream temperature and the amount of condensation from pitot and static pressures measured on the tunnel centerline. The chief advantage of their method is that it does not require use of the assumed Clausius-Clapeyron equation (A-1), being based only on the fundamental flow relationships. Using this method, the data under discussion has been plotted in Fig. 29, which shows the theoretical isentropes and saturation curve on static pressure vs. free-stream temperature coordinates together with the experimental data.

Nagamatsu and Willmarth's method was also used in the computation of the free-stream parameters in Fig. 36, along with other methods to be discussed later.

The pitot-static pressure data was used in an attempt to clarify some of the uncertainty about the true speed of propagation of an infinitesimal wave, which was discussed on page 4. Using quantities computed by Nagamatsu and Willmarth's procedure, experimental values of $\mathring{a}$, $\tilde{a}$, and $dP/d\rho$ were calculated and plotted against distance from the throat in Fig. 30, and for a single location in Table I.

The difference between the square root of $dP/d\rho$ and the theoretical characteristic velocity $\mathring{a}$ is significant, indicating that the exact equality of these quantities, which is characteristic of the isentropic flow of a perfect gas, probably does not exist in the two-phase fluid.

This discrepancy indicates that the passage of a sound wave is not isentropic; i.e., that the wave frequency is too high to permit droplets to follow all temperature and velocity fluctuations of the vapor, and hence that $\mathring{a}$ is not exactly the characteristic sound velocity. However, this does not mean that $\mathring{a}$ cannot be close to the true velocity; this plot is merely an indication that $dP/d\rho$ for a passage of a sound wave is not equal to the free-stream value, and does not throw any light on the true pressure-density relationship for passage of such a wave.

The characteristic velocity as determined by the wedge pressure measurements (Cf. Appendix C-5) falls between $\mathring{a}$ and $\tilde{a}$, and appears to match quite closely the value as determined by wave angle measurements in Ref. 10. However, no conclusions can be drawn from a single measurement of this type, particularly in view of the fact that this value was obtained using an empirical correction for the nonuniformity of flow over the wedge.

The effect of increased stagnation temperature on the character of the flow in the neighborhood of the saturation point is illustrated by Fig. 31, showing the relatively low temperatures required to increase the saturation Mach number. The effect of this supersaturation is to relax the stagnation temperature criteria for condensation-free flow as given by Fig. 41, and the results of this test have been indicated approximately by the dashed curve of that figure.

B. Validity of Pitot Measurements

An important concern in this investigation was the validity of

pitot pressure measurements in a two-phase fluid. The essentially normal shock wave at the mouth of a pitot tube is always sufficiently strong to eventually cause full reevaporation of the condensed phase, but the effect of this reevaporation (and, in particular, the effect of the time delay involved) on the pitot reading was unknown.

An ordinary pitot probe measures the pressure necessary to cancel that component of momentum of the flow which is perpendicular to the plane of the probe's mouth. In this respect, it would appear that the pitot measurements in a condensing flow would be satisfactory regardless of the reevaporation process. However, although momentum considerations seem to indicate no difficulty in making these measurements, there is another possible effect in the condensing flow which may or may not affect the pitot reading. If the reevaporation process behind the probe bow wave were sufficiently slow, some of the droplets, being unable to follow the gas streamlines because of their greater inertia, might pass through the mouth of the probe and evaporate inside it, absorbing energy from the gas. Any error caused by this effect must of necessity be small, since the momentum-pressure balance appears to be satisfied; however, the information on this particular characteristic of the condensing flow was lacking, and it was considered worthwhile to prove the validity of the pitot readings by experimental methods.

The apparatus of Fig. 10 was used for this purpose. As described on page 19, a normal shock was created at the mouth of a cylindrical channel and a pitot probe was traversed through the wave. It would be expected that, if any error were caused by a reevaporation delay as

described above, the measured pressure would change as the probe moved farther downstream of the normal shock until reevaporation was complete, at which point the pitot reading would become constant. Fig. 32 shows the results of the traverse, along with a free-stream pitot survey of the test section. Location of the shock wave region indicated in this figure was determined by measurement of enlarged schlieren photographs. Figs. 15 and 16 are typical of these photographs, and show the normal shock with the pitot probe in two different positions.

It is clear from Fig. 32 that the measured pitot pressure remains constant through and downstream of the normal shock region, leading to the conclusion that the effect of reevaporation delay is small enough not to affect the readings of the probe. The measurements far upstream of the normal shock wave follow the free-stream survey. It might be expected that a discontinuous change in the pitot pressure gradient should occur at the normal shock, but it must be remembered that the data taken just upstream of the shock is affected by factors such as interaction of the normal shock with the probe boundary layer and bow wave, which are apt to be rather complicated. However, these effects cannot affect the conclusions of the test, since the probe, when traversed in the upstream direction, shows no change in measured pressure until well upstream of the shock region.

The probe used in this test was .042" in diameter, and since this was the smallest diameter pitot probe used for measurements in the free stream, all pitot pressure data may be considered to be reliable with respect to reevaporation effects.

C. Oblique Shock Wave Tests

1. Wedge Surface Pressure Data

It has been demonstrated earlier in the text that no systematic set of equations can be written to describe the flow in the transition region between the isentrope and the saturation curve. Thus, the oblique shock tests were all performed at a nominal test-section Mach number sufficiently high to insure that the model was always in a region of saturated expansion.

The first series of these tests was performed with the 10° half-angle wedge of Fig. 8, and consisted of measurement of wedge surface pressures at flow deflection angles θ of from zero to twenty degrees. The investigation of the negative flow deflection angles was prohibited, and that of small positive angles severely limited, by a tendency for the flow to separate from the wedge. This separation tendency is illustrated by Figs. 17 and 18, which show the flow over the wedge at inclinations of 0° and -1° respectively.

The primary interest in this series of tests was the determination of pressure coefficients at the various angles of attack. In this respect, unfortunately, the source flow of the tunnel test section proved to be a major disadvantage, and the accuracy of some of the results has of necessity been impaired. The data obtained with this wedge is summarized in Figs. 33 and 34, which plot the wedge surface pressure against distance from the leading edge and surface pressure against flow deflection angle. An important result of Fig. 34 is the determination of $dp/d\theta$ in the neighborhood of $\theta = 0$. This quantity,

along with the free-stream static pressure, may be used as a measure of the significant Mach number of the flow (as is shown in Appendix C-5), and hence as an indication of the speed of propagation of an infinitesimal wave. This value of "$\bar{a}$" is given in Table I and in Fig. 30, together with the various other values obtained by different methods, and has been discussed earlier in the text.

The approximate experimental pressure coefficients, although certainly not accurate because of the non-parallel test section flow, have been plotted against angle of attack in Fig. 35. In addition to the experimental data (which has been included only to illustrate approximate trends), this figure includes plots of pressure coefficient as calculated for the following conditions by the methods of Appendix C-6:

(a) Saturated expansion theory.

(b) Isentropic expansion of a perfect gas having the same pressure and "significant" Mach number $\bar{M}$ at the wedge leading edge as in (a).

(c) Isentropic expansion of a perfect gas having the same pressure and area ratio at the wedge leading edge as in (a)

(d) Isentropic expansion of a perfect gas having the same pressure and theoretical characteristic Mach number $\mathring{M}$ at the wedge leading edge as in (a).

(e) Use of the hypersonic slender-body approximation with $\mathring{M}$ as similarity parameter.

2. Pitot and Static Pressure Surveys Behind an Oblique Shock

The models of Figs. 11 and 12 were used to obtain pitot and static pressures behind and in the neighborhood of an oblique shock wave. The original purpose of these models was to supply data necessary to compute free-stream temperature and amount of condensation by local measurements of wave angle and pitot and static pressures just behind the oblique shock.

Values of T and g were computed for two angles of attack by the methods of Appendix C-3 and are given in Table II and Fig. 36 for the various experimental techniques. Figs. 37 and 38 show the pitot and static pressure surveys behind the oblique shock wave at one angle of attack. Originally it was intended to obtain the shock wave angle from schlieren photographs such as Fig. 19, but it was found that the measurement of the schlieren photographs was accurate only to about a half degree (previous to the redesign of the optical system). Consequently, the wave angles illustrated in Fig. 39 were obtained by plotting reference points from pitot rake surveys similar to Fig. 37, since the location of the probes was known to within .001" in the vertical plane and to within .002" in the horizontal plane, giving an accuracy of the order of 0.1° in the wave angle. However, although the wave angle could be accurately measured, the position of the wave itself was somewhat in doubt due to the finite (.018" diameter) size of the pitot probes. The definition of the shock was thus limited to a "region" whose maximum thickness was determined by the pitot surveys (Cf. Fig. 37) and whose order of magnitude is indicated in Fig. 38. In the computations, the data at the downstream edge of this shock "region" was considered as the "local" data.

The methods used for the determination of the quantities needed for the calculation of Table II and Fig. 36 are as follows:

(a) Measurement of the pitot and static pressures at a local point just down-stream of the shock "region", thus giving the Rayleigh Mach number behind the shock. (Since all oblique shocks tested here were of sufficient strength to cause full reevaporation of the condensed phase, no Mach number ambiguity existed in the flow field behind the shock.)

(b) Measurement of the static pressure ratio across the oblique shock.

(c) Bleeding a weak wave from one of the wedge static pressure orifices, and using this to determine the Mach number down-stream of the shock by the procedure of Appendix C-3. (Note: Application of this method requires accurate determination of the flow inclination behind the oblique shock).

(d) Graphical integration of the pitot-static data as described previously on page 26.

(e) Use of the approximate method discussed in Appendix C-4.

Table II indicates a fair grouping of the results as computed by the graphical integration method of Ref. 7, the approximate method of Appendix C-4, and the wedge static pressure ratio method. As pointed out in Appendix C-3, this particular wedge method is likely to be more accurate than the others, since an estimate of the flow inclination

behind the shock is not required here. The method using the pitot-static pressure ratio behind the oblique shock shows some departure from the main grouping, probably because of the inaccuracy of estimation of the flow inclination in this region (Cf. Appendix C-3), while the results of the wave-bleed method, requiring two uses of the estimated flow inclination, are so far off as to render this method inadequate.

Figs. 36a and 36b both indicate that, in the region of fully-developed condensing flow well downstream of the saturation point, the approximation method of Appendix C-4 is sufficiently within the scatter of the so-called exact method of Ref. 7 as to be of value in the calibration of unheated hypersonic tunnels.

A further "spot-check" on the oblique shock theory was performed by the use of this data. The method is indicated in Appendix C-7, and showed an experimental discrepancy from the theory of only 1%. Although a check of this type certainly cannot be used as proof of the theory, it offers some support to the conclusions of the theory's accuracy which were deduced earlier in the text, and, in addition, verifies the method used for the determination of the pseudo-Mach number $\tilde{M}$.

3. Flow Inclination Behind an Oblique Shock

The last of the oblique shock experiments was conducted with the models of Figs. 13 and 14, which were used to measure the flow inclination behind an oblique shock and the wave angle itself.

Data for a flow inclination of 20° to the free stream is given in Fig. 40. It was discovered that the flow inclinations close to the

shock wave or to the plate could not be obtained, even with the small wedge used in the tests, probably because of the interference by the wedge shock waves. The extremely limited range of valid data, as illustrated by Fig. 40, thus prevented the attainment of the test objective, which was to measure the flow inclination in the immediate downstream neighborhood of the oblique shock. It was attempted to extrapolate the existing data to the shock wave without success, and as a result the additional check on free-stream temperature and amount of condensation could not be made. Some of this data, however, was useful in approximating the flow inclinations behind the oblique waves for the application in various calculations, and are referred to in several instances in the calculations of Appendix C.

It is suggested to possible future investigators that a blunt probe of the general design described by Ref. 16 might afford better results in this type of measurement.

D. Qualitative Discussion of the Application to Wind Tunnel Testing

The foregoing discussion has illustrated two major points: (a) the good correspondence of the saturated expansion theory with the actual measurements in the condensing flow, and (b) the facility of using this theory for the computations of various flow parameters and for the reduction of the pressure data. Before the application of condensed-air wind tunnel data can be considered for practical problems, however, several points must be cleared up.

The most important gap in this connection is the present lack of a universal significant flow parameter. Until such a quantity has been derived and measured in a wind tunnel, the theory of pressure coefficients

on slender bodies and thin wings (which will be the primary models considered for testing in hypersonic tunnels) cannot be applied accurately. The measurements made in this investigation indicate close comparison between the velocities $\bar{a}$ and $\overset{o}{a}$, and if $\overset{o}{a}$ should turn out to be sufficiently close to the true characteristic velocity, the problem of a similarity parameter for slender bodies will be solved.

Another major difficulty which can never be completely overcome in a hypersonic wind tunnel utilizing condensing air is the simulation of high stagnation temperature on an airplane or missile traveling at hypersonic speeds. The major effects of this discrepancy in stagnation temperature will be in the boundary layer and in the wave drag, and it will certainly cause differences in shock wave characteristics, pressure gradients, and turbulent effects such as flow separation and wakes. In this respect, data obtained in cold or insufficiently heated wind tunnels will probably be unsatisfactory for conversion to free-flight conditions until additional knowledge of temperature characteristics is available to correct for the effects of this difference in the stagnation temperatures.

It should be pointed out, however, that it is the difference in temperature which is the primary difficulty in these respects, and not the effects of condensation. With regard to the boundary layer, the effect of free-stream air condensation is probably quite small close to a body surface, as only the extreme outer portion of the wind tunnel boundary layer contains any liquid phase. Since by far the greatest contribution to the momentum thickness integral occurs in the inner boundary layer region close to the body surface, condensation will probably affect the conventional boundary layer theories and measurements

only with regard to the differences it creates in the free-stream flow, which are readily accounted for by the use of the saturated expansion theory.

Suppose now that the effect of temperature difference may be corrected for, the significant Mach number $\bar{M}$ is available, and it is desired to obtain the free-flight normal forces on a wedge-shaped body by means of model tests in a hypersonic wind tunnel using condensing air.

First consider the case of a slender body at small angles of attack, which is probably typical of the majority of models to be tested in hypersonic tunnels. For an assumed inviscid flow, the forces of interest here* are the induced drag and lift coefficients, both of which depend directly on the pressure coefficient. If the forces are measured in the wind tunnel, the free-flight conditions corresponding to these measurements are readily obtainable.

The local pressure coefficient on a slender body at small angles of attack is given for a perfect gas at hypersonic speeds by Smelt (Ref. 17) as $C_p = \frac{2\theta}{\sqrt{M^2-1}} + \frac{\gamma+1}{2}\frac{\theta^2 M^2}{M^2-1} + \frac{\gamma+1}{6}\frac{\theta^3 M^4}{(M^2-1)^{3/2}} + \cdots$

* Problems such as wave drag, viscous drag, flow separation effects, and turbulent wakes are outside the scope of this investigation, but must be considered from both the theoretical and experimental standpoints before application of the condensed-air wind tunnel can be made. Since viscous and turbulent effects in the neighborhood of body surfaces take place at air velocities sufficiently low that no liquid phase is present, it is possible that these phenomena will be quite similar in condensing and non-condensing flows, and that the difference in measured forces may be small. This cannot be determined, however, until an experimental investigation of viscous and turbulent phenomena is made in the two-phase fluid.

The measured wind tunnel forces thus correspond to the forces at the following flight conditions in a perfect gas (the subscript $(\ )_c$ is used to denote known free-stream parameters of the condensing wind tunnel air, and free-flight conditions are written with no subscript):

$$M = \bar{M}_c$$

$$\rho U^2 = \gamma P M^2 = \rho_c U_c^2 = \gamma P_c \tilde{M}_c^2$$

or

$$P = P_c \left(\frac{\tilde{M}_c}{\bar{M}_c} \right)^2$$

(The temperature conditions cannot be matched, as discussed previously.) This result is valid for the case of infinitesimal disturbances. Thus, the wind tunnel measurements give the induced drag and lift coefficients variations on a slender wedge-shaped body traveling in free-flight at Mach number $M = \bar{M}_c$ and at an altitude corresponding to an ambient pressure $P = P_c(\tilde{M}_c/\bar{M}_c)^2$.

This relation holds for any slender body at small angles of attack, and hence may be applied to thin, double-wedge airfoils and similar types of simple bodies. The non-viscous forces on slender ogive and conical shapes, although not treated here experimentally, involve only the parameters of Mach number and free-stream dynamic pressure, and hence are subject to the same correspondence of wind tunnel and free-flight parameters given above. The limiting flow deflection angle for which this correspondence holds true is approximately 8 degrees, as indicated by the departure of the slender-body approxi-

mation from the theoretical curve of Fig. 35.

The case of wedge-shaped bodies of large vertex angle (or of slender bodies at large angles of attack) is much more involved due to the appreciable reevaporation which takes place in the shock waves, a phenomenon which was considered negligible in the treatment of slender bodies. Another major difficulty is illustrated by the case of a large-angle double-wedge airfoil, in which the amount of condensed phase increases due to the expansion around the center ridge (possibly involving some characteristic condensation time delay), producing flow characteristics which are markedly different on the different surfaces of the airfoil.

This additional complexity, while it does not preclude the use of the similarity parameters for Mach number and altitude as given above, requires application of the rather complicated shock relationships of Appendix B in order to estimate the necessary corrections. This can be done, of course, (e.g., the theoretical pressure coefficients on a wedge for condensing and non-condensing flows is presented in Fig. 35) but the error involved in making the correction according to theory, compounded with the stagnation temperature and boundary layer corrections required in any case, would result in a rather questionable set of wind tunnel data.

In consequence of this discussion, it appears that hypersonic tunnels utilizing condensed air have a possible application in the testing of slender bodies at small angles of attack, using the Mach number and altitude similarity parameters given above to relate wind tunnel and free-flight perfect gas conditions, but that the prohibitive errors

involved in correcting force measurements at large angles of attack or on blunt bodies require that other wind tunnel methods be employed.

Despite this limitation, however, it must be remembered that at free-flight Mach numbers beyond the capacity of heated tunnels, all aerodynamic shapes must of necessity conform to "slender body" requirements, and large angles of attack are practically impossible. It is in this field of operation that the methods of testing in condensing air are most likely to find their best application, subject of course to the development of an adequate method of correcting for the discrepancy in stagnation temperatures.

V. CONCLUSIONS

1. Pitot pressure measurements made in the flow of a condensing gas are unaffected by the size of tubes used in the tests and by the reevaporation effects in or behind the probe bow wave for the stagnation pressures of these tests, and may be considered to be correct from this standpoint.

2. For the Reynolds and Mach numbers of this investigation, the proper dimensions have been obtained for free-stream static pressure probes in the two-phase fluid by experimental methods.

3. Appreciable amounts of supersaturation of air were observed (of the order of about .75 Mach number, or about 12°C) despite the contamination of the wind tunnel air by oil droplets and small amounts of carbon dioxide.

4. The saturated expansion theory describes the unheated wind tunnel flow quite accurately at area ratios greater than those corresponding to about Mach number 6. There is a marked departure from the theory in the neighborhood of the onset of the condensation due to the breakdown of the supersaturated state, but the flow returns to the saturation curve after a moderately short delay. No condensation shocks are observed in the breakdown region, the process apparently being of a comparatively gradual nature.

At very high area ratios a slight deviation from the assumed Clausius-Clapeyron vapor-pressure equation was observed, due to an assumption of constant latent heat over the entire range, but this may be easily corrected by the proper selection of the latent heat for

the particular region of flow under consideration.

5. The passage of an infinitesimally weak wave in the two-phase fluid is probably not isentropic, or at least the pressure-density relationship for such a passage is not the same as the free-stream value derived by measurement of the pressure and density gradients. The velocity of sound as calculated by the wedge measurements appears to corroborate the value obtained by measurement of weak wave angles (Ref. 10), and also appears to be close to the theoretical characteristic velocity based on the saturated expansion assumptions.

6. Based on the validity of the saturated expansion theory, an experimentally simple approximate method for the determination of the two-phase flow parameters has been checked, and provides results accurate to within the experimental scatter of the exact methods in the region of fully-developed condensing flow.

7. An application of the condensed-air hypersonic wind tunnel appears to be possible in the testing of slender bodies at very high Mach numbers. Two major obstacles to this application are the present lack of a significant Mach number based on the true characteristic sound velocity and the lack of an adequate theory to correct for the difference in the stagnation temperatures between the free-flight and wind tunnel conditions. It is possible that the boundary layer effects (other than those introduced by the temperature discrepancy) will not be very different in the corresponding condensing and non-condensing flows.

VI. RECOMMENDATIONS

1. Further measurements of $dP/d\theta$ on a wedge surface in the neighborhood of zero flow inclination should be made in a uniform condensing flow field at several area ratios and stagnation pressures in order that the true characteristic velocity of sound be determined, and a theoretical model for the droplet-vapor interaction be devised on the basis of the results.

2. Wedge, cone, and ogive pressure coefficients should be determined in a uniform condensing flow field in order that empirical relationships may be developed to permit the use of the condensed-air hypersonic wind tunnel data.

3. The boundary layer investigations should be made to determine the effects of the condensation on skin friction, heat transfer, flow separation, and wakes. The emphasis here should be on the correlation of this information with similar effects in a corresponding non-condensing flow.

4. The effects of the differences in the stagnation temperature on the aerodynamic characteristics of bodies at hypersonic Mach numbers should be determined theoretically and experimentally, and a method of correcting for these differences be devised. This investigation should include the effect of local expansions in the neighborhood of the models, since such expansions, by changing the amount of condensed phase, can severely affect the measured pressure coefficients on the model surfaces. A method of accounting for the effects of dissociation of air components at very high free-flight stagnation temperatures should also be investigated.

REFERENCES

1. Stever, H. G.: "A Modification of the Theory of Kinetics of Condensation and Its Application to Air Condensation in Hypersonic Wind Tunnels". Contributed paper, Division of Fluid Mechanics, American Physical Society Meeting, Charlottesville, Va., December 28, 29, 30, 1949.

2. Tolman, R. C.: "Effect of Droplet Radius on Surface Tension". Journal of Chemical Physics, Volume 17, No. 3, March 1949, Pages 333-343.

3. Charyk, J. and Lees, L.: "Condensation of the Components of Air in Hypersonic Wind Tunnels". Princeton University Aeronautical Engineering Laboratory Report No. 127, March 1948.

4. Probstein, R. F.: "Time Lag in Self-Nucleation of Supersaturated Vapor". Princeton University Aeronautical Engineering Laboratory Report No. 168, November 27, 1950.

5. Oswatitsch, K.: "Condensation Phenomena in Supersonic Nozzles". RTP Translation No. 1905.

6. Head, R. M.: "Investigations of Spontaneous Condensation Phenomena". Ph.D. Thesis, California Institute of Technology, 1949.

7. Nagamatsu, H. T. and Willmarth, W. W.: "Condensation of Nitrogen in a Hypersonic Nozzle". Hypersonic Wind Tunnel Memorandum No. 6, Guggenheim Aeronautical Laboratory, January 15, 1952.

8. Arthur, P. D. and Nagamatsu, H. T.: "Effects of Impurities on the Supersaturation of Nitrogen in a Hypersonic Nozzle". Hypersonic Wind Tunnel Memorandum No. 7, Guggenheim Aeronautical Laboratory, California Institute of Technology, February 15, 1952.

9. Buhler, R. D.: "Recent Results on the Condensation Investigation". Hypersonic Wind Tunnel Memorandum No. 1, Guggenheim Aeronautical Laboratory, California Institute of Technology, July 9, 1950.

10. Coles, D. and Nagamatsu, H. T.: "Experimental Techniques and Preliminary Test Data from the GALCIT 5" Hypersonic Wind Tunnel". Hypersonic Wind Tunnel Memorandum, in preparation, Guggenheim Aeronautical Laboratory, California Institute of Technology.

11. Buhler, R. D., Jackson, P., and Nagamatsu, H. T.: "Oblique Shock Waves with Evaporation; Method of Calculating Free-Stream Temperature and Amount of Condensation from Wedge Tests; Remarks on the Pressure Coefficient in Hypersonic Tunnels". Hypersonic Wind Tunnel Memorandum No. 3, Guggenheim Aeronautical Laboratory, California Institute of Technology, April 10, 1951.

12. Wagner, K.: "Wasserbau Versuchs Anstalt". Kochel Report No. A-3, 1942.

13. Buhler, R. D.: "Methods for Determining the Mach Number in Hypersonic Wind Tunnels". Hypersonic Wind Tunnel Memorandum No. 2, Guggenheim Aeronautical Laboratory, California Institute of Technology, August 21, 1950.

14. Wegener, Stollenwerk, Reed, and Lundquist: "NOL Hyperballistics Tunnel No. 4 Results I: Air Liquefaction". NAVORD Report 1742, January 4, 1951.

15. Bogdonoff, S. M. and Lees, L.: "Study of the Condensation of the Components of Air in Supersonic Wind Tunnels: Part I". Princeton University Aeronautical Engineering Laboratory Report No. 146, May 25, 1949.

16. Fusfield, R. D.: "A Probe for Measuring Flow Inclination in a Supersonic Air Stream". Journal of the Aeronautical Sciences, Volume 18, No. 5, May 1951, Page 356.

17. Smelt, R.: "Problems of Missiles at Extreme Speeds". Symposium on Ordnance Aeroballistics, U. S. Naval Ordnance Laboratory, White Oak, Maryland, March 1, 1950.

18. Millikan, C. B.: "Lecture Notes: Compressible Fluid Aerodynamics". California Institute of Technology, 1948.

19. Courant and Friedrichs: "Supersonic Flow and Shock Waves". Interscience Publishers, Inc., 1948.

20. "Charts and Tables for Hypersonic Flow". Hypersonic Wind Tunnel Memorandum No. 4, Guggenheim Aeronautical Laboratory, California Institute of Technology, May 15, 1951.

APPENDIX A

A-1. NOTATION

a	Isentropic velocity of sound in a perfect gas
$\tilde{a}$, $\overset{o}{a}$, $\overset{v}{a}$, $\bar{a}$	Velocities to be defined in A-2
A	Nozzle cross-section area
C_p	Pressure Coefficient
c_p	Specific heat at constant pressure of the vapor phase
E	Condensation parameter to be defined in Appendix B
g	Fraction of mixture by mass which is in the condensed phase
h	Specific enthalpy of the mixture
L	Latent heat of condensation per unit mass of air
M	Mach number (general)
$\tilde{M}$, $\overset{o}{M}$, $\bar{M}$	Particular "Mach numbers" to be defined in A-2
$M( )$	Mach number as calculated from a quantity ( ) by one-dimensional perfect gas methods
P	Free-stream static pressure
P_o	Stagnation pressure
P_o'	Pitot pressure, or stagnation pressure behind a normal shock
q	Dynamic pressure
R	Gas constant per unit mass

s	Specific entropy
T	Free-stream temperature
T_o	Stagnation temperature
u	Air velocity normal to a shock wave
v	Air velocity tangential to a shock wave
w	Free-stream air velocity
x	Axial distance from the wind tunnel throat
γ	Ratio of specific heats of the vapor phase
θ	Flow inclination angle
μ	Characteristic angle of an infinitesimal wave
ρ	Density of the mixture
σ	Shock wave angle

Subscripts

$( )_o$	Settling tank (stagnation)
$( )_1$	Location in the nozzle at which the expansion becomes saturated
$( )_2$	Free-stream location downstream of "1"
$( )_3$	Location downstream of shock wave
$( )^*$	Nozzle throat
$( )_v$	Vapor phase
$( )_c$	Corrected for free-stream flow inclination
$( )$	Mixture of both phases (no subscript)
$( )_N$	Component normal to a shock wave
$( )_w$	At the surface of a wedge

A-2. OUTLINE OF THE THEORY (REF. 9)

Fundamentally, the theory assumes that the expansion takes place along the dry isentrope up to the saturation point, after which it follows the saturation curve for air. The saturation curve, as explained on page 7, is simply the Clausius-Clapeyron Equation

$$\frac{dP}{dT} = \frac{L}{R}\,\frac{P}{T^2} \tag{A-1}$$

with L/R determined from Wagner's data (Ref. 12), and is plotted in Fig. 20. The vapor phase is assumed to follow the perfect gas laws with $\gamma = 1.4$.

The basic equations are

Continuity: $$\frac{d\rho}{\rho} + \frac{dw}{w} + \frac{dA}{A} = 0 \tag{A-2}$$

Momentum: $$w\,dw + \frac{dP}{\rho} = 0 \tag{A-3}$$

Energy: $$w\,dw + c_p\,dT - L\,dg = 0 \tag{A-4}$$

Since the pressure depends only on the amount of vapor present (i.e., the specific volume of the condensed phase is negligible compared to that of the vapor), the equation of state is written as

$$\frac{dP}{P} - \frac{d\rho}{\rho} - \frac{dT}{T} + \frac{dg}{1-g} = 0 \tag{A-5}$$

or, in the integrated form,

$$P = \rho(1-g)RT \tag{A-5a}$$

where

$$\rho_v = \rho(1-g)$$

The fundamental assumption implies the following:

$$\text{for } T > T_1 \qquad P = P_0 (T/T_0)^{\frac{\gamma}{\gamma-1}}$$

$$\text{for } T < T_1, \qquad P = P(T) \qquad \text{as given by Eq. (A-1)} \tag{A-6}$$

Solutions for the various flow parameters in terms of measurable quantities may now be easily found using these equations. Free-stream temperature T is determined directly by integration of Eq. (A-1):

$$\frac{1}{T} = \frac{1}{T_1} - \frac{\log_e P/P_1}{L/R} \tag{A-7}$$

where state "1" is determined from stagnation conditions and the isentropic perfect gas relationships.

To find the amount of condensed phase g, successive use of Eqs. (A-5a) and (A-1) gives

$$\frac{dP}{\rho} = \frac{dP}{P}(1-g)RT$$

$$= (1-g)L\frac{dT}{T}$$

and the application of the momentum and energy Eqs. (A-3) and (A-4) gives

$$-w\,dw = (1-g)L\frac{dT}{T}$$

$$-L\,dg + c_p\,dT = (1-g)L\frac{dT}{T}$$

or

$$\frac{dg}{dT} + \frac{(1-g)}{T} - \frac{c_p}{L} = 0$$

Integrating,

$$g = \frac{c_p}{L}T\log_e\frac{T}{T_1} + \left(1 - \frac{T}{T_1}\right) \tag{A-8}$$

where T is given by Eq. (A-7).

The free-stream velocity w is now directly obtainable from the integrated energy equation

$$w = \left[w_1^2 + 2Lg + 2c_p (T_1 - T) \right]^{1/2} \qquad \text{(A-9)}$$

where w_1 is obtainable from the knowledge of P_1/P_o and T_1 by standard methods.

The mixture density ρ is easily found from the equation of state (A-5a):

$$\rho = \frac{p}{(1-g) RT}$$

or, in terms of the area ratio, by integration of the continuity equation (A-2):

$$\rho = \rho_1 \frac{w_1}{w} \frac{A_1}{A} \qquad \text{(A-10)}$$

Thus, all the necessary flow parameters may be determined (within the framework of the initial assumptions), requiring only a pressure measurement in the free-stream, given stagnation conditions, and a knowledge of P and T at the reference station "1". In practice, however, a departure from the fundamental assumption prevents application of the theory in so direct a manner in some regions of the flow. The theory as outlined above is based on the assumption that the condensation begins at the intersection of the saturation curve with the isentrope, and the expansion then continues along the saturation curve. This does not occur in practice, however, as is clearly illustrated by Fig. 28. The supersaturation which occurs in the wind tunnel is followed by a breakdown to the saturation curve which is not at present amenable to simple analysis, and which certainly does not even roughly

approximate the assumption of saturated expansion from the theoretical dewpoint. Thus, integration of Eq. (A-1), upon which depends the entire analysis, cannot be carried out over this region.

Velocity of Sound

To obtain a general form of the characteristic sound velocity for an isentropic expansion of the mixture independently of any assumptions about the interaction between droplets and vapor, consider the non-steady form of the continuity and momentum Equations (A-2) and (A-3) for one-dimensional flows:

$$\frac{\partial \rho}{\partial t} + \rho \frac{\partial w}{\partial x} + w \frac{\partial \rho}{\partial x} = 0 \qquad \text{(A-2a)}$$

$$\frac{\partial w}{\partial t} + w \frac{\partial w}{\partial x} + \frac{1}{\rho} \frac{\partial P}{\partial x} = 0 \qquad \text{(A-3a)}$$

or, if it is assumed that some relation exists between pressure and density of the two-phase fluid, Eq. (A-3a) can be written as

$$\frac{\partial w}{\partial t} + w \frac{\partial w}{\partial x} + \frac{1}{\rho} \left[\frac{dP}{d\rho}\right]_s \frac{\partial \rho}{\partial x} = 0 \qquad \text{(A-3b)}$$

Using the method of Ref. 18, the equation for lines of discontinuous derivatives in the x - t plane (i.e., the characteristics) is obtained directly:

$$\frac{dx}{dt} = w \pm \left[\frac{dP}{d\rho}\right]_s^{1/2}$$

Thus, the speed of propagation of an infinitesimal wave in the two-phase fluid may be defined as the square root of $dP/d\rho$, regardless of the nature of the interaction between vapor and droplets.

Note that in the foregoing discussion the only assumption has been that of some arbitrary relationship between the pressure and density for the isentropic expansion. However, in order to define this pressure-density relationship, the interaction of the droplets and vapor during passage of a sound wave must be considered, as was discussed on page 5 .

Now, if the passage of the wave is assumed to be such that no heat transfer occurs between the vapor and droplets,* but that the droplets follow velocity fluctuations, a sound velocity for the mixture may be defined as follows:

Since the vapor phase is assumed to follow the perfect gas laws,

$$\frac{P}{\rho_v^{\gamma}} = \text{Constant}$$

And, from the definition of density,

$$\rho_v = \rho(1-g)$$

Then

$$\left[\frac{dP}{d\rho}\right]_g = \frac{\partial P}{\partial \rho_v}\,\frac{\partial \rho_v}{\partial \rho}$$

$$= (1-g)\gamma RT \qquad (\text{since } P \equiv P_v)$$

Thus, a velocity of sound based on the assumed type of interaction is defined by

$$\tilde{a} \equiv \sqrt{(1-g)\gamma RT} \qquad \text{(A-11)}$$

Now, if the droplets are so large that they follow neither temperature nor velocity fluctuations with passage of a sound wave, the

---

* This of course requires that g = constant during passage of the wave.

mixture may be considered to be a perfect gas with inert particles, and thus

$$\frac{dP}{d\rho_v} = \gamma \frac{P}{\rho_v} = \gamma RT$$

Thus, this velocity of sound is

$$a = \sqrt{\gamma RT} \tag{A-12}$$

Now, if the droplets are so small and the wave frequency so low that complete thermal and dynamic equilibrium is maintained during passage of a sound wave (i.e., the passage is isentropic with respect to the mixture) another sound velocity may be derived.

Consider the equations of vapor pressure and state:

$$\frac{dP}{P} - \frac{L}{RT^2} dT = 0 \tag{A-1}$$

$$\frac{dP}{P} - \frac{d\rho}{\rho} - \frac{dT}{T} + \frac{dg}{1-g} = 0 \tag{A-5}$$

Now the property of constant entropy of the mixture during passage of the wave may be brought in as follows:

From the definition of entropy and the first law of thermodynamics,

$$ds = \frac{dh}{T} - \frac{1}{\rho} \frac{dP}{T}$$

but, for the mixture,

$$dh = c_p dT - L dg \quad *$$

---

* Actually, $dh = c_p(1-g)dT + c_L g dT - L dg$ but since g is small, the error involved by taking $c_L = c_p$, where c_L = specific heat of the liquid phase, will be small.

Thus

$$ds = \frac{c_p dT}{T} - \frac{L dg}{T} - \frac{1}{\rho}\frac{dP}{T} \equiv 0$$

Applying the integrated equation of state, Eq. (A-5a),

$$\frac{c_p dT}{T} - \frac{L dg}{T} - R(1-g)\frac{dP}{P} = 0$$

$$\frac{\gamma R}{\gamma-1}\frac{dT}{T} - \frac{L dg}{T} - R\frac{dP}{P} + gR\frac{dP}{P} = 0$$

And, by the use of Eq. (A-1) on the last term, the condition of constant entropy becomes

$$\left(\frac{\gamma}{\gamma-1} + \frac{Lg}{RT}\right)\frac{dT}{T} = \frac{dP}{P} + \frac{L}{RT}dg \qquad \text{(A-13)}$$

Making the proper substitutions in Eqs. (A-1), (A-5), and (A-13), and using the integrated equation of state (A-5a), we obtain

$$\frac{dP}{d\rho} = \frac{(1-g)RT}{1 - \frac{2RT}{L} + \frac{\gamma}{(\gamma-1)}\frac{1}{(1-g)}\left(\frac{RT}{L}\right)^2}$$

and defining

$$\overset{\circ}{a}^2 \equiv \left[\frac{dP}{d\rho}\right]_S$$

the speed of propagation of an isentropic infinitesimal wave may be written as*

$$\overset{\circ}{a} = \left[\frac{(1-g)RT}{1 - \frac{2RT}{L} + \frac{\gamma}{(\gamma-1)}\frac{1}{(1-g)}\left(\frac{RT}{L}\right)^2}\right]^{1/2} \qquad \text{(A-14)}$$

---

* $\overset{\circ}{a}$ has also been derived as the theoretical characteristic sound velocity by considering the matrix of the five basic equations (A-1) through (A-5), and using the general method of Ref. 19.

A fourth velocity of sound for the two-phase fluid is derived in Ref. 10 on the assumption that the droplets follow thermal motions of the vapor with passage of a weak wave, but not velocity fluctuations. Experimental results, however, seem to indicate that this "isothermal" velocity is not of as much significance as the others derived above.

These various velocities of sound have each been discussed and derived on the basis of definite assumptions concerning the nature of the interaction between droplets and vapor. However, it is quite reasonable to suppose that the actual interaction which takes place in the flow of a condensing gas might be a combination of two or more of the assumed types. In this case, the possibilities of theoretical analysis no longer exist (at least insofar as the present theory is concerned), and the significant sound velocity must necessarily be determined experimentally. Once this has been done, of course, it is quite possible that a theoretical model may be set up to represent the actual interaction process. The subject of experimental results has been discussed on page 27 and illustrated in Table I and Fig. 30, using the notation $\bar{a}$ to represent the significant or true characteristic sound velocity as measured experimentally.

In order to perform experimental analyses utilizing a condensing fluid, it is necessary to define some sort of similarity parameter similar to the Mach number in a perfect gas. By defining the various sound velocities above, we have introduced five possible "Mach numbers" as defined in the usual way by taking the ratio of fluid velocity to each of the local sound velocities discussed.

If the passage of a sound wave is isentropic with respect to the

vapor phase only, i.e., if the sound velocity is

$$\tilde{a} = \sqrt{(1-g)\gamma RT}$$

then we may define the pseudo-Mach number

$$\tilde{M} = \frac{w}{\tilde{a}} \tag{A-15}$$

To observe the significance of this parameter,

$$\tilde{M}^2 = \frac{w^2}{\tilde{a}^2} = \frac{w^2}{(1-g)\gamma RT} = w^2\left(\frac{\rho}{\gamma P}\right)$$

or

$$\frac{\frac{1}{2}\rho w^2}{P} = \frac{1}{2}\gamma \tilde{M}^2 \tag{A-16}$$

Thus, $\tilde{M}$ is a true similarity parameter, in that its square is a direct measure of the ratio of dynamic to static pressure. As such, and in the absence of a valid model for the true characteristic Mach number $\bar{M}$ as defined by

$$\bar{M} = w/\bar{a} \tag{A-17}$$

the pseudo-Mach number $\tilde{M}$ has been used throughout the text as the primary flow parameter with which to discuss the two-phase fluid flow.

The quantity $\overset{\circ}{M}$ as defined by

$$\overset{\circ}{M} = w/\overset{\circ}{a} \tag{A-18}$$

is of interest here in that it is the theoretical characteristic Mach number for full thermal equilibrium, and as such could be represented by

$$\sin \overset{\circ}{\mu} = 1/\overset{\circ}{M} \tag{A-19}$$

Thus, $\overset{\circ}{M}$ is merely the theoretical counterpart of the true characteristic Mach number $\bar{M}$.

APPENDIX B

SHOCK WAVES IN A TWO-PHASE FLUID

The fundamental theory of the normal and oblique shock waves in condensing flow is given in Ref. 11.

The process of the evaporation of the droplets just after a shock wave is as yet unknown, but does not prevent an analysis from being made in the ordinary manner by considering states upstream and downstream of the wave. The basic equations are

Continuity: $$\rho_2 u_2 = \rho_3 u_3 \tag{B-1}$$

Momentum component normal to the wave:

$$\rho_2 u_2^2 + P_2 = \rho_3 u_3^2 + P_3 \tag{B-2}$$

Tangential momentum component:

$$V_2 = V_3 \tag{B-3}$$

Energy: $$\frac{u_2^2}{2} + c_p T_2 - L g_2 = \frac{u_3^2}{2} + c_p T_3 - L g_3 \tag{B-4}$$

where, as before, c_p and L are assumed constant.

State: $$\frac{P}{\rho(1-g)} = RT \tag{B-5}$$

Vapor pressure: (assuming the flow is saturated both upstream and downstream of the shock)

Upstream: $$\log_e \frac{P_2}{P_1} = \frac{L}{R}\left[\frac{1}{T_1} - \frac{1}{T_2}\right] \tag{B-6a}$$

Downstream: $$\log_e \frac{P_3}{P_i} = \frac{L}{R}\left[\frac{1}{T_i} - \frac{1}{T_3}\right] \tag{B-6b}$$

where i represents an arbitrary reference point.

It should be noted that in the case of a shock strong enough to cause complete reevaporation (to be discussed below), $g_3 = 0$, and Eq. (B-6b) can no longer be used.

The normal component of the pseudo-Mach number $\tilde{M}$ is defined by

$$\tilde{M}_N = \frac{u}{\tilde{a}} = \frac{u}{\sqrt{(1-g)\gamma RT}} \tag{B-7}$$

and the generalized shock relations may now be calculated in terms of this parameter.

Using the equation of state Eq. (B-5), Eq. (B-2) becomes

$$P_3\left[\frac{u_3^2}{(1-g_3)RT_3} + 1\right] = P_2\left[\frac{u_2^2}{(1-g_2)RT_2} + 1\right]$$

or, using Eq. (B-7),

$$\frac{P_3}{P_2} = \frac{1+\gamma\tilde{M}_{2N}^2}{1+\gamma\tilde{M}_{3N}^2} \tag{B-8}$$

Arranging Eq. (B-2) in a different form, and using Eq. (B-1) and (B-5),

$$\frac{u_3}{u_2} = 1 - \frac{1}{\gamma\tilde{M}_{2N}^2}\left(\frac{P_3}{P_2} - 1\right) \tag{B-9}$$

and

$$\frac{u_3}{u_2} = \frac{1 + \frac{1}{\gamma\tilde{M}_{2N}^2}}{1 + \frac{1}{\gamma\tilde{M}_{3N}^2}} \tag{B-10}$$

Now, by substituting Eq. (B-10) into the energy equation (B-4),

$$\frac{\tilde{M}_{2N}^2\left[\tilde{M}_{2N}^2+\frac{2}{\gamma-1}+E_2\right]}{\left(1+\gamma\tilde{M}_{2N}^2\right)^2}=\frac{\tilde{M}_{3N}^2\left[\tilde{M}_{3N}^2+\frac{2}{\gamma-1}+E_3\right]}{\left(1+\gamma\tilde{M}_{3N}^2\right)^2} \tag{B-11}$$

where

$$E_i=\frac{2q_i}{1-q_i}\left[\frac{1}{\gamma-1}-\frac{L}{\gamma R T_i}\right] \tag{B-12}$$

The assumption that the flow is saturated both upstream and downstream of the shock wave implies that Eqs. (B-6a) and (B-6b) may be combined:

$$\log_e\frac{P_3}{P_2}=\frac{L}{RT_2}\left[1-\frac{T_2}{T_3}\right] \tag{B-6c}$$

By substituting Eq. (B-8) into Eq. (B-6c), the temperature ratio can be obtained in terms of $\tilde{M}_2$ and $\tilde{M}_3$, and also as a function of $\tilde{M}_2$ and u_3/u_2 by the use of Eq. (B-9). If now we consider one more relation:

$$\frac{v_3}{v_2}=\frac{\tan(\sigma-\theta)}{\tan\theta} \tag{B-13}$$

which is a direct consequence of Eq. (B-3), sufficient information is available with which to plot the shock polar and a full set of shock wave charts (Ref. 11) for any strength shock wave, using Eqs. (B-5) through (B-13).

In the present investigation it was intended to limit the testing of oblique shocks to those which were sufficiently strong to cause full reevaporation of condensed phase. The criteria for full reevaporation were determined as follows:

For each value of $\tilde{M}_2$, E_2 may be obtained for given stagnation conditions by the use of the theory of Appendix A-2 and Eq. (B-12). Then M_{3N}^2 may be computed as a function of the wave angle σ for each $\tilde{M}_2$, using Eq. (B-11) with $E_3 = 0$, and P_3/P_2 then plotted against σ using Eq. (B-8).

In order that the wave strength be just sufficient to cause full reevaporation, Eq. (B-6c) is used with the Eqs. (A-5a), (B-1), (B-8), and (B-10) (with $g_3 = 0$) combined in the form

$$\frac{T_3}{T_2}\,\frac{1}{(1-g_2)} = \frac{(\gamma \tilde{M}_{2N}^2+1)^2}{(\gamma \tilde{M}_{3N}^2+1)^2}\,\frac{M_{3N}^2}{\tilde{M}_{2N}^2}$$

to give

$$\log_e \frac{P_3}{P_2} = \frac{L}{RT_2}\left[1-(1-g_2)\left(\frac{\gamma \tilde{M}_{2N}^2+1}{\gamma M_{3N}^2+1}\right)^2\left(\frac{M_{3N}}{\tilde{M}_{2N}}\right)^2\right] \qquad \text{(B-14)}$$

Thus, P_3/P_2 has been calculated as two separate functions of σ for each $\tilde{M}_2$, and the intersection will give the minimum wave angle necessary to produce complete reevaporation of the condensed phase at each value of $\tilde{M}_2$. To find the flow inclination angle corresponding to this wave angle, Eqs. (B-10) and (B-13) are combined:

$$\tan(\sigma-\theta) = \left[\frac{1+\frac{1}{\gamma \tilde{M}_{2N}^2}}{1+\frac{1}{\gamma M_{3N}^2}}\right]\tan\sigma \qquad \text{(B-15)}$$

Fig. 21 was constructed on this basis, and shows the wave angles and flow deflection angles required for full reevaporation as a function of $\tilde{M}_2$ and stagnation pressure for $T_o = 300^\circ K$.

In the analysis of the experimental results, the relations derived in this section for the general case were specialized to apply to the full reevaporation shocks by letting $g_3 = 0$ and omitting Eqs. (B-6b) and (B-6c).

APPENDIX C

APPLICATION OF THE THEORY TO EXPERIMENTAL DATA

C-1 Theoretical Determination of Pressure Ratios in Condensing Air Flow

(a) Static-to-Stagnation Pressure Ratio P/P_o

A value for P/P_o is assumed, and A/A^* corresponding to the value is calculated by using Eqs. (A-7) through (A-10). The reference state "1" is chosen at the intersection of the isentrope and the saturation curve corresponding to the particular stagnation pressure considered. By selecting a range of P/P_o, a plot of theoretical effective A/A^* vs. P/P_o may be constructed.

(b) Static-to-Pitot Pressure Ratio P/P_o'

Consider the bow wave at the mouth of a pitot probe, behind which the flow is fully reevaporated. For each P_2/P_o as selected in (a), the quantities T_2, w_2, g_2, and A_2/A^* are known; hence $\tilde{M}_2$ is known. Eqs. (B-11) and (B-12) with $g_3 = 0$ may be used to calculate M_3 (for a normal shock $\tilde{M}_{2N} = \tilde{M}_2$ and $M_{3N} = M_3$).

Now P/P_o' may be obtained by

$$\frac{P_2}{P_o'} = \frac{P_2}{P_3}\frac{P_3}{P_o'} = \left(\frac{1+\gamma M_3^2}{1+\gamma \tilde{M}_2^2}\right)\left(1+\frac{\gamma-1}{2}M_3^2\right)^{\frac{-\gamma}{\gamma-1}} \qquad \text{(C-101)}$$

(c) Pitot-to-Stagnation Pressure Ratio P_o'/P_o

Once (a) and (b) have been computed, this ratio is obtained directly:

$$\frac{P_o'}{P_o} = \frac{P}{P_o} \frac{1}{P/P_o'} \qquad \text{(C-102)}$$

The "Mach numbers" corresponding to each of these pressure ratios may be obtained from Ref. 20 as functions of area ratio. The results, along with the experimental data, have been plotted in Figs. 27a and 27b, together with the perfect gas isentrope. The pressure ratios as calculated here were also used to plot the saturation curve in Figs. 28 and 31.

C-2 Criteria for Condensation-Free Flow

Saturation curves are plotted on P/P_o versus temperature coordinates for various stagnation pressures, and the intersections of these curves with the isentropes for various stagnation temperatures are found. The intersections are then plotted on Mach number versus stagnation temperature axes (Cf. Fig. 41) and constitute the theoretical criteria for condensation-free flow. However, as indicated in Figs. 28 and 31, the wind tunnel air supersaturates slightly before condensation begins. The dashed curve of Fig. 41 represents a rough estimate of the maximum Mach number attainable without condensation in an actual wind tunnel when typical values of supersaturation are considered.

C-3 Computation of Free-Stream Temperature and Amount of Condensed Phase Utilizing Oblique Shock Wave Measurements

The equations of Appendix B may be applied to the computation of the free-stream temperature (and thus to the determination of all other flow parameters) using only local measurements in the region of a strong oblique shock wave in a saturated two-phase fluid.

The following measurements are given:

(1) Shock wave angle σ

(2) Free-stream flow inclination θ_2

(3) Free-stream P_2/P_o' (just upstream of the shock wave)

(4) Pitot pressure P_{03}' (just downstream of the wave)

(5) Static pressure P_3 (just downstream of the wave)

The free-stream pitot-static pressure ratio determines the Rayleigh Mach number $M_2(P/P_o')$, which may be converted into the pseudo-Mach number $\tilde{M}_2$, accurate to better than 1%, by the use of Fig. 26 with a very rough estimate of the condensation parameter E. The measurements of σ and θ_2 give

$$\tilde{M}_{2N} = \tilde{M}_2 \sin \sigma_c \tag{C-301}$$

where

$$\sigma_c = \sigma - \theta_2 \tag{C-302}$$

The Mach number M_3 behind the shock wave may now be determined by two methods, which act as checks against each other.

(a) Direct measurement of static and pitot pressures behind the wave supply a determination of M_3 from the Rayleigh formula; however, this then requires an estimate of the flow angle θ_3 behind the wave in order to calculate M_{3N}; i.e.,

$$M_{3N} = M \sin (\sigma - \theta_3) \tag{C-303}$$

The necessary estimate of θ_3 was supplied (to approximate accuracy) by the data obtained with the model of Fig. 13, a sample plot of which was given in Fig. 40. Once M_{3N} is known, E_2 may be calculated from Eq. (B-11), with $E_3 = 0$. Then g and T are obtained by simultaneous solution of Eq. (B-12) and the integrated energy equation (A-4) written in the form

$$g_2 = \frac{1 + \frac{\gamma-1}{2}\tilde{M}_2^2 - \frac{T_o}{T_2}}{\frac{\gamma-1}{2}\tilde{M}_2^2 - \frac{(\gamma-1)}{\gamma}\frac{L}{RT_2}} \tag{C-304}$$

(b) Measurement of static pressures upstream and downstream of

the shock wave provide the static pressure ratio P_3/P_2, and M_{3N} may be computed directly from Eq. (B-8). Once M_{3N} is known, the procedure is the same as that given above in (a).

In addition to these methods, another (approximate) determination of M_3 may be made by measuring the angle of a weak wave in the condensation-free region behind the oblique shock. This is done by the following method:

Estimate the flow inclination θ_3 at the desired downstream point using data obtained with the model of Fig. 13. Then the weak wave angle (as determined by pitot rake survey) may be used to find the Mach angle* μ_3. Thus, M_3 is known, and M_{3N} is estimated by Eq. (C-303). The procedure for the determination of g and T is then the same as for the other methods.

This latter procedure is of questionable accuracy in that it requires two uses of the approximation to the flow angle behind the oblique shock, whereas the other methods involve only one or none at all. Table II shows that the results differ widely from those of the other two methods at the value of wedge surface inclination for which this particular test was made.

C-4 Approximate Methods of Computing Free-Stream Flow Parameters by Simple Pressure Measurements at a Single Point

An experimentally simple method has been devised for calculating g and T, and hence all other flow parameters, to fairly good accuracy.

---

* Ref. 10 includes a calculation of the Mach angle correction due to strength of the wave, and demonstrates that for waves of the strength used in the present investigation, the correction is of the order of magnitude of the experimental error.

The procedure, which involves measurement of the static pressure and the knowledge of the stagnation conditions, is simply to assume the validity of the saturated expansion theory, and thus to use without modification the theoretical computations of Appendix A. As indicated in Table II and Fig. 36, the error incurred by the use of this method is of the order of magnitude of the experimental scatter observed in the application of so-called exact methods, and hence would certainly be suitable for use wherever high orders of accuracy are not essential, and simplicity of measurement is important.

C-5 Theoretical Treatment of Slender Bodies (Ref. 11)

For the treatment of the two-dimensional slender body (i.e., small-angle wedge), consider the oblique shock wave at its leading edge to be of infinitesimal strength; i.e., to be a Mach wave. The characteristic velocity of sound for the theoretical treatment will be taken to be $\overset{o}{a}$ as defined in Appendix A, and the equations will then be rederived for the actual case using the true sound velocity $\bar{a}$.

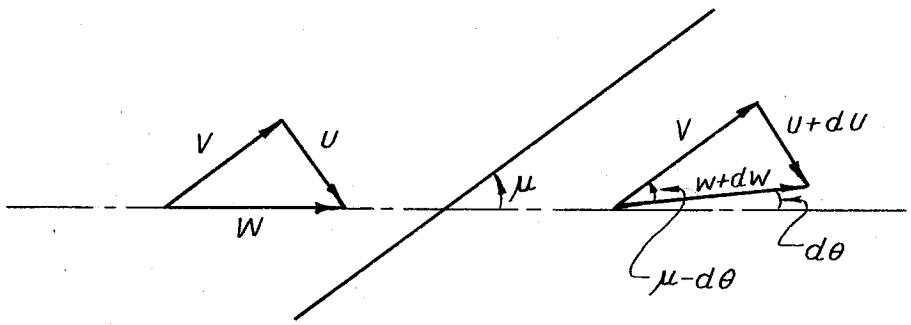

Following Ref. 11, the geometry of the wave requires that

$$U = V \tan \mu$$

$$U+dU = V \tan (\mu - d\theta)$$

Or, neglecting second-order terms,

$$\frac{dU}{U} = -\frac{d\theta}{\sin\mu \cos\mu}$$

If $\overset{o}{a}$ is the characteristic sound velocity, the Mach angle μ is given by Eq. (A-19):

$$\sin\mu = \frac{1}{\overset{o}{M}} = \frac{\overset{o}{a}}{w} \tag{A-19}$$

and thus

$$\left(\frac{du}{u}\right)_{\overset{o}{a}} = -\frac{\overset{o}{M}^2}{\sqrt{\overset{o}{M}^2-1}}\, d\theta \tag{C-501}$$

where the subscript $(\ )_{\overset{o}{a}}$ indicates that the derivation is based on this particular characteristic velocity.

Using the normal momentum component equation,

$$\rho u du + dP = 0$$

or

$$\frac{dP}{P} = -\frac{w^2 \sin\mu}{P/\rho}\,\frac{du}{u}$$

and from Eqs. (C-501) and (A-16),

$$\left(\frac{dP}{P}\right)_{\overset{o}{a}} = \frac{\gamma \tilde{M}^2}{\sqrt{\overset{o}{M}^2-1}}\, d\theta \tag{C-502}$$

Finally, the pressure coefficient is written

$$\overset{o}{C}_p = \left(\frac{dP}{P}\right)_{\overset{o}{a}} \left(\frac{P}{\tfrac{1}{2}\rho w^2}\right)$$

or

$$\overset{o}{C}_p = \frac{2 d\theta}{\sqrt{\overset{o}{M}^2-1}} \tag{C-503}$$

Now, suppose the above analysis is repeated, using the true characteristic sound velocity $\bar{a}$ instead of the theoretical quantity $\overset{o}{a}$. The treatment is identical, and the results are

$$\left(\frac{du}{u}\right)_{\bar{a}} = -\frac{\bar{M}^2}{\sqrt{\bar{M}^2-1}}\, d\theta \tag{C-504}$$

$$\left(\frac{dP}{P}\right)_{\bar{a}} = \frac{\gamma \tilde{M}^2 d\theta}{\sqrt{\tilde{M}^2 - 1}} \qquad \text{(C-505)}$$

$$\bar{C}_p = \frac{2 d\theta}{\sqrt{\bar{M}^2 - 1}} \qquad \text{(C-506)}$$

where again, the subscript $(\ )_{\bar{a}}$ denotes use of this characteristic velocity, and where $\bar{M}$ is defined in the usual way by Eq. (A-17).

Eq. (C-505) immediately suggests a method for the determination of the still unknown characteristic velocity $\bar{a}$ in terms of the measurable parameters. Rearranging this equation,

$$\bar{M} = \left[1 + \frac{\gamma^2 \tilde{M}^4}{\left(\frac{1}{P}\frac{dP}{d\theta}\right)^2}\right]^{1/2} \qquad \text{(C-507)}$$

or

$$\bar{a} = W \left[1 + \frac{\gamma^2 \tilde{M}^4}{\left(\frac{1}{P}\frac{dP}{d\theta}\right)^2}\right]^{-1/2} \qquad \text{(C-508)}$$

Thus, by the measurement of $dP/d\theta$ on a wedge surface at $\theta = 0$, and computing the free-stream velocity by the method of Ref. 7 or the procedures described earlier in this Appendix, the quantity $\bar{a}$ may be measured. This has been done, and the result included in Fig. 30 and Table I.

C-6 Calculation of Wedge Pressure Coefficients (Non-Viscous)

1. Saturated Expansion Theory

(a) Flow Inclinations Sufficiently Large to Cause Complete Reevaporation (Cf. Fig. 21)

The quantities T_2, g_2, $\tilde{M}_2$, and P_2 upstream of the wedge are assumed to be known (from experimental measurements), and $g_3 = 0$. Assume a value for the static pressure rise P_3/P_2 across the shock. Then, solving Eq. (B-14) for $(\tilde{M}_{3N} / \tilde{M}_{2N})^2$

$$\left(\frac{\tilde{M}_{3N}}{\tilde{M}_{2N}}\right)^2 = \left[1 - \frac{\log_e \frac{P_3}{P_2}}{\frac{L}{RT^2}}\right] \frac{(1-g_3)}{(1-g_2)} \frac{1}{\left(\frac{P_3}{P_2}\right)^2} \tag{C-601}$$

and, from Eq. (B-8),

$$\tilde{M}_{2N}^2 = \frac{\frac{P_3}{P_2} - 1}{\gamma\left[1 - \frac{P_3}{P_2}\left(\frac{\tilde{M}_{3N}}{\tilde{M}_{2N}}\right)^2\right]} \tag{C-602}$$

Eq. (B-15) gives

$$\tan(\sigma-\theta) = (\tan\sigma)\left[\left(\frac{P_3}{P_2}\right)\left(\frac{\tilde{M}_{3N}}{\tilde{M}_{2N}}\right)^2\right] \tag{C-603}$$

and this, together with the definition of the normal component of $\tilde{M}_2$,

$$\sin^2\sigma = \left(\frac{\tilde{M}_{2N}}{\tilde{M}_2}\right)^2 \tag{C-604}$$

supplies the shock angle σ and the deflection angle θ for each assumed P_3/P_2.

The pressure coefficient is then given by

$$C_p = \frac{P_3 - P_2}{\frac{1}{2}\rho w^2} = \frac{2\left(\frac{P_3}{P_2} - 1\right)}{\gamma \tilde{M}_2^2} \tag{C-605}$$

(b) Partial Evaporation Shocks (Cf. Fig. 21)

In order to determine the wedge surface pressures as a function of the flow inclination θ, first assume a value for the shock angle σ. Thus all upstream parameters and $\tilde{M}_{2N}$ are now known. The following equations are available: Eqs. (B-8), (B-11), (B-6c), and the equation just preceding Eq. (B-14), with $g_3 \neq 0$,

$$\frac{T_3}{T_2}\,\frac{(1-g_3)}{(1-g_2)} = \frac{\left[\gamma \tilde{M}_{2N}^2 + 1\right]^2}{\left[\gamma \tilde{M}_{3N}^2 + 1\right]^2}\,\frac{\tilde{M}_{3N}^2}{\tilde{M}_{2N}^2} \qquad \text{(C-606)}$$

These equations involve only four unknown parameters: T_3, g_3, $\tilde{M}_{3N}$, and P_3, and thus, a simultaneous solution is theoretically possible. However, due to the enormous complexity of the system, an approximate method will be used.

A value for P_3/P_2 is assumed. Then, instead of calculating an exact value for g_3, a rough estimate is made that g_3 varies linearly with P_3/P_2, changing from g_2 to zero as P_3/P_2 goes from unity to the minimum value of 5.53 for complete evaporation under the given upstream conditions, i.e.,

$$g_3 = g_2\left[\frac{5.53 - P_3/P_2}{4.53}\right] \qquad \text{(C-607)}$$

Physically, this approximation is probably very close to the actual case, and furthermore, the effect of small variations in g_3 on the calculations necessary to determine σ and θ for the assumed P_3/P_2 is small. Once g_3 is known, the procedure for determination of C_p as a function of θ is the same as that given above in (a). The theoretical curve of Fig. 35 was plotted using these methods.

2. Perfect Gas Theory

The pressure ratio P_3/P_2 is found for each value of θ by use of the shock polar charts of Ref. 20. The pressure coefficient is then given directly by

$$C_p = \frac{2\left(\frac{P_3}{P_2} - 1\right)}{\gamma M_2^2} \qquad \text{(C-608)}$$

where M_2 is taken to be numerically equal to $\overset{\circ}{M}_2$, $\bar{M}_2$, and $M(A_2/A^*)$ for comparison with corresponding pressure coefficients in the two-phase fluid.

3. Slender-Body Approximation

The hypersonic slender-body approximation as given in Ref. 17 is

$$C_p = \frac{2\theta}{\sqrt{M^2-1}} + \frac{\gamma+1}{2}\,\frac{\theta^2 M^2}{M^2-1} + \frac{\gamma+1}{6}\,\frac{\theta^3 M^4}{(M^2-1)^{3/2}} + \cdots \qquad \text{(C-609)}$$

Thus, for any given Mach number, the pressure coefficient is determined directly for each value of the flow inclination. This equation has been included in Fig. 35, using the theoretical characteristic Mach number $\overset{\circ}{M}$. (Note: The difference between using $\overset{\circ}{M}$ and $\bar{M}$ in these calculations is too small to appear in the scale of Fig. 35.)

4. Experimental Results

The data of Fig. 33 was used to obtain P_3 at a point on the wedge surface corresponding to the point at which the free-stream pressure P_2 as used in (1) above was measured. The pressure coefficient is then given by Eq. (C-605). It should be noted that these results

give only a rough idea of the actual pressure coefficient, since the non-parallel test-section flow probably introduces an error which cannot be corrected for with any reasonable degree of accuracy.

C-7 Experimental "Spot-Check" of the Oblique Shock Theory

By making a sufficiently large number of independent measurements in a local neighborhood of an oblique shock wave, an equation derived from the considerations of Appendix B may be duplicated experimentally, and the accuracy of the resulting identity examined. If Eq. (B-15) is substituted into Eq. (B-9) and the resulting expression solved for $\tilde{M}_2^2$, we obtain

$$\tilde{M}_2^2 = \frac{\tilde{M}_{2N}^2}{\sin^2\sigma} = \frac{1}{\gamma \sin^2\sigma} \frac{\left[\frac{P_3}{P_2} - 1\right]}{\left[1 - \frac{\tan(\sigma-\theta)}{\tan\sigma}\right]} \qquad \text{(C-701)}$$

The measurements used to check this identity at $\theta_w = 30^\circ$ and $\theta_w = 34^\circ$ were made in the neighborhood of a single point on the oblique shock wave as follows:

(a) $\tilde{M}_2$ was determined from pitot and static pressures and Fig. 26.

(b) σ was determined from pitot rake data as plotted in Fig. 37, and was corrected for free-stream flow inclination by Eq. (C-302).

(c) P_3/P_2 was determined directly by static pressure probe measurements.

(d) θ was estimated from data similar to that of Fig. 40.

The numerical results for the two wedge angles selected satisfied the identity within 1.1% for $\theta_w = 30^\circ$ and within 0.5% for $\theta_w = 34^\circ$.

LIST OF ILLUSTRATIONS

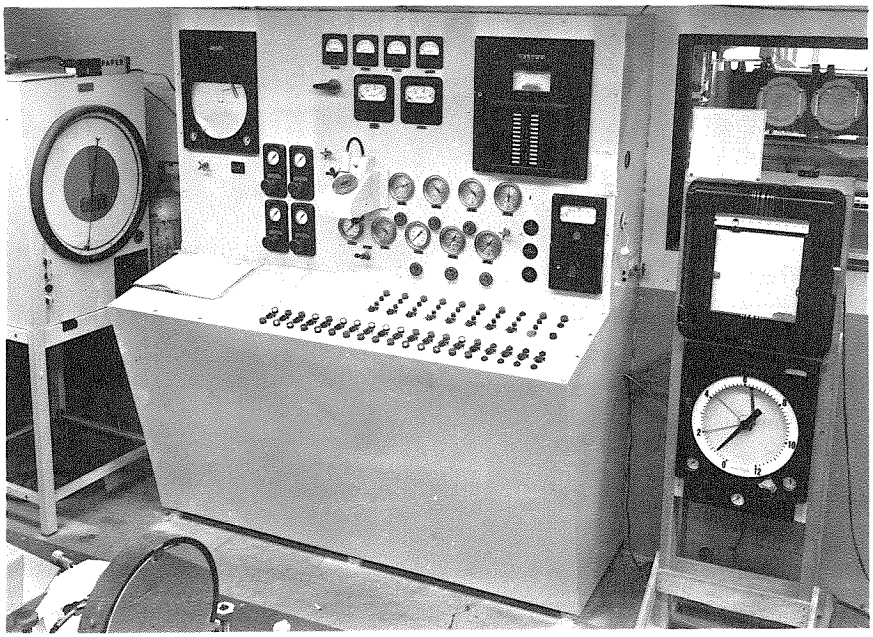

FIGURE 1
GALCIT 5" HYPERSONIC WIND TUNNEL
CONTROL PANEL

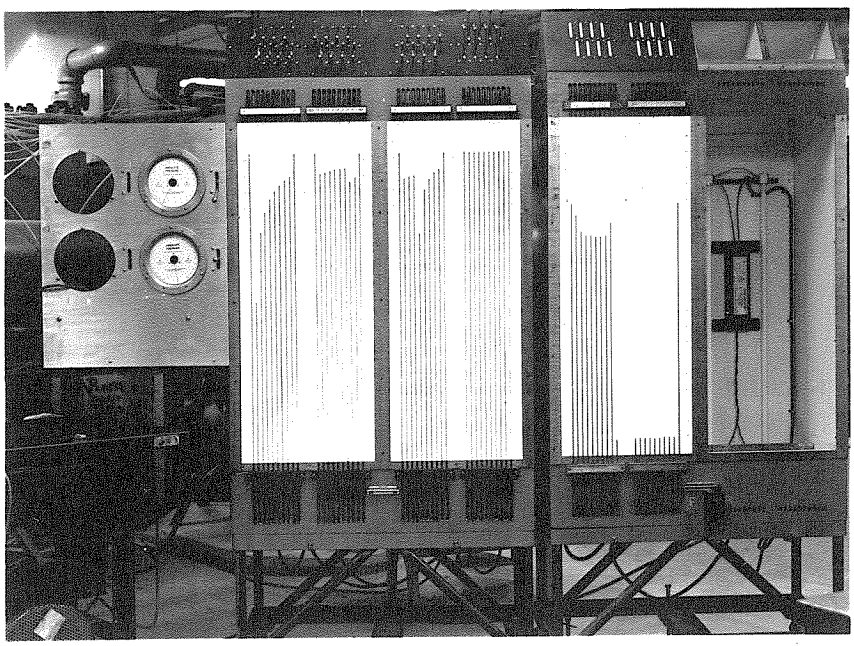

FIGURE 2
GALCIT 5" HYPERSONIC WIND TUNNEL
MANOMETER BOARD

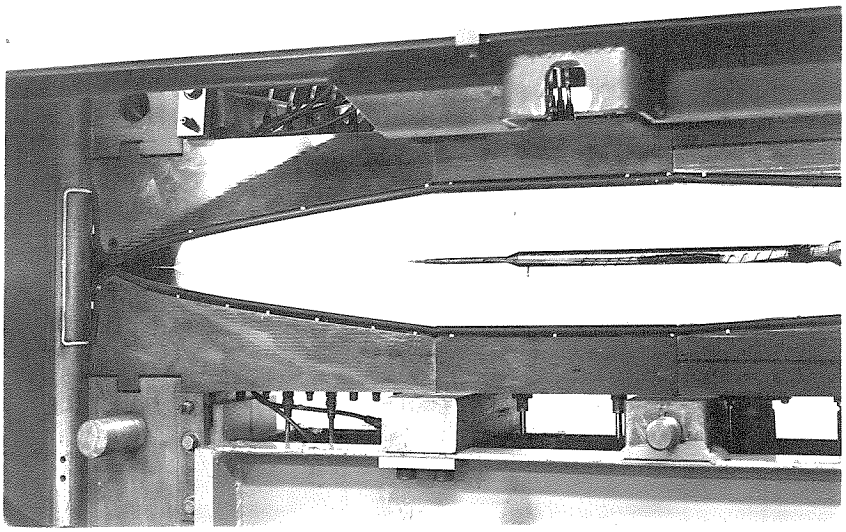

FIGURE 3
GALCIT 5" HYPERSONIC WIND TUNNEL
TEST SECTION WITH M = 8.9 NOZZLE

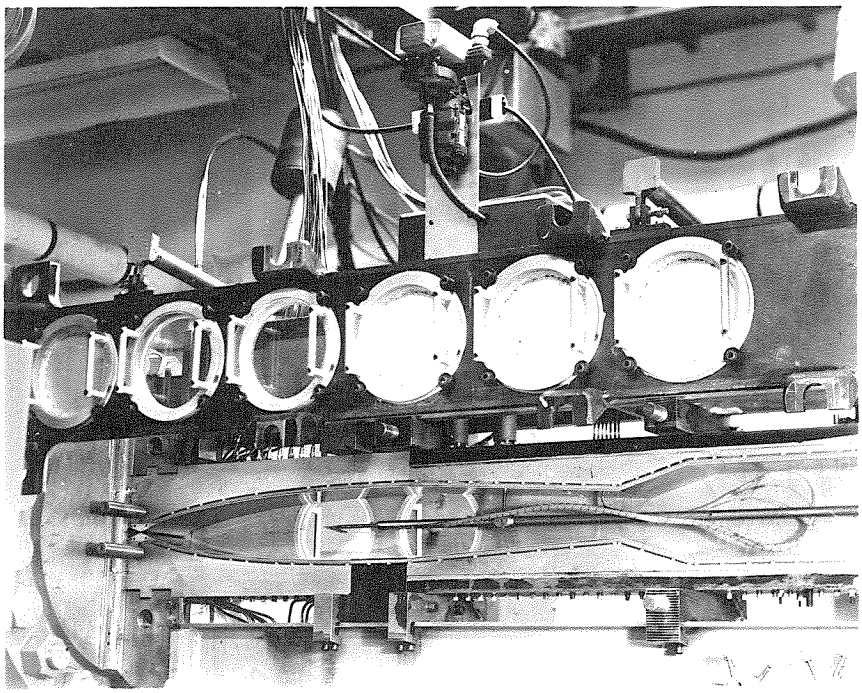

FIGURE 4
GALCIT 5" HYPERSONIC WIND TUNNEL
TEST SECTION WITH M = 6 NOZZLE

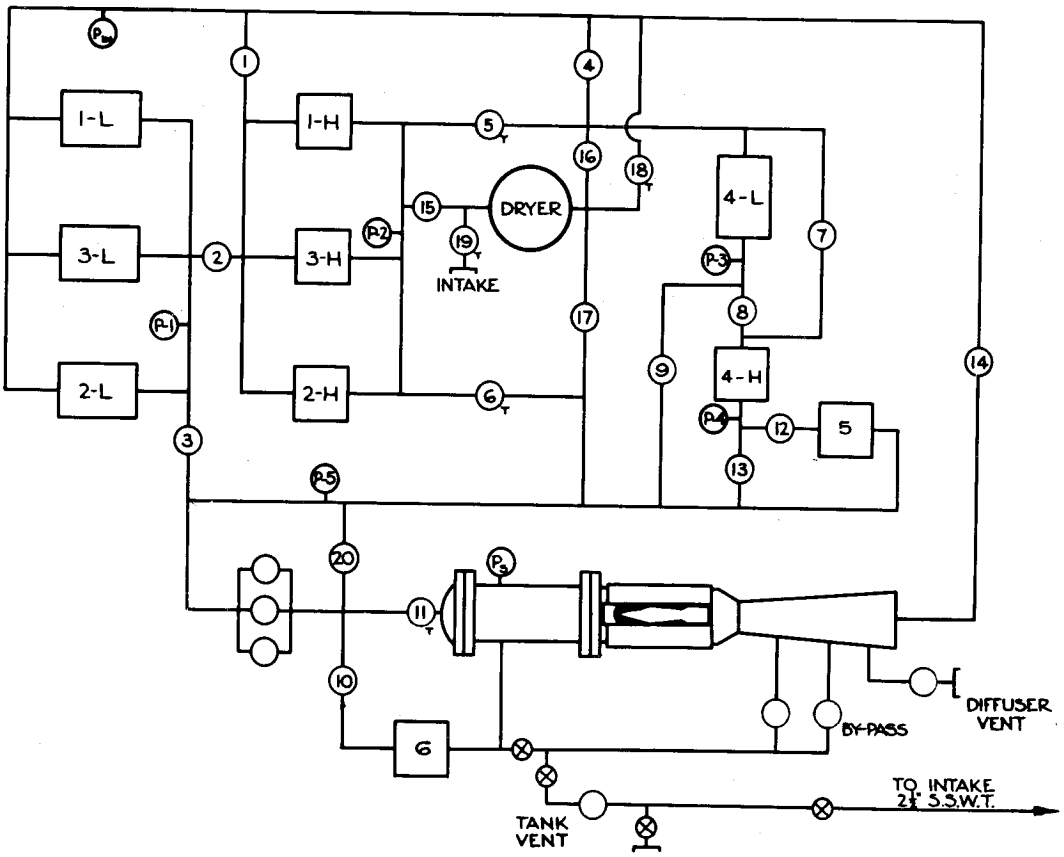

FIGURE 5
SCHEMATIC DIAGRAM OF GALCIT 5"
HYPERSONIC WIND TUNNEL

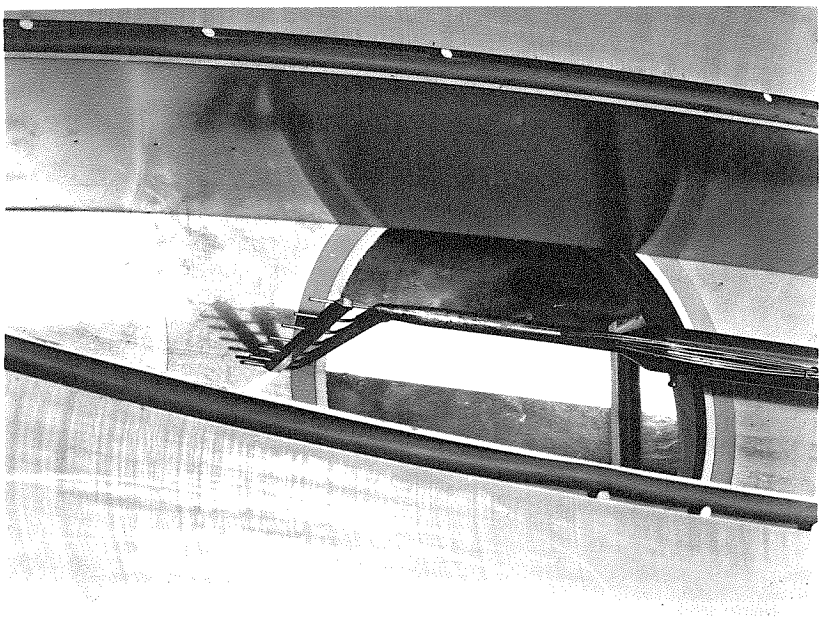

FIGURE 6
SEVEN-TUBE PITOT PRESSURE RAKE

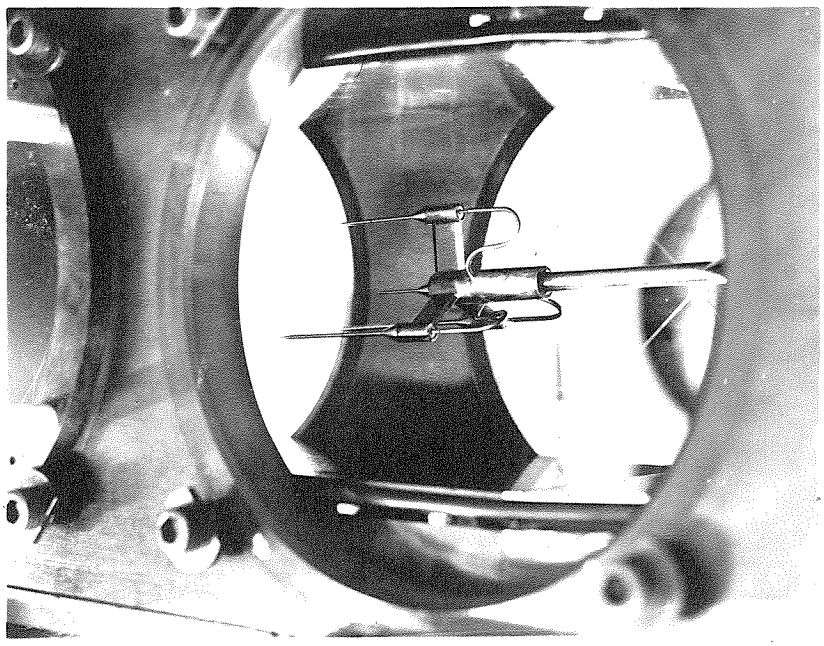

FIGURE 7
EQUIPMENT FOR CALIBRATION OF
STATIC PRESSURE PROBES

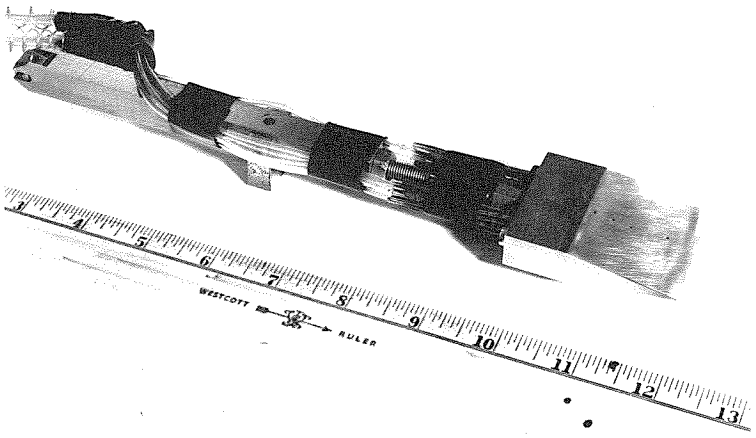

FIGURE 8
10° HALF-ANGLE WEDGE

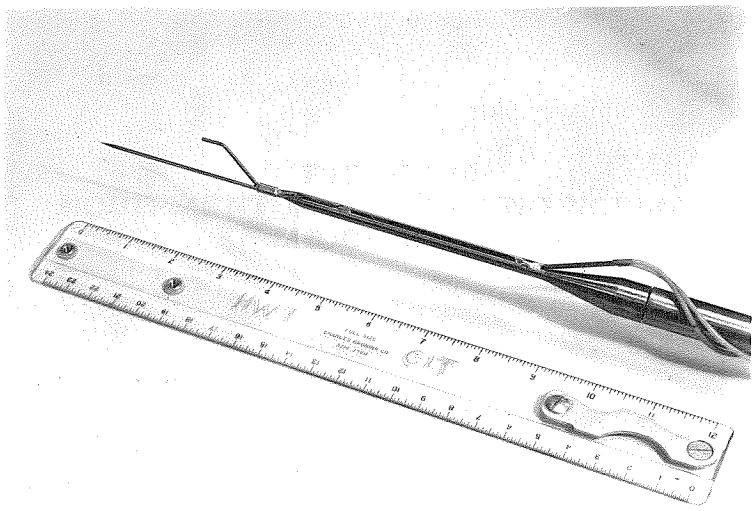

FIGURE 9
PITOT-STATIC PRESSURE PROBE

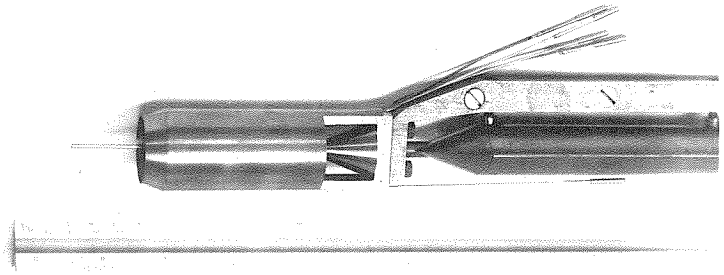

FIGURE 10
EQUIPMENT FOR CREATING NORMAL
SHOCK WAVE

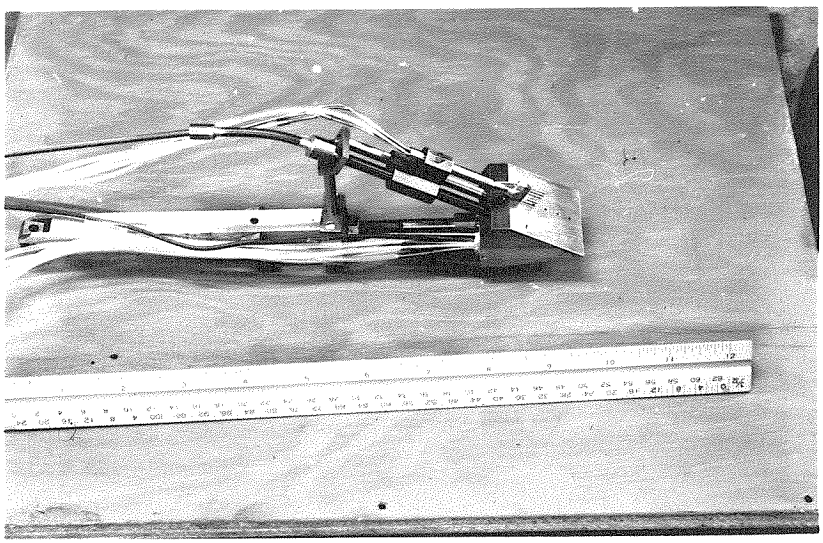

FIGURE 11
40° WEDGE WITH ADJUSTABLE PITOT
PRESSURE RAKE

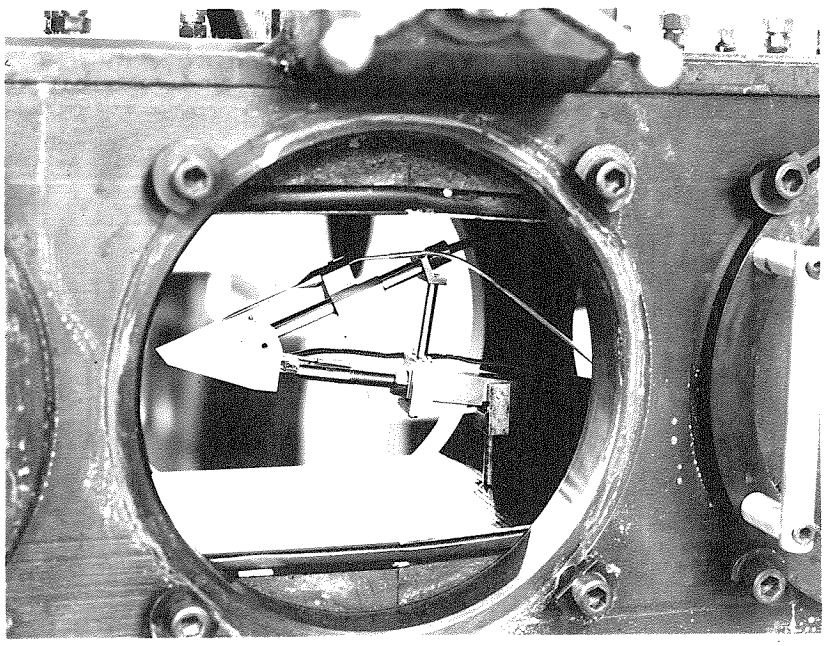

FIGURE 12
40° WEDGE WITH ADJUSTABLE STATIC
PRESSURE PROBE

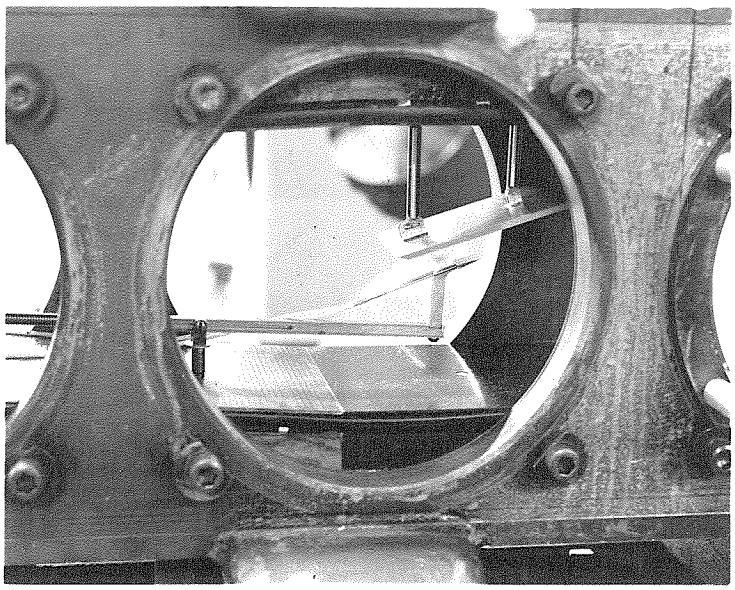

FIGURE 13
INCLINED FLAT PLATE WITH WEDGE TO
MEASURE FLOW INCLINATION

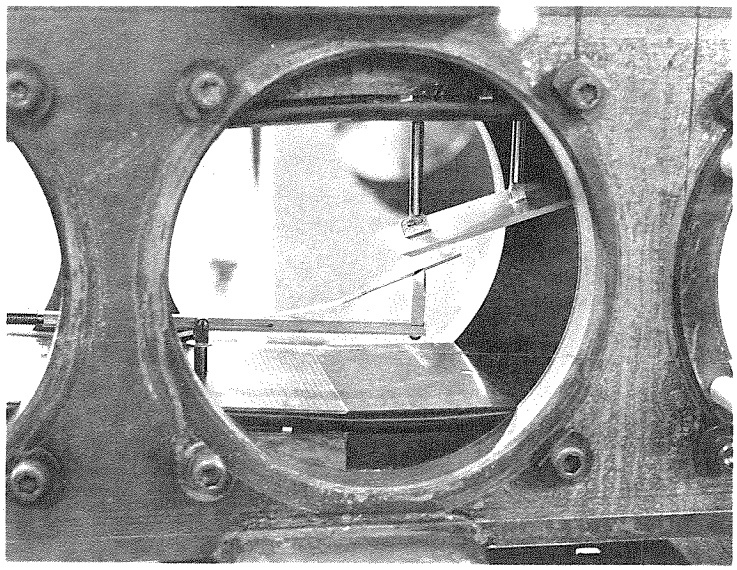

FIGURE 14
INCLINED FLAT PLATE WITH PITOT
PRESSURE PROBE TO CHART OBLIQUE
SHOCK WAVE

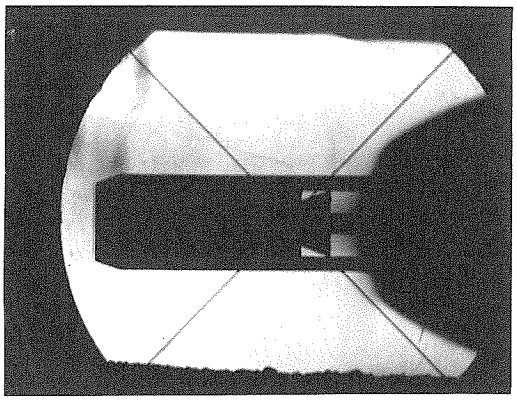

FIGURE 15
NORMAL SHOCK STANDING AT MOUTH
OF CHANNEL (KNIFE EDGE VERTICAL)

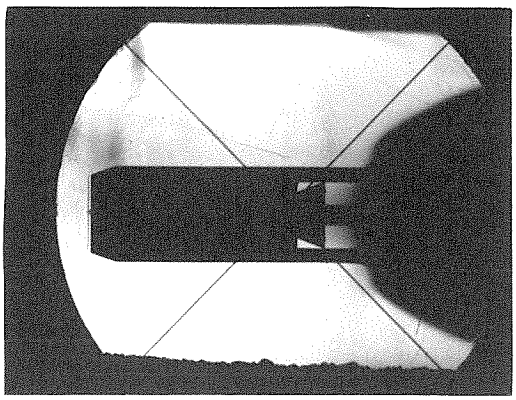

FIGURE 16
PITOT PRESSURE PROBE IN REGION OF
NORMAL SHOCK (KNIFE EDGE VERTICAL)

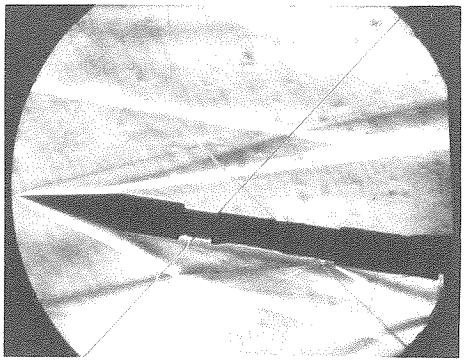

FIGURE 17
TOP SURFACE OF WEDGE AT 0° FLOW INCLINATION, SHOWING TENDENCY TOWARD SEPARATION

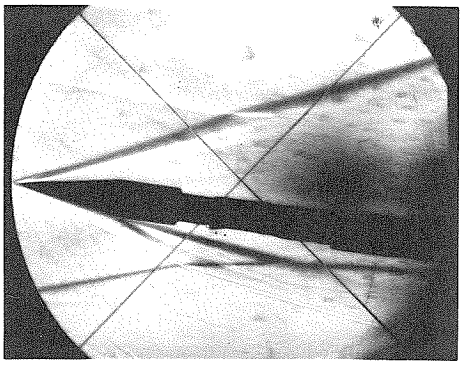

FIGURE 18
TOP SURFACE OF WEDGE AT -1° FLOW INCLINATION, SHOWING SEPARATION (KNIFE EDGE HORIZONTAL)

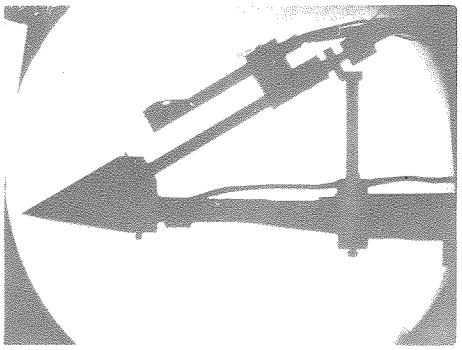

FIGURE 19
OBLIQUE SHOCK WAVE ON 40° WEDGE (KNIFE EDGE PARALLEL TO SHOCK)

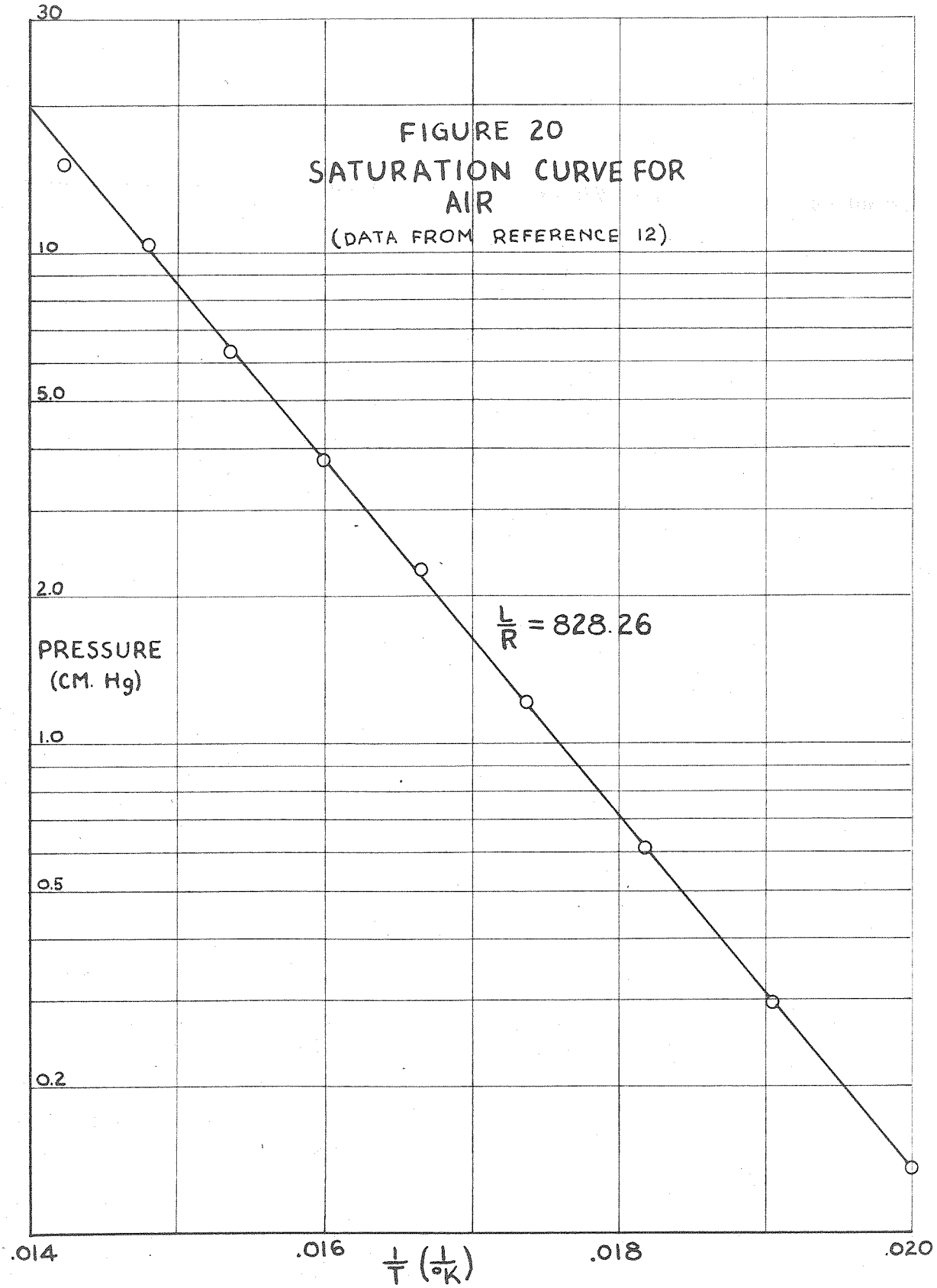

FIGURE 20
SATURATION CURVE FOR AIR
(DATA FROM REFERENCE 12)

FIGURE 21
CRITERIA FOR FULL RE-EVAPORATION BEHIND OBLIQUE SHOCK WAVES

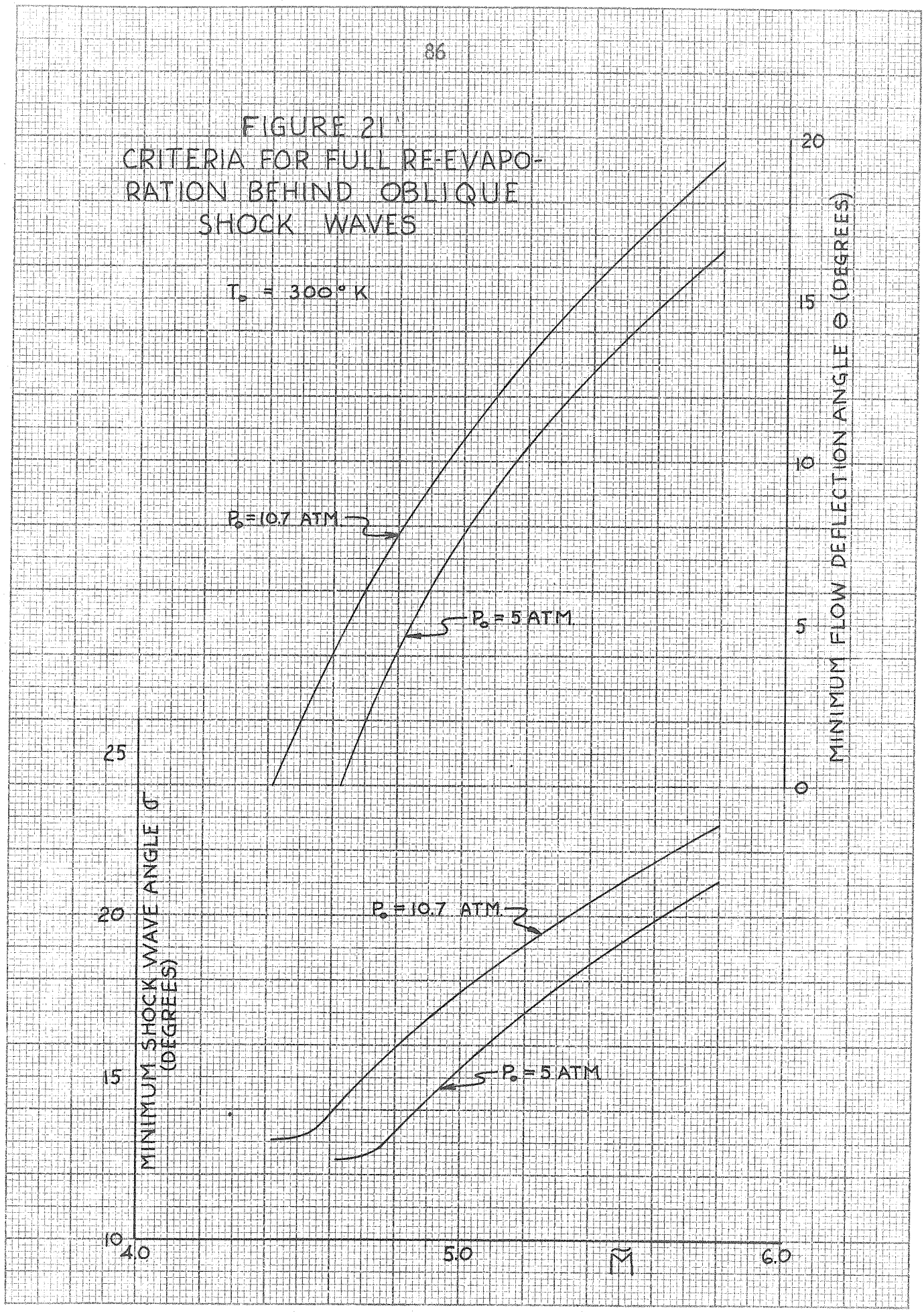

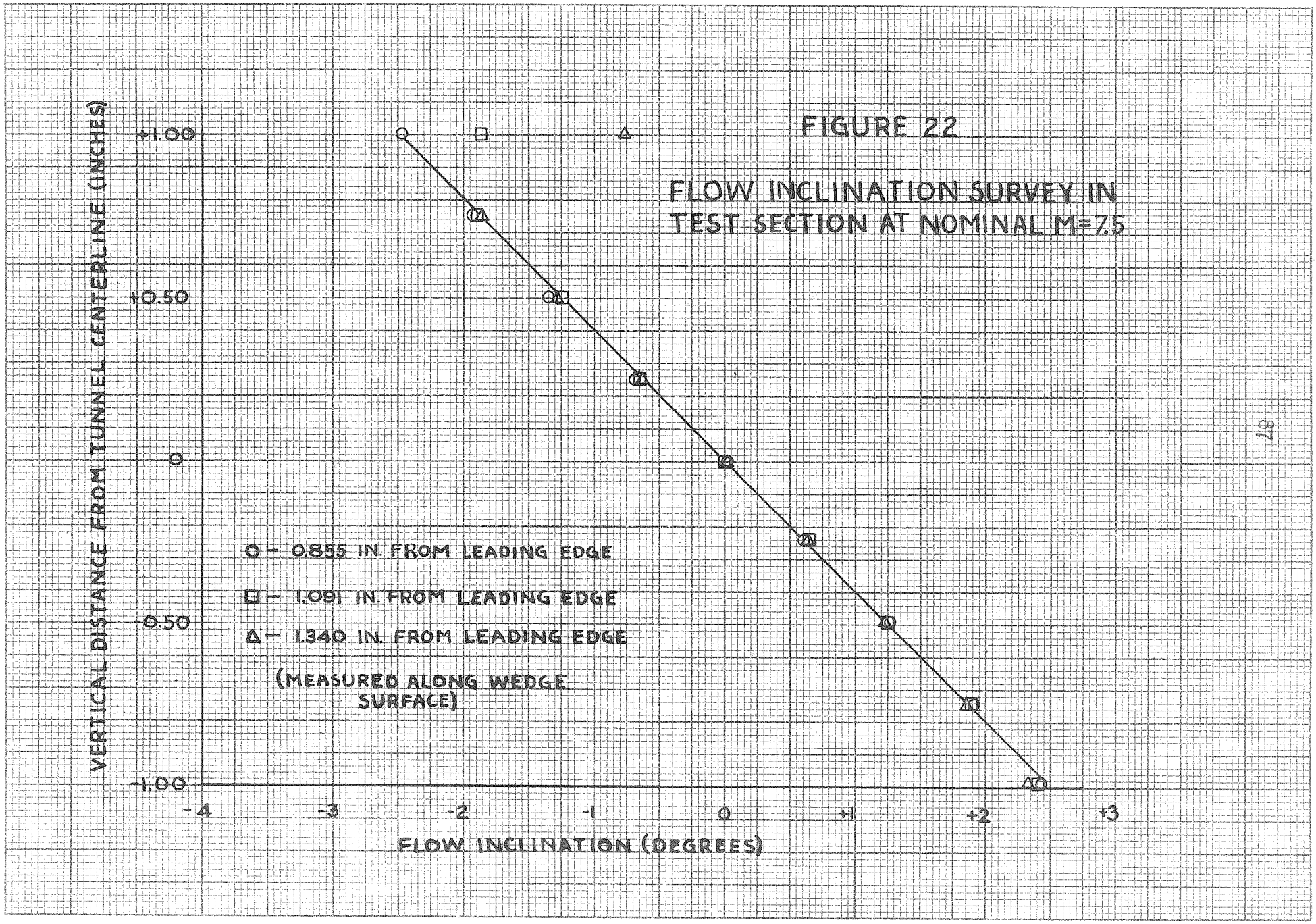
FIGURE 22
FLOW INCLINATION SURVEY IN TEST SECTION AT NOMINAL M=7.5
VERTICAL DISTANCE FROM TUNNEL CENTERLINE (INCHES)
+1.00
+0.50
0
-0.50
-1.00
-4
-3
-2
-1
0
+1
+2
+3
FLOW INCLINATION (DEGREES)
○ - 0.855 IN. FROM LEADING EDGE
□ - 1.091 IN. FROM LEADING EDGE
Δ - 1.340 IN. FROM LEADING EDGE
(MEASURED ALONG WEDGE SURFACE)

FIGURE 23

PITOT PRESSURE SURVEY OF TEST SECTION:
HORIZONTAL PLANE

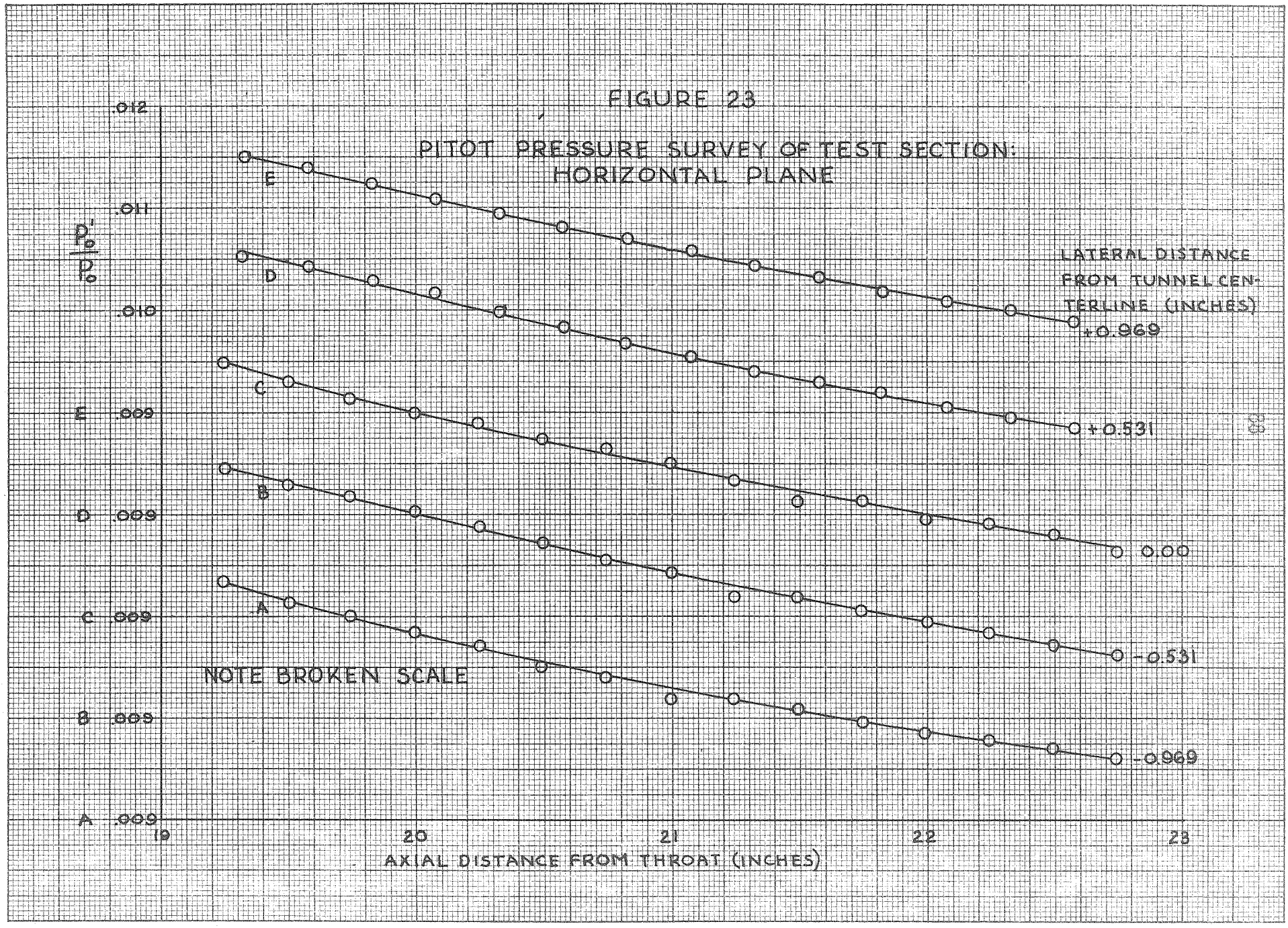

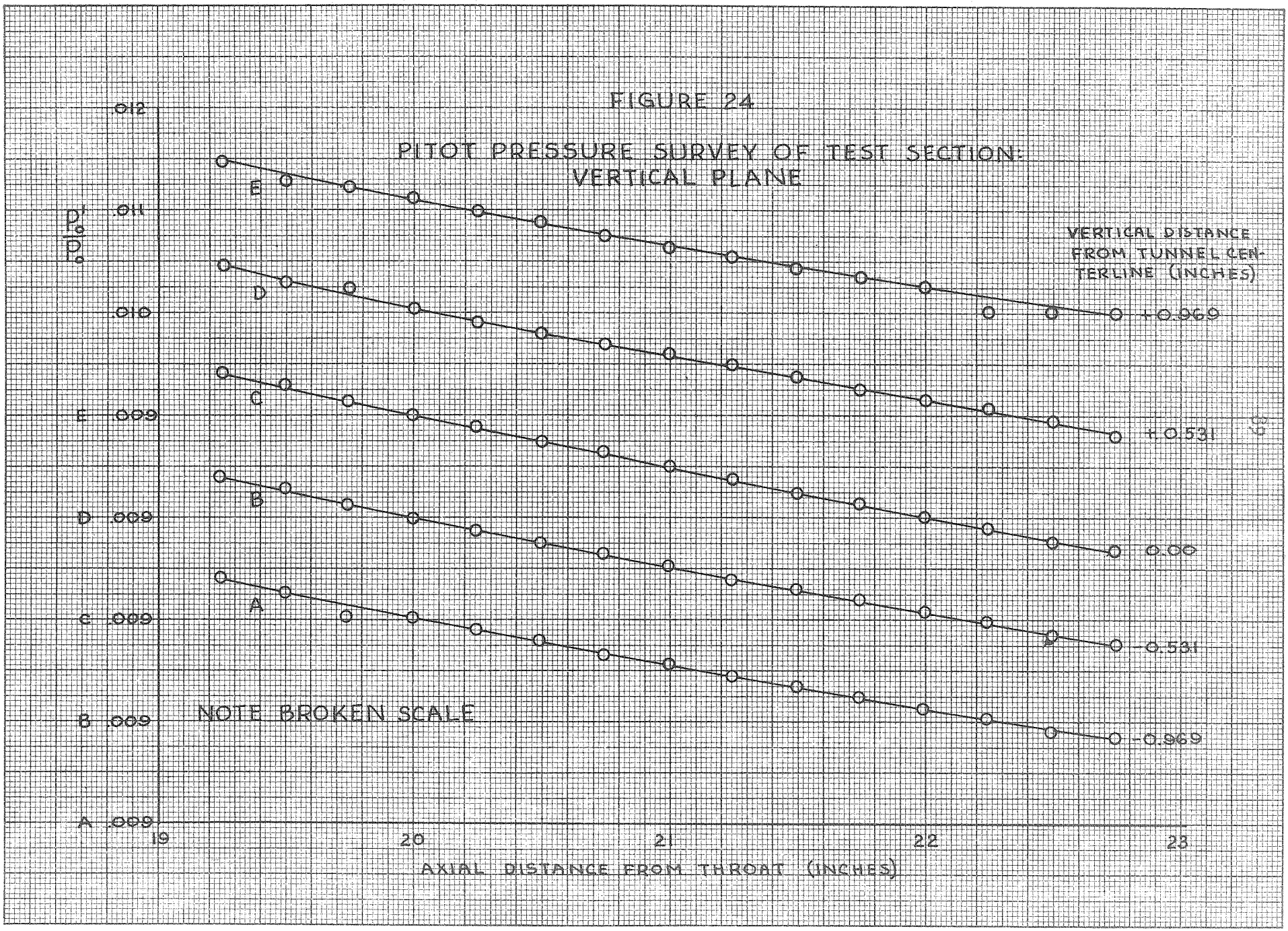
FIGURE 24
PITOT PRESSURE SURVEY OF TEST SECTION: VERTICAL PLANE
P'o/Po
.012
.011
.010
.009
.009
.009
.009
.009
E
D
C
B
A
VERTICAL DISTANCE FROM TUNNEL CENTERLINE (INCHES)
+0.969
+0.531
0.00
-0.531
-0.969
NOTE BROKEN SCALE
19
20
21
22
23
AXIAL DISTANCE FROM THROAT (INCHES)

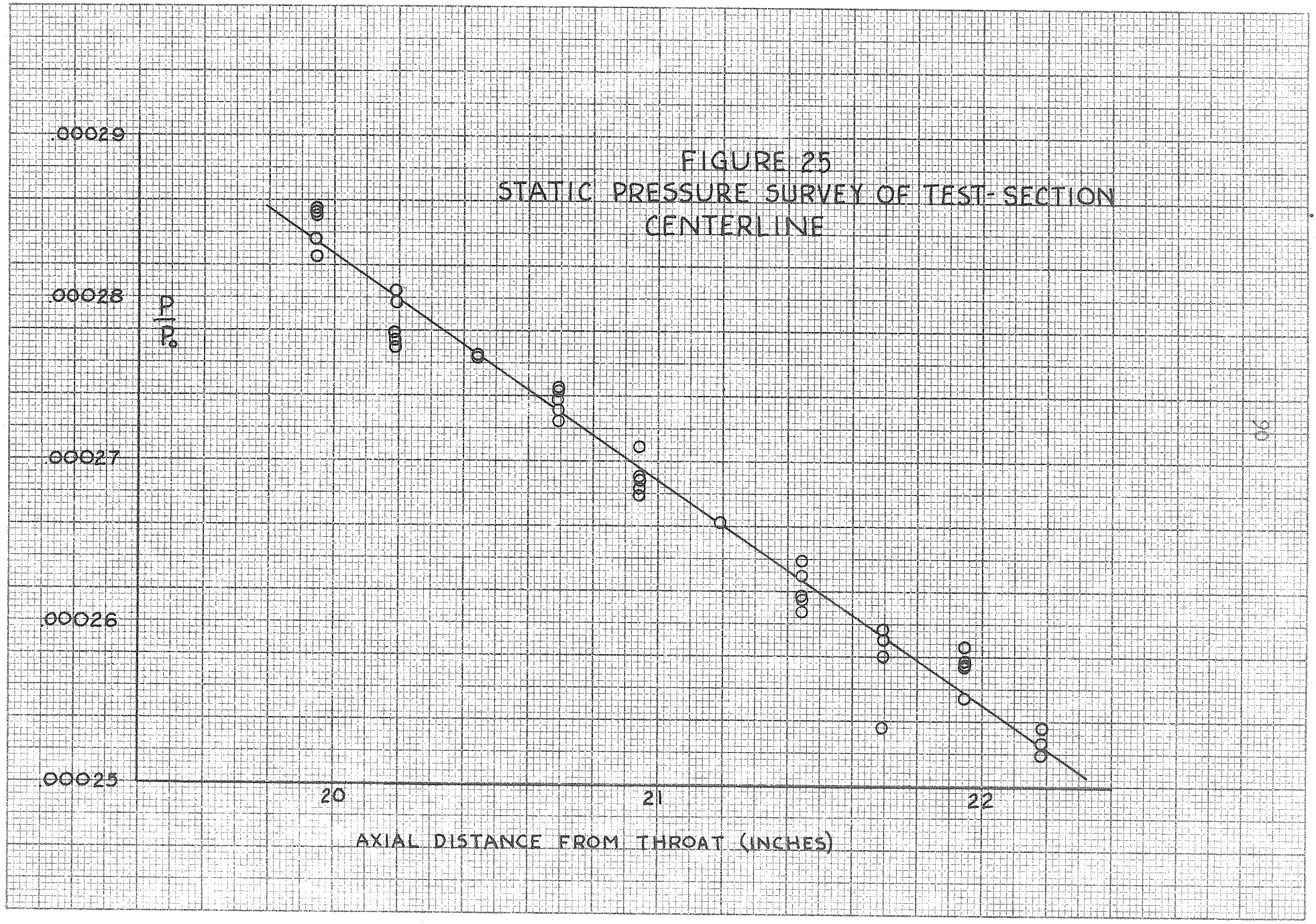

FIGURE 25
STATIC PRESSURE SURVEY OF TEST-SECTION CENTERLINE

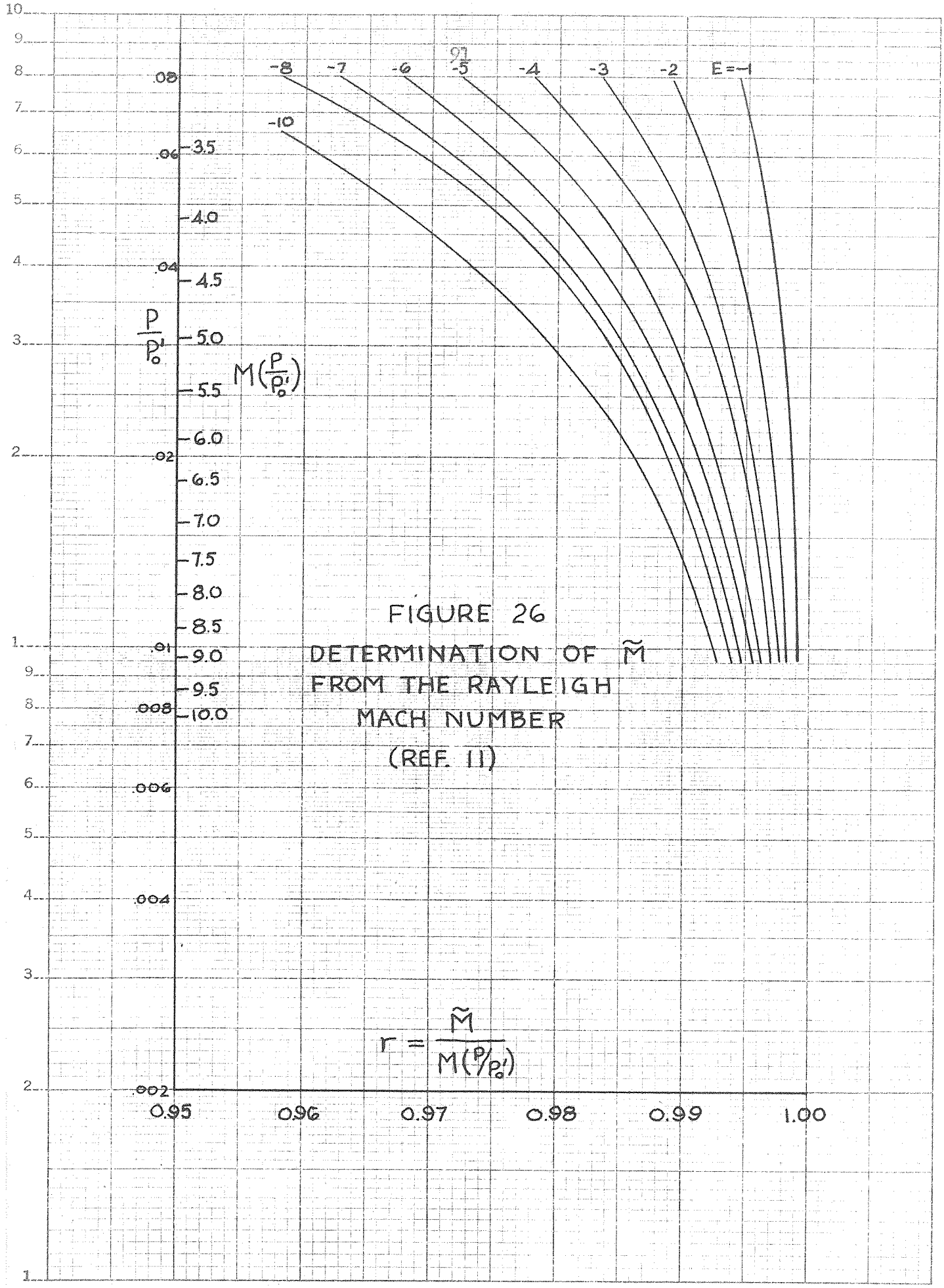

FIGURE 26
DETERMINATION OF $\tilde{M}$
FROM THE RAYLEIGH
MACH NUMBER
(REF. 11)

FIGURE 27a

DETECTION OF CONDENSATION BY PRESSURE RATIOS

P_o = 10.7 ATM.

T_o = 300° K

NOMINAL M = 7.5

[NOTE: EXPERIMENTAL EFFECTIVE AREA RATIO WAS OBTAINED FROM MEASUREMENTS OF P_o'/P_o]

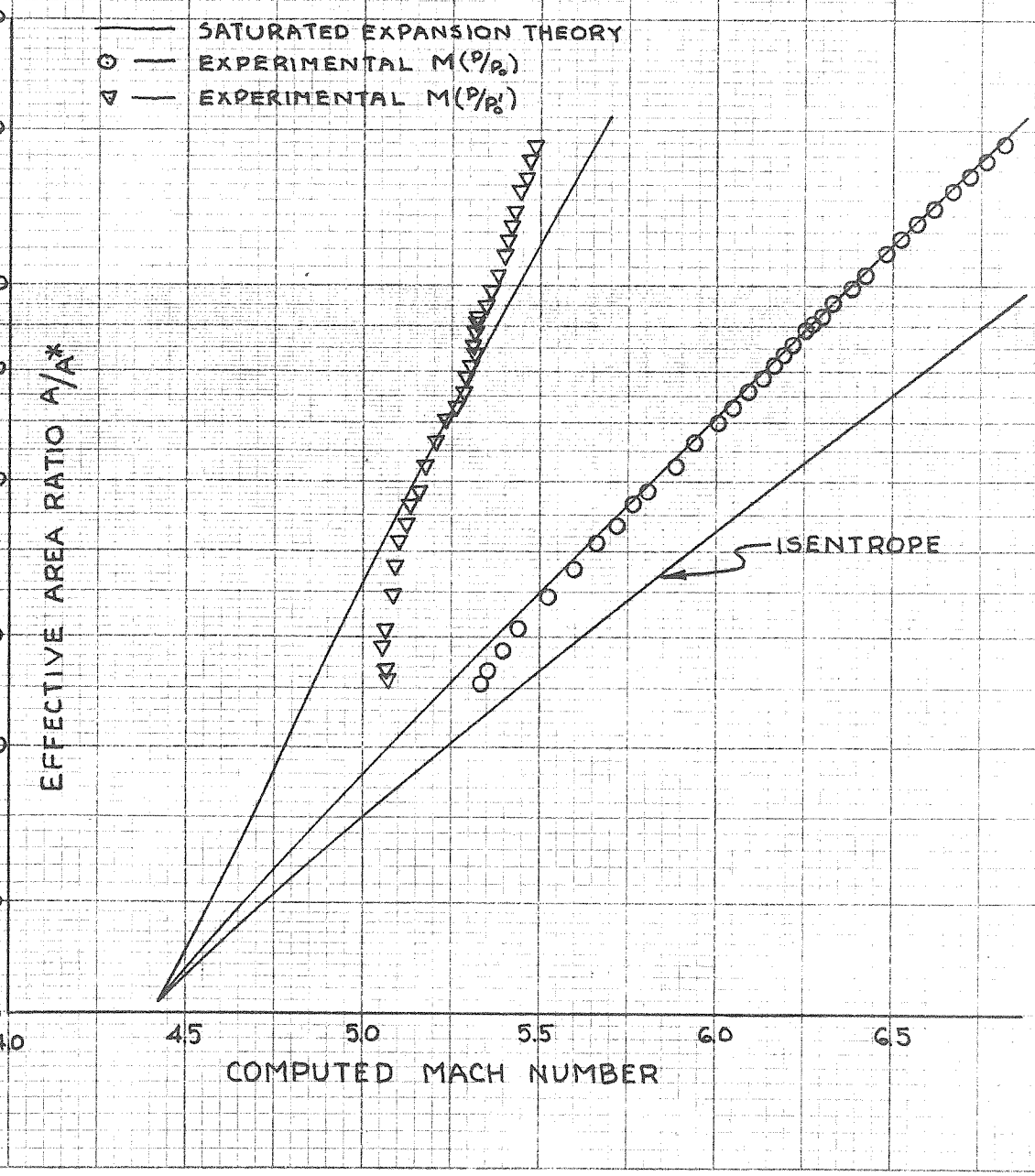

FIGURE 27b

DETECTION OF CONDENSATION BY PRESSURE RATIOS

P_o = 5 ATM

T_o = 300° K

NOMINAL M = 6

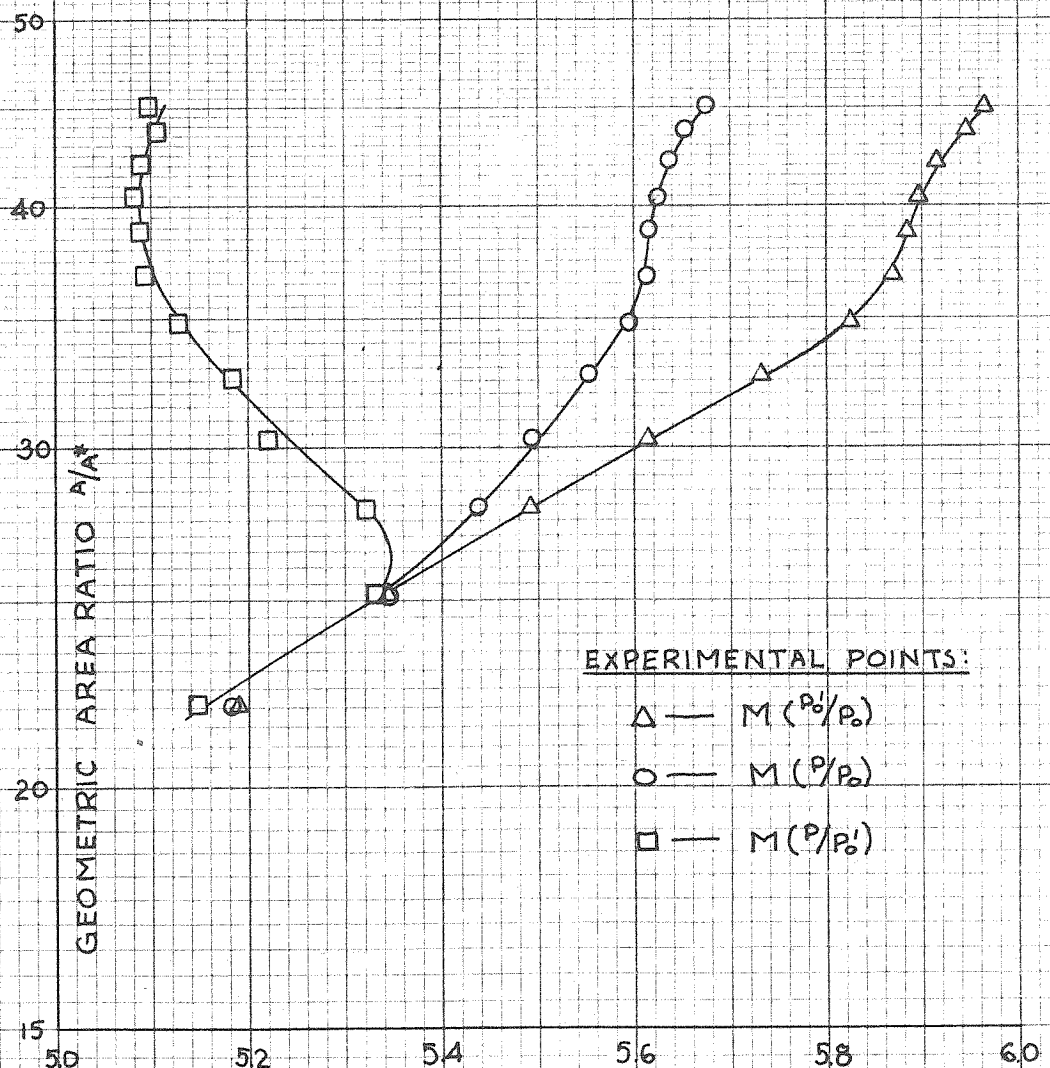

FIGURE 28
STATIC-PITOT PRESSURE RATIO VS. PITOT-STAGNATION PRESSURE RATIO

$T_o = 300°K$

⊙ — $P_o = 10.7$ ATM

△ — $P_o = 5$ ATM.

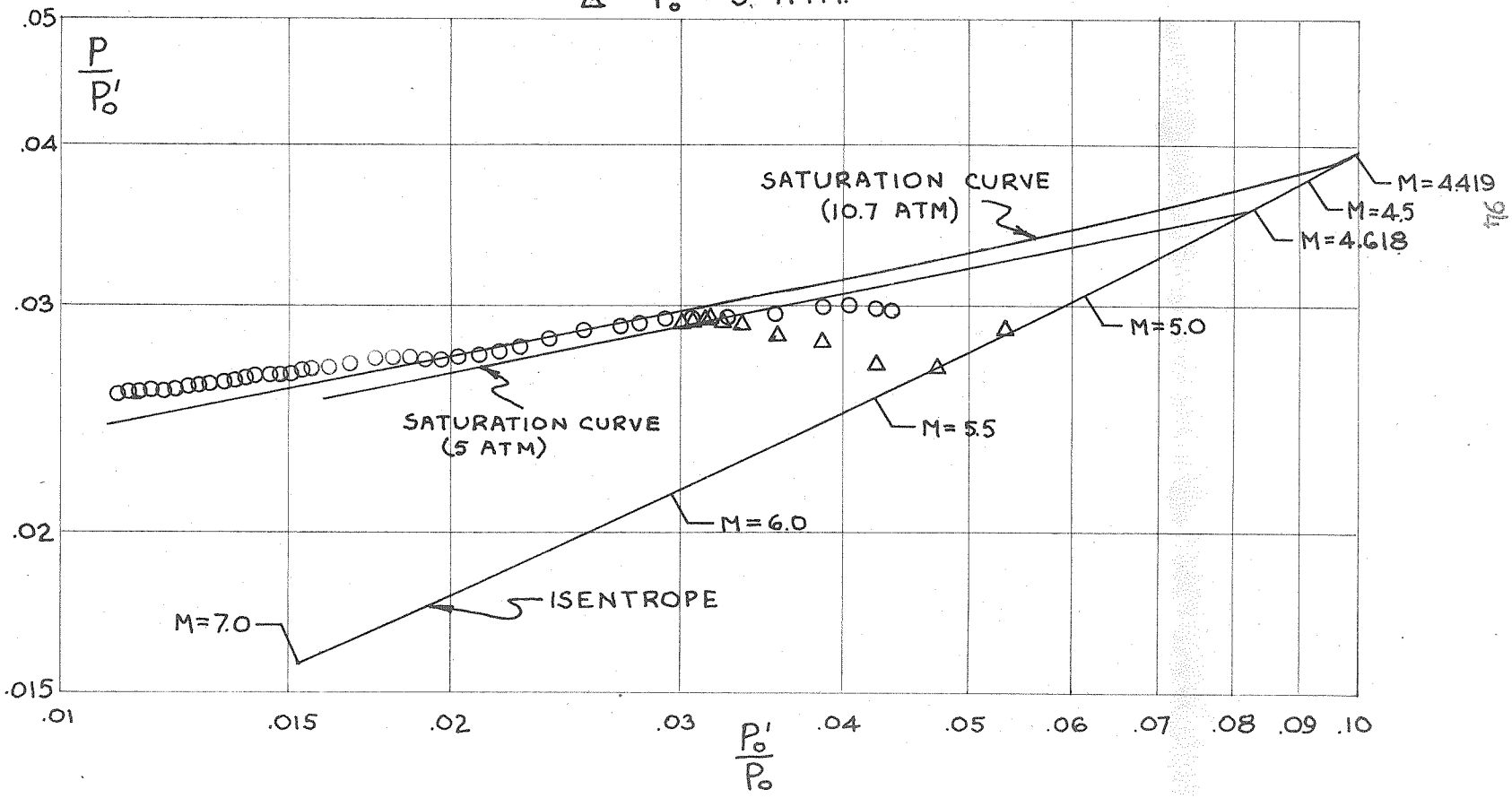

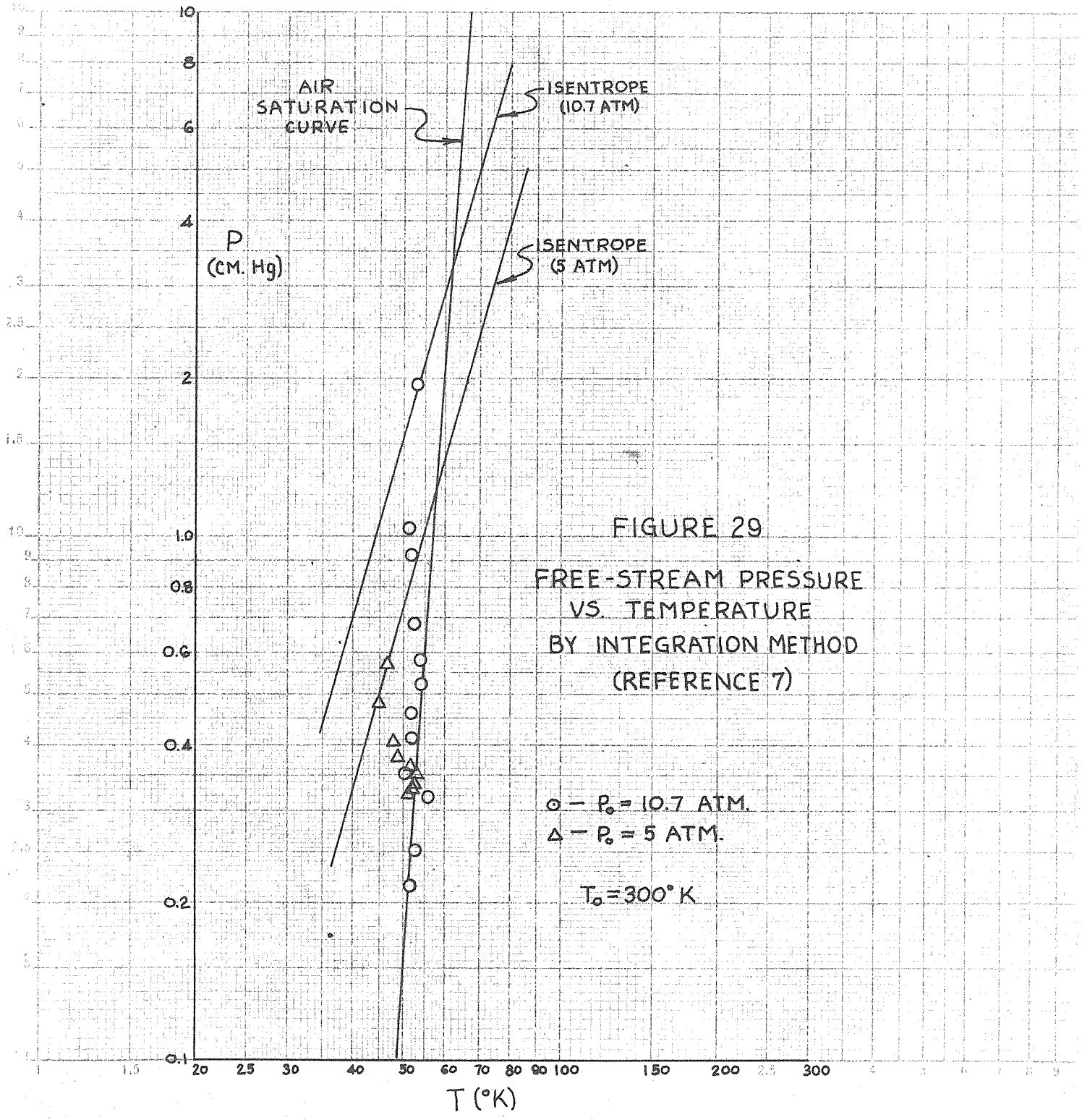

FIGURE 29

FREE-STREAM PRESSURE VS. TEMPERATURE BY INTEGRATION METHOD (REFERENCE 7)

○ — P_o = 10.7 ATM.

△ — P_o = 5 ATM.

T_o = 300° K

FIGURE 30
COMPARISON OF EXPERIMENTAL VALUES OF SPEEDS OF SOUND

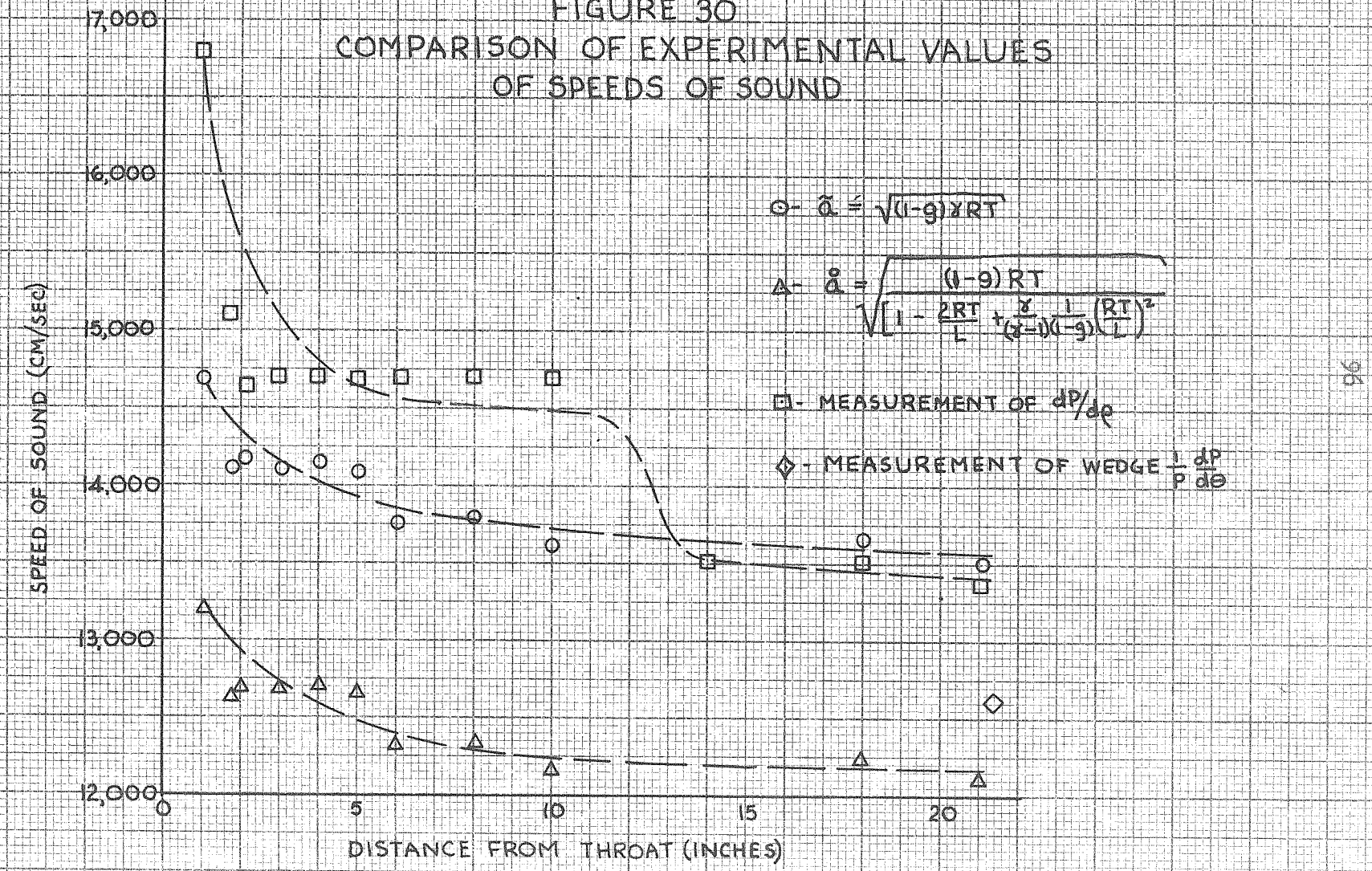

FIGURE 31
EFFECT OF INCREASED STAGNATION TEMPERATURE ON THE CHARACTER OF THE FLOW AT NOMINAL MACH NO. 6

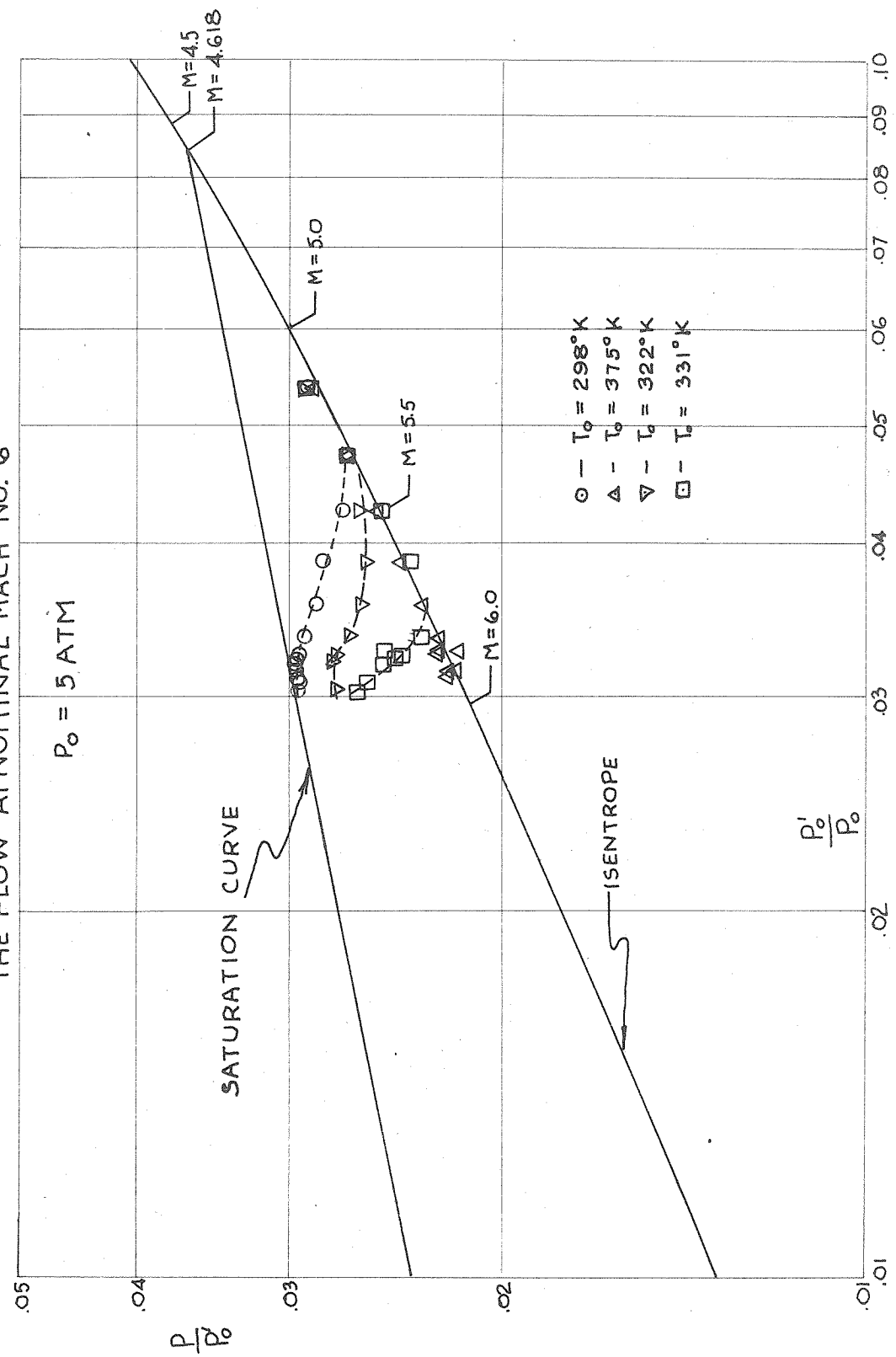

FIGURE 32

EFFECT OF RE-EVAPORATION ON PITOT PROBE MEASUREMENTS

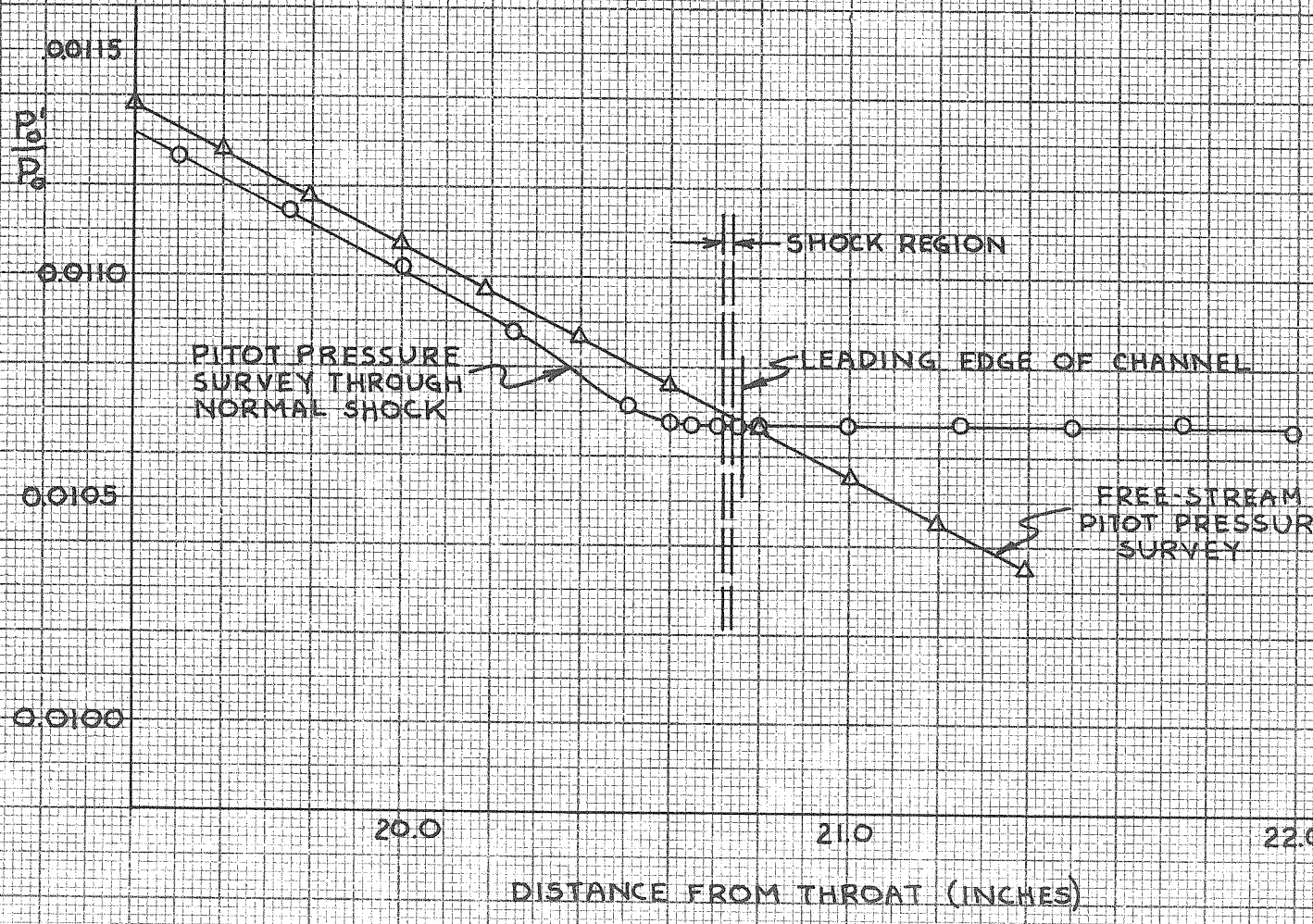

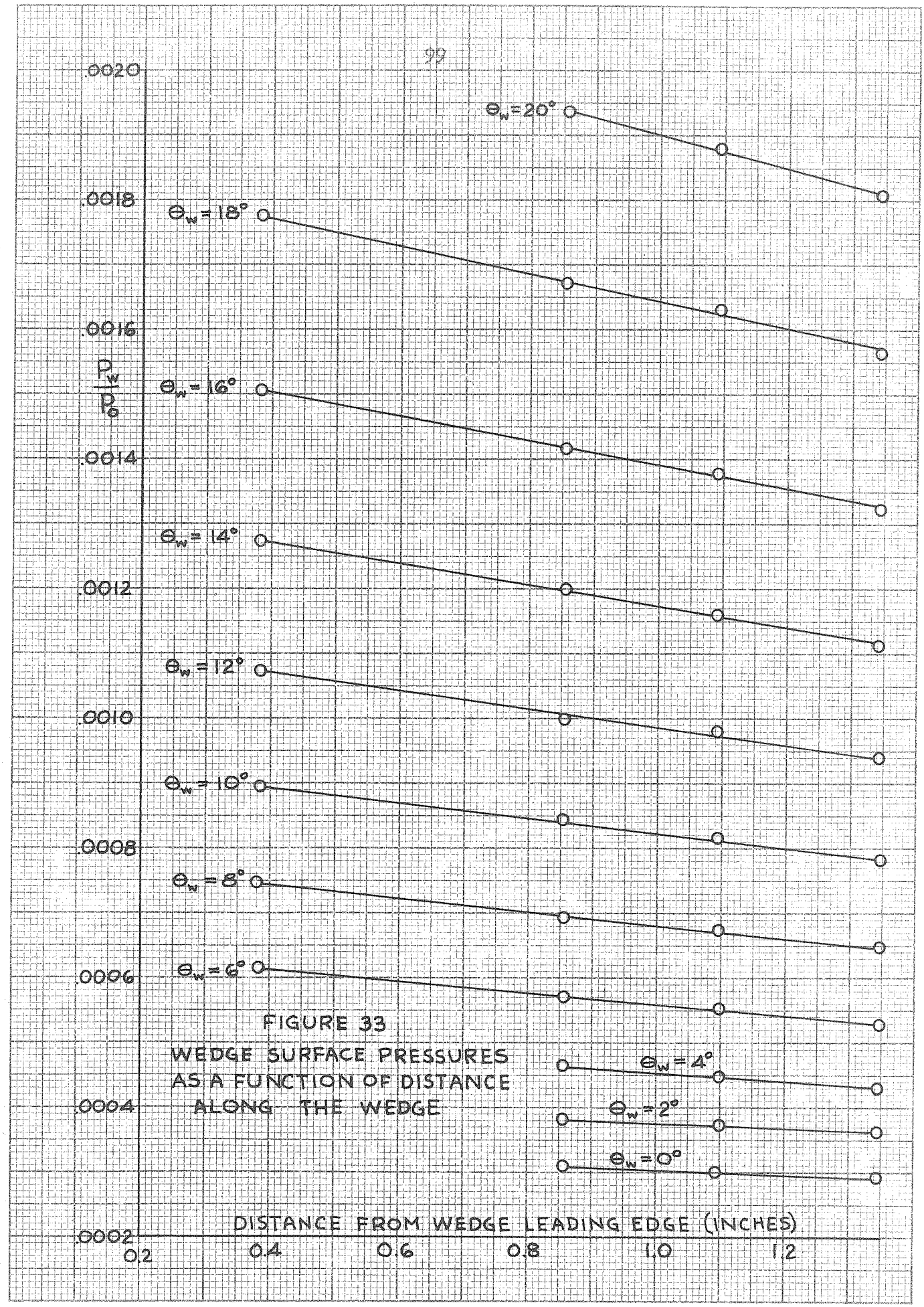

FIGURE 33
WEDGE SURFACE PRESSURES
AS A FUNCTION OF DISTANCE
ALONG THE WEDGE

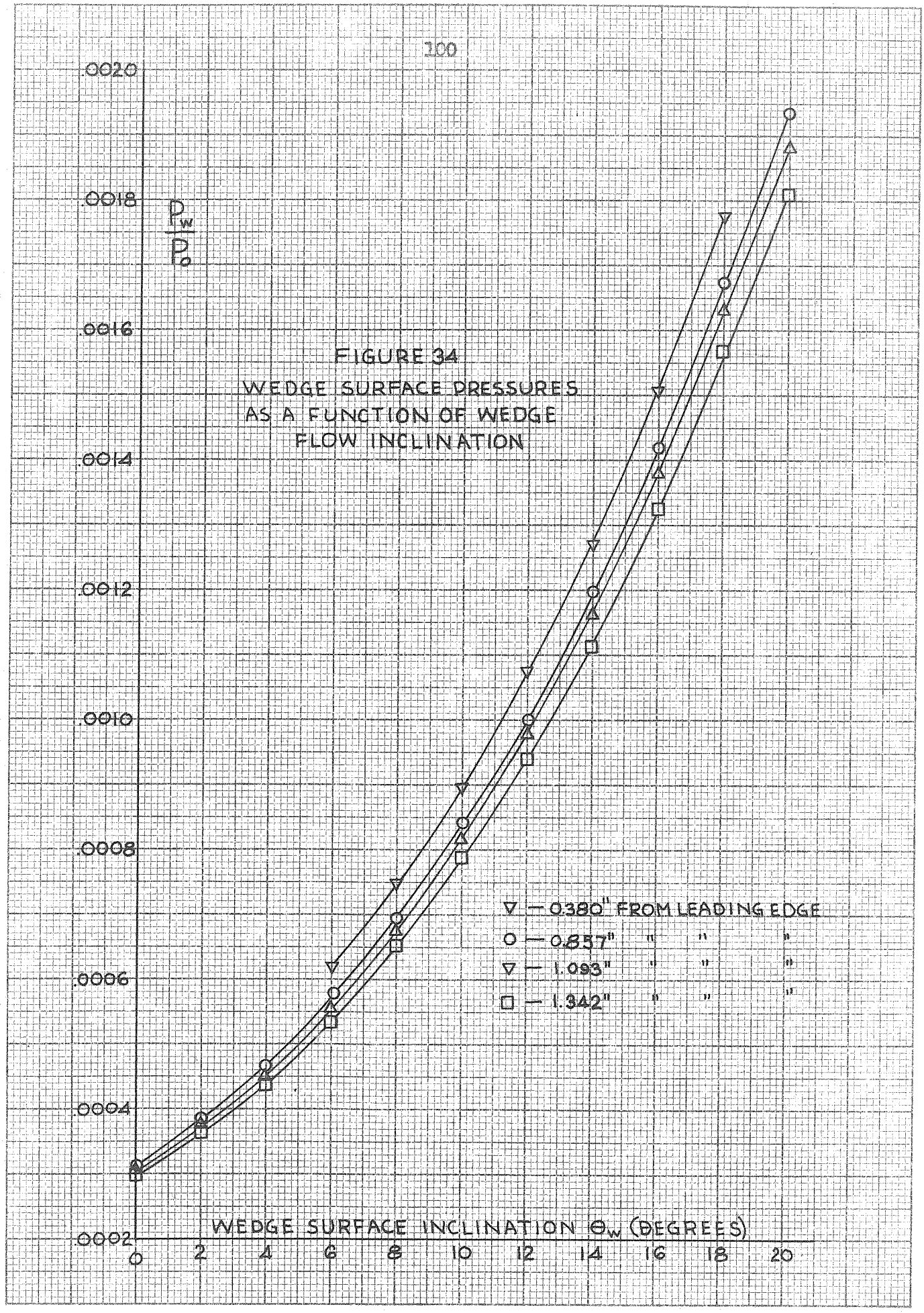

FIGURE 34
WEDGE SURFACE PRESSURES AS A FUNCTION OF WEDGE FLOW INCLINATION

FIGURE 35
WEDGE PRESSURE COEFFICIENTS

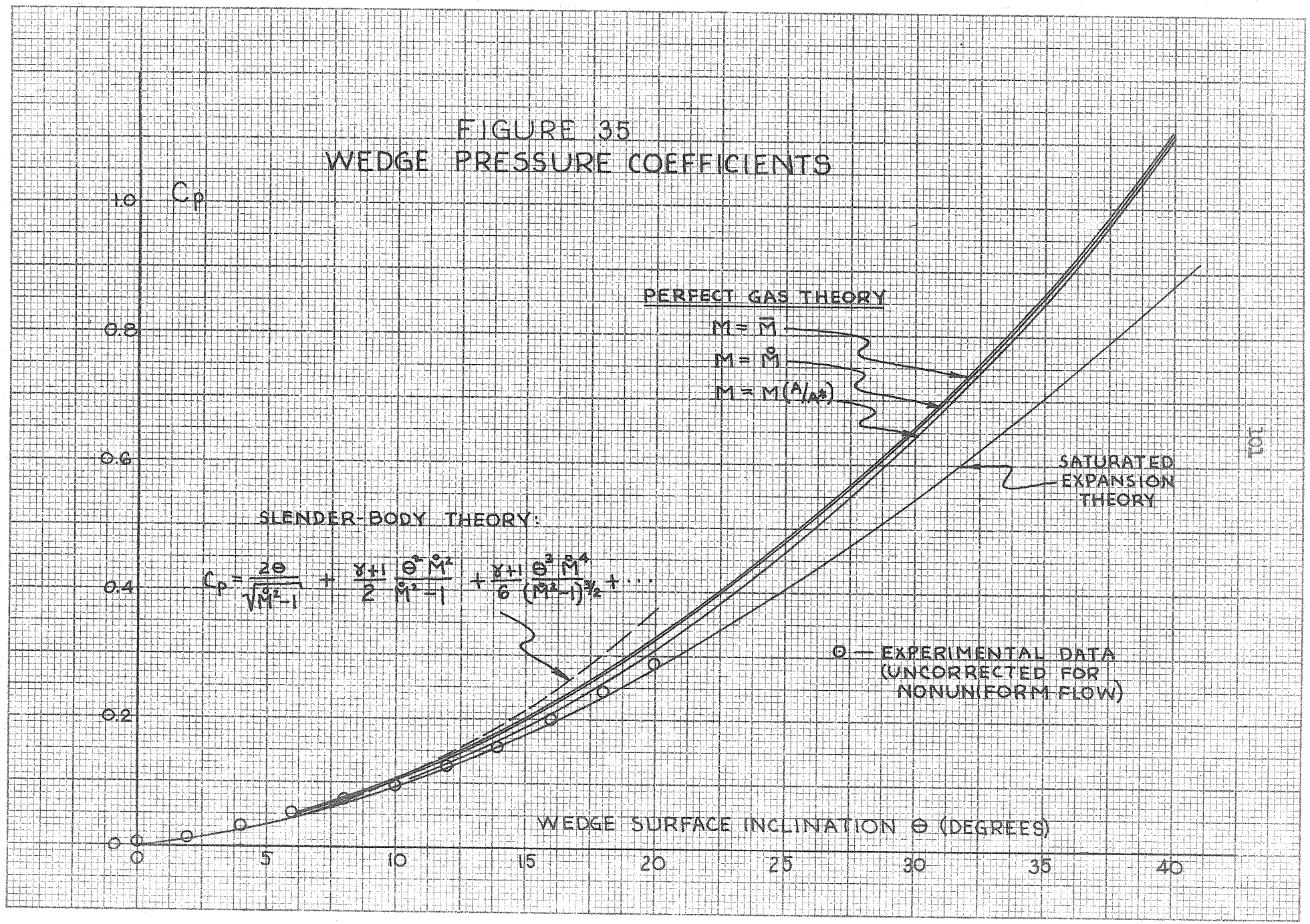

FIGURE 36a

COMPARISON OF MEASUREMENTS OF AMOUNT OF CONDENSED PHASE BY VARIOUS METHODS

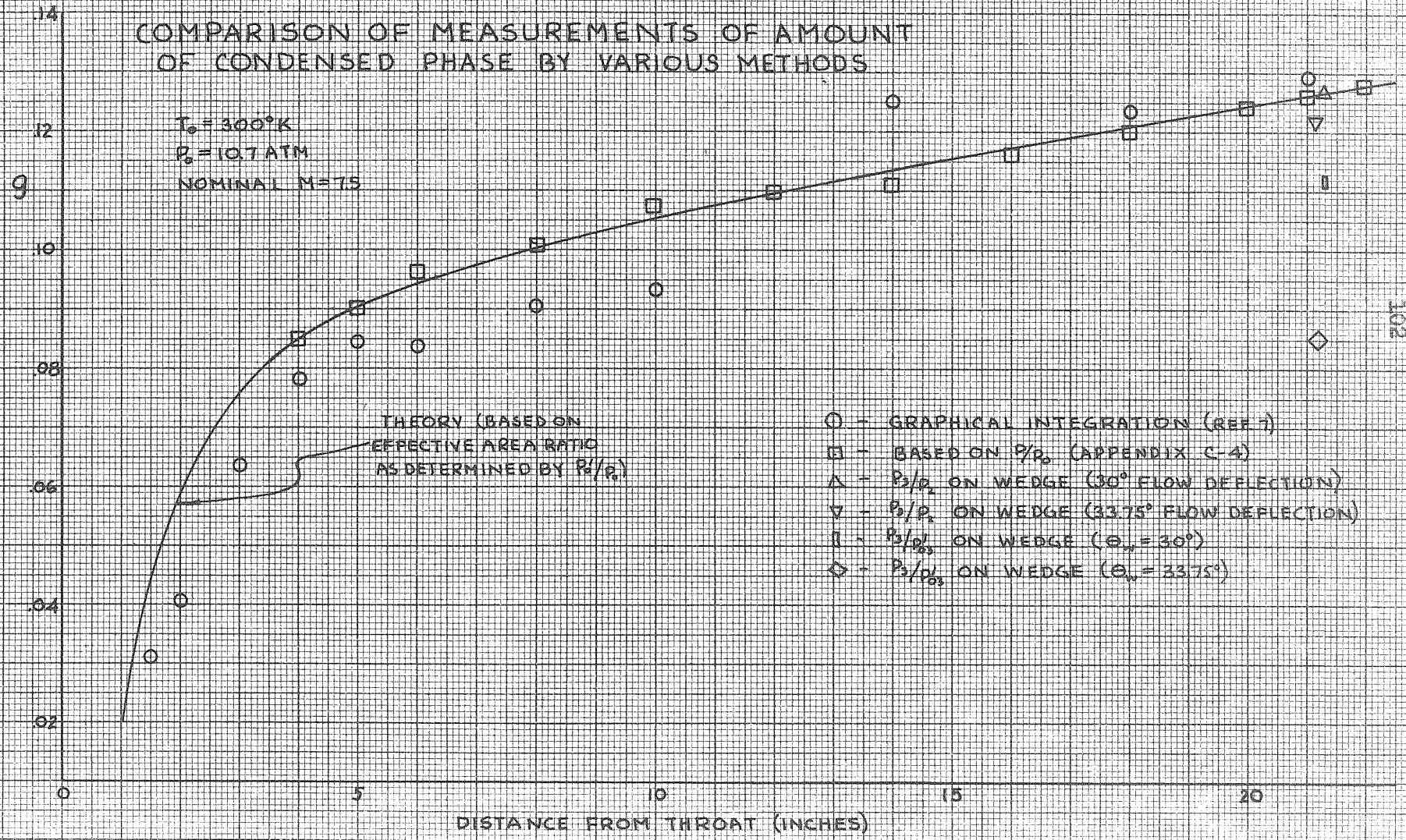

FIGURE 36 b

COMPARISON OF FREE-STREAM TEMPERATURE MEASUREMENTS BY VARIOUS METHODS

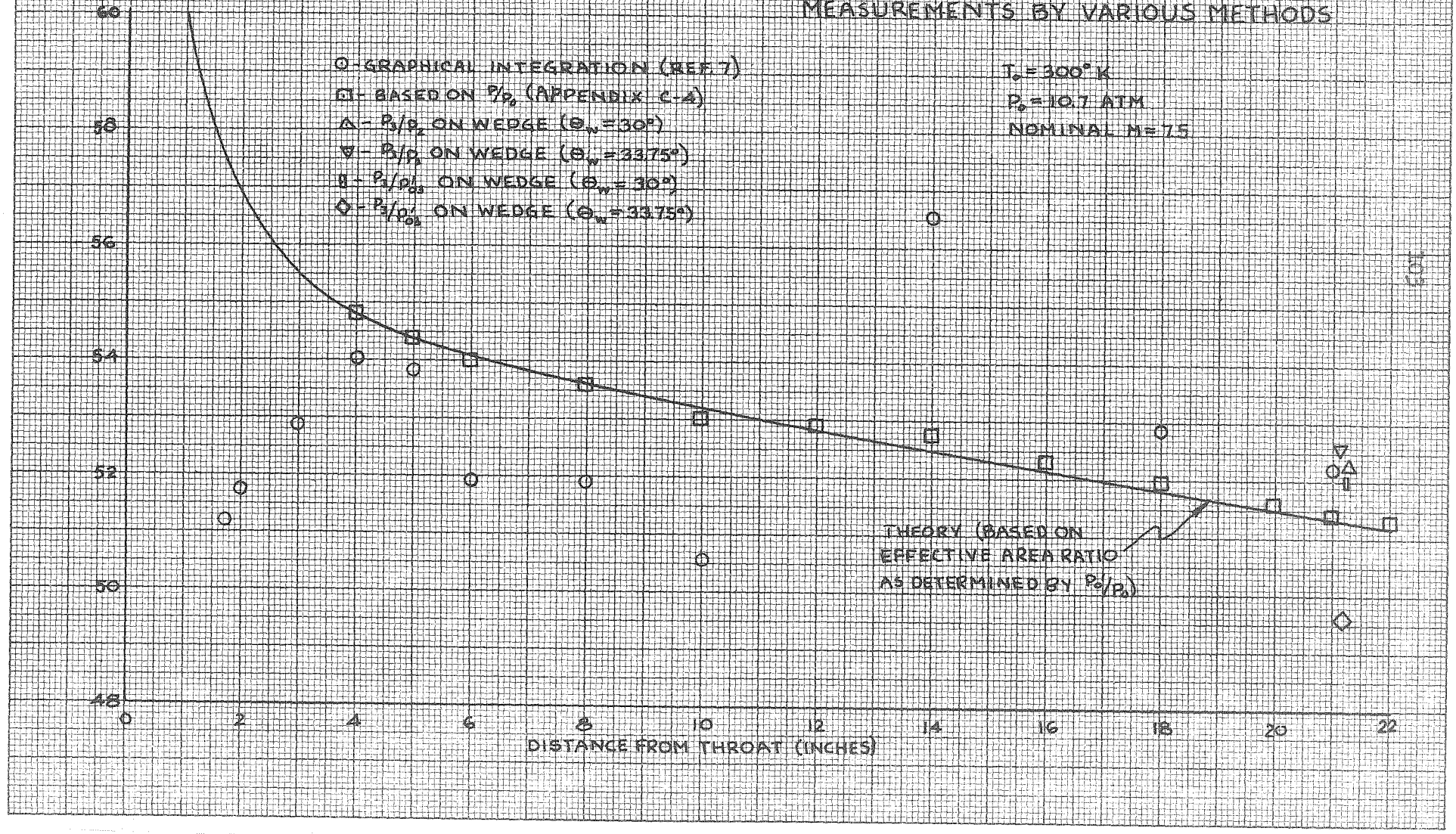

FIGURE 37
PITOT PRESSURE SURVEY BEHIND OBLIQUE SHOCK
(30° FLOW DEFLECTION)

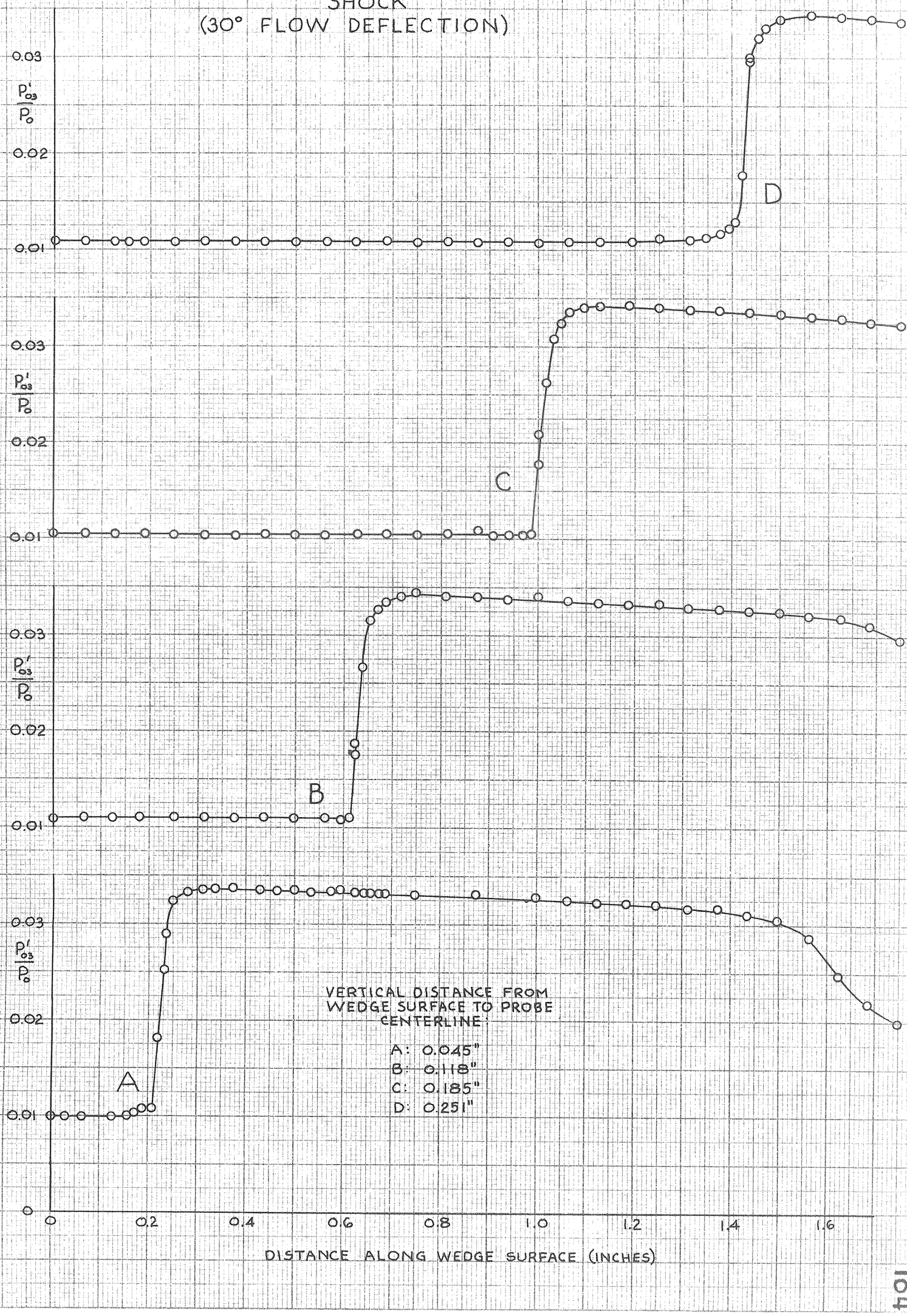

VERTICAL DISTANCE FROM WEDGE SURFACE TO PROBE CENTERLINE:

A: 0.045"
B: 0.118"
C: 0.185"
D: 0.251"

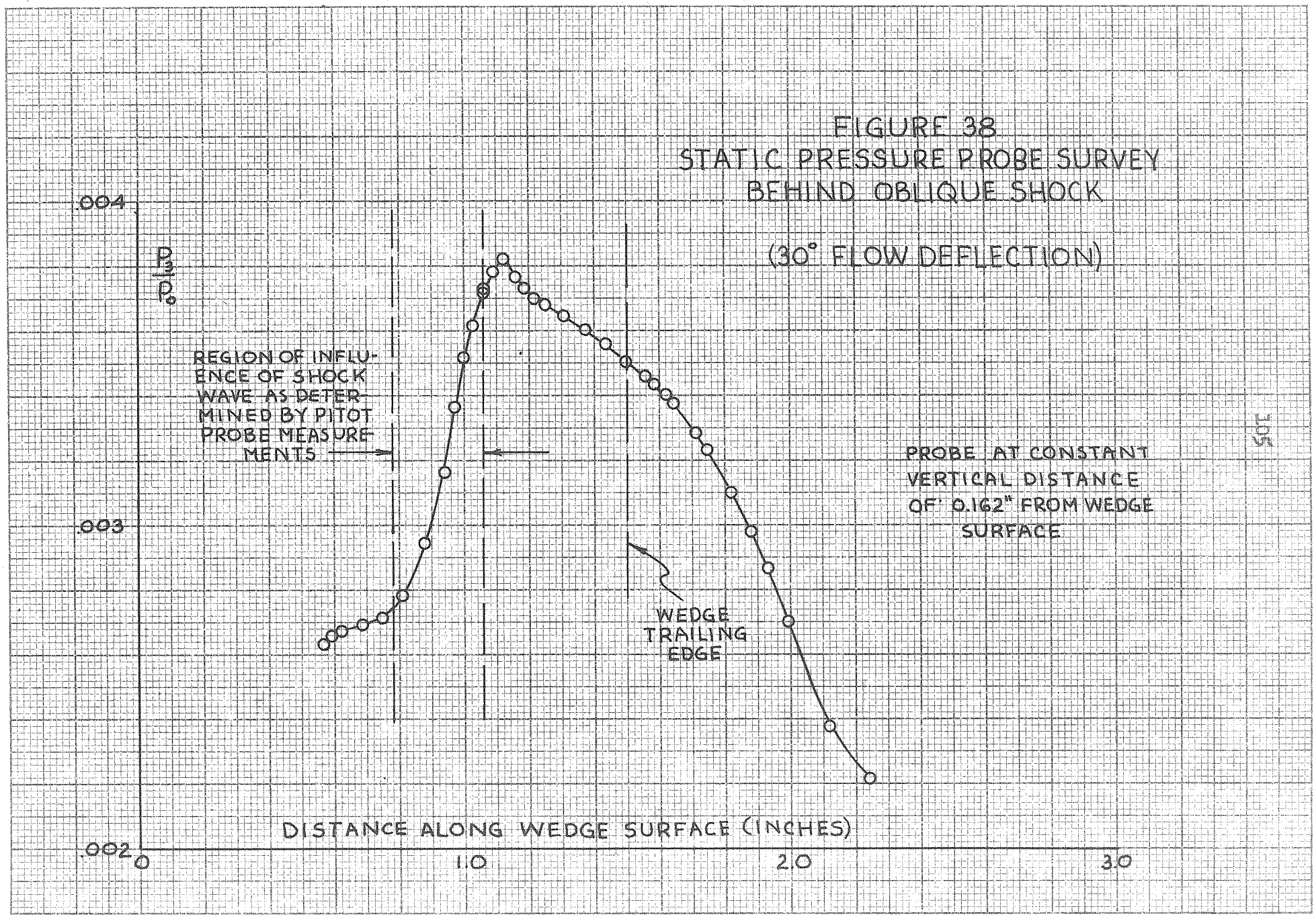
FIGURE 38
STATIC PRESSURE PROBE SURVEY
BEHIND OBLIQUE SHOCK
(30° FLOW DEFLECTION)
.004
.003
.002
$\frac{P_3}{P_0}$
REGION OF INFLUENCE OF SHOCK WAVE AS DETERMINED BY PITOT PROBE MEASUREMENTS
PROBE AT CONSTANT VERTICAL DISTANCE OF 0.162" FROM WEDGE SURFACE
WEDGE TRAILING EDGE
DISTANCE ALONG WEDGE SURFACE (INCHES)
0
1.0
2.0
3.0
305

FIGURE 39

SHOCK WAVE ANGLE AS A FUNCTION OF WEDGE SURFACE ANGLE

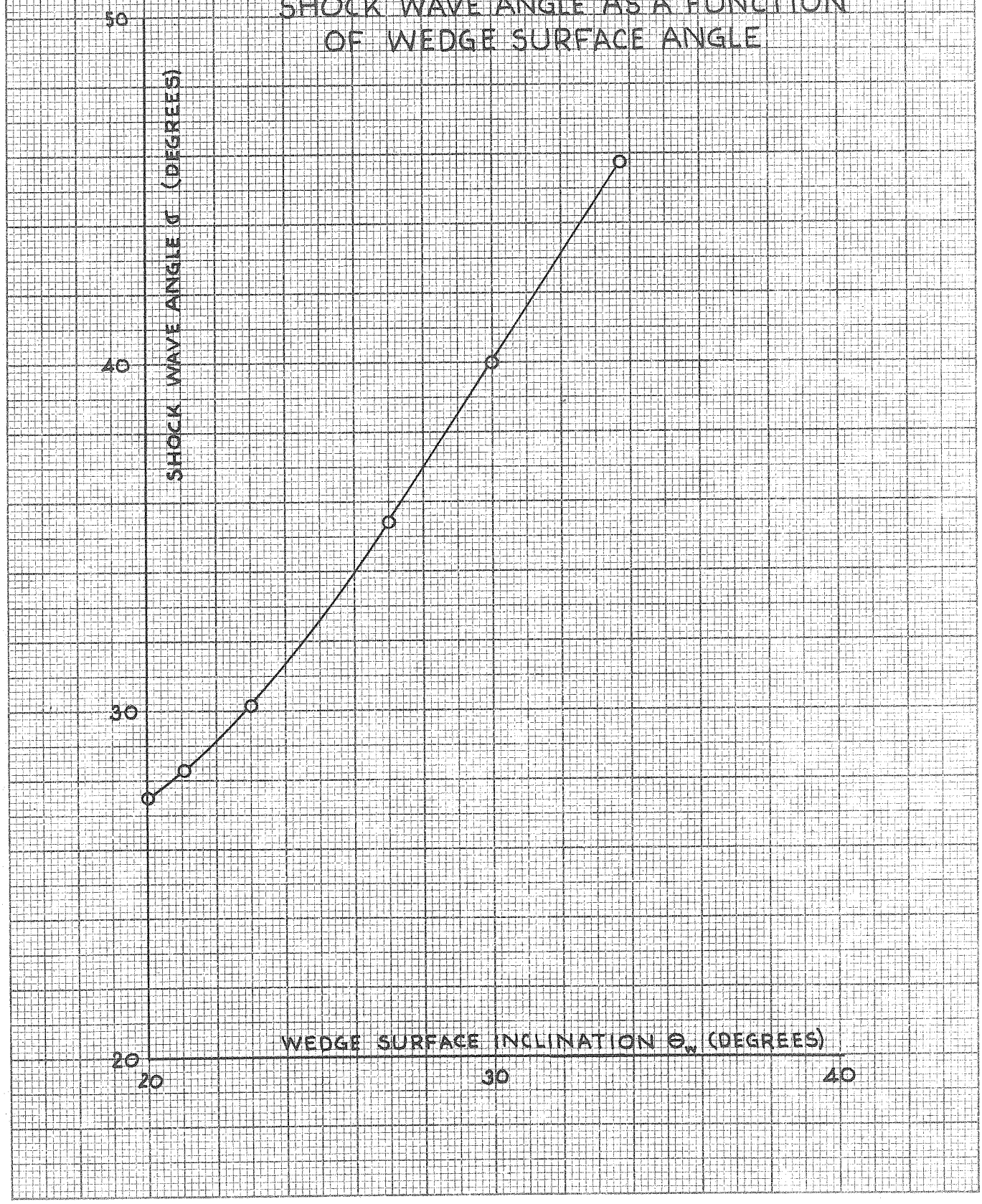

FIGURE 40

FLOW INCLINATION Θ BEHIND AN OBLIQUE SHOCK IN SOURCE FLOW

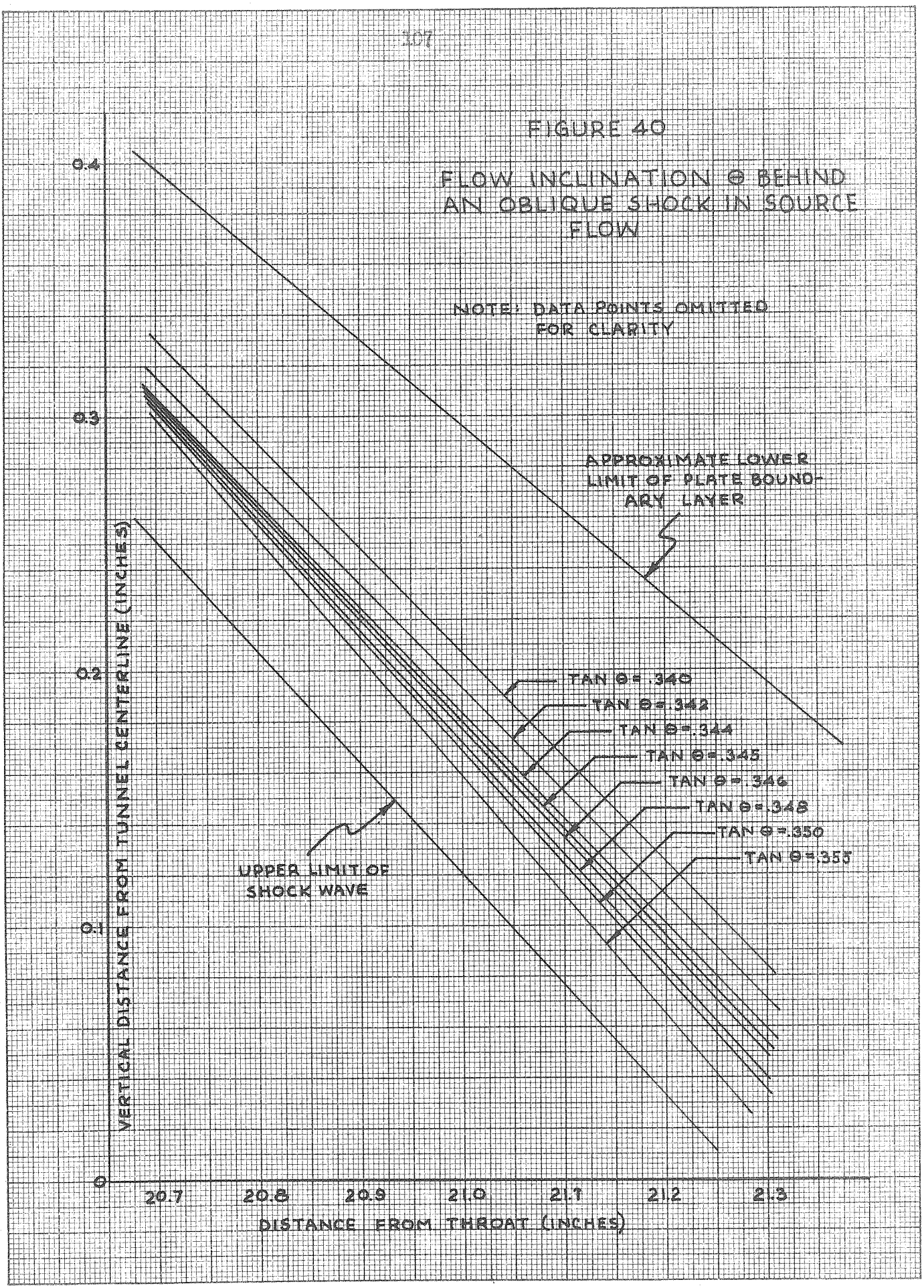

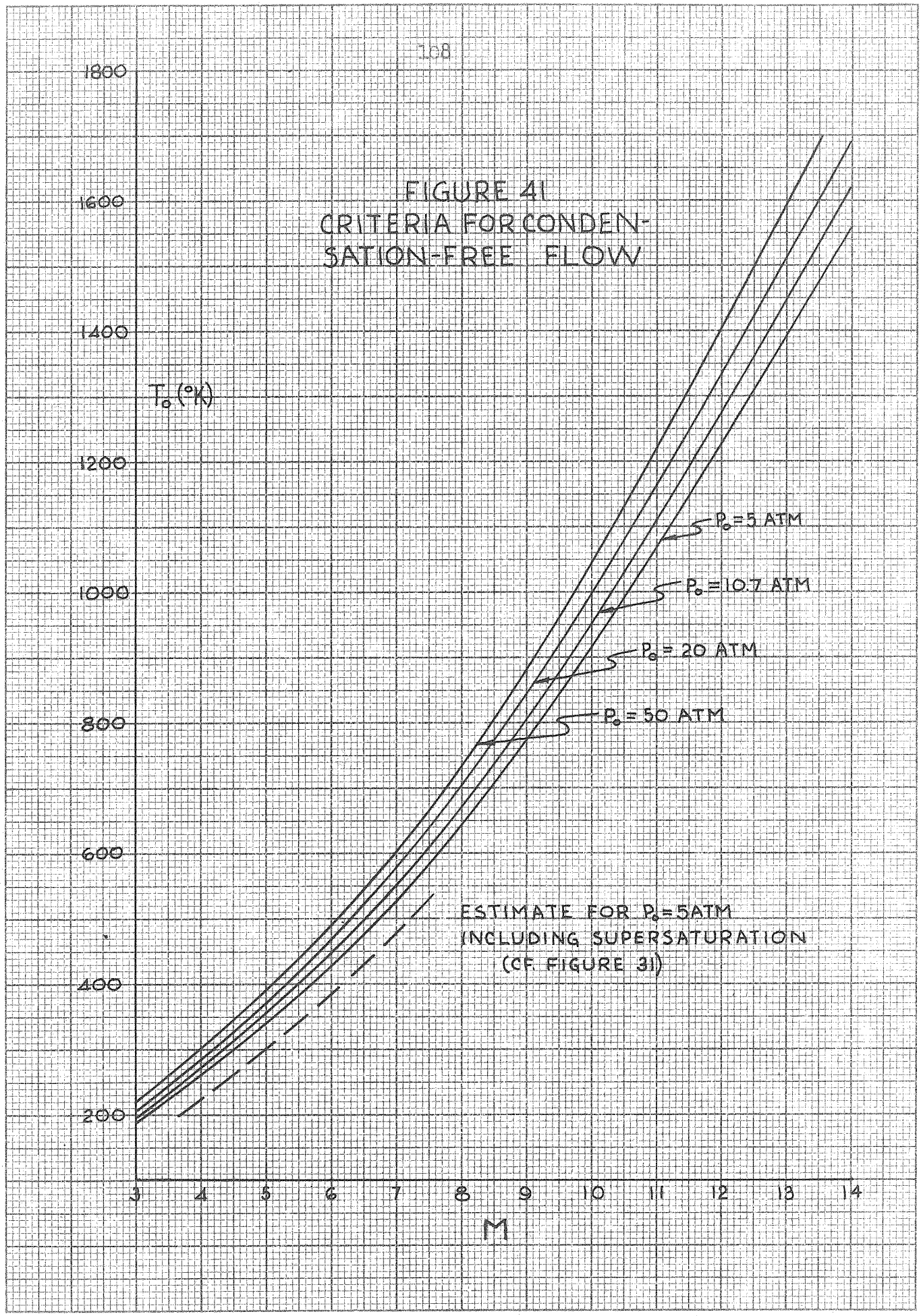

FIGURE 41
CRITERIA FOR CONDEN-
SATION-FREE FLOW

LIST OF TABLES

TABLE I

COMPARISON OF EXPERIMENTAL DETERMINATIONS OF VARIOUS SPEEDS OF SOUND AT ONE AREA RATIO OF 149

SYMBOL	EXPRESSION	VALUE (CM/SEC)
$\tilde{a}$	$\sqrt{(1-g)\gamma RT}$	13,500
$\check{a}$	$\sqrt{\gamma RT}$	14,460
$\mathring{a}$	$\left[\frac{(1-g)RT}{1-\frac{2RT}{L}+\frac{\gamma}{(\gamma-1)(1-g)}\frac{1}{\left(\frac{RT}{L}\right)^2}}\right]^{\frac{1}{2}}$	12,100
$\bar{a}$	[DETERMINED BY WEDGE MEASUREMENT OF $dp/d\theta$]	12,560
$\sqrt{\frac{dp}{d\rho}}$	(MEASURED BY PITOT-STATIC PRESSURE SURVEY)	13,370

TABLE II

VALUES OF FREE-STREAM TEMPERATURE AND AMOUNT OF CONDENSED PHASE AS DETERMINED BY VARIOUS EXPERIMENTAL METHODS AT ONE AREA RATIO OF 149

METHOD	T(°K)	g
GRAPHICAL INTEGRATION (REF. 7)	52.21	.1293
P/P_o (APPENDIX C-4)	51.45	.1260
WEDGE: P_3/P_2 ($\theta_w = 30°$)	53.3	.1265
WEDGE: P_3/P_2 ($\theta_w = 33.75°$)	52.6	.1220
WEDGE: P_3/P'_{o3} ($\theta_w = 30°$)	52.0	.112
WEDGE: $(P_3/P'_{o3}$ ($\theta_w = 33.75°$)	49.6	.085
WEDGE: WAVE BLEED BEHIND SHOCK	69.2	.257
SATURATED EXPANSION THEORY	51.40	.1265